Identifying the location of the drug binding site(s) in P-glycoprotein

Rituparna Mittra

February 2021

A thesis submitted for the degree of Doctor of Philosophy of The Australian National University.

DECLARATIONS

I, Rituparna Mittra, declare that I am the sole author of this thesis and all the results presented are my own original work.

Word count: 36,578

……..

Rituparna Mittra

ACKNOWLEDGEMENTS

Firstly, I would like to thank my supervisor and friend, Associate Professor Richard Callaghan for not only giving me the opportunity to pursue my PhD at his laboratory, but also for his unsurpassed patience and guidance over the years. Getting to this point has been quite a journey with several personal speed bumps, many of which Richard has helped me over. I value Richard's support and his straightforward attitude to many things in life. I also value his determination and perseverance and have been fortunate enough to have built a friendship with him over many years of curry and wine. I hope we continue this. Thank you for putting up with me and for believing I had it in me to one day become the scientist that I am. I owe you a depth of gratitude.

I would also like to thank my co-supervisors, Associate Professors Ian Kerr and Megan O'Mara for their help and guidance over the years. To the rest of the Callaghan laboratory, I thank each one of you for your support both within the lab and beyond it. I have many cherished memories and luckily gained some long-lasting friendships.

Most importantly, I would like to thank my family for their unparalleled belief, support, and unconditional love over the years on this journey. I wish my grandmother were alive to enjoy this milestone; I miss her every day. To my parents - you have dreamed for me from the day I was born and done everything to make sure I had the best opportunities in life. I am everything today because of you both. Thank you. To my brother, thank you for challenging me, pushing me, and cheering me on every step of my journey in life. You believed in me when I did not. To my husband and best friend - one of the best things that came out of this PhD was meeting you in Canberra. I love you; thank you for sticking by me through all the difficult times and most of all thank you for giving me the two greatest inspirations in my life – Emilia and Riaan. Mili and Riaan – this is for you both.

ABSTRACT

P-glycoprotein (P-gp), an ABC transporter protein, is characterized by its ability to recognise, bind, and efflux over 300 chemically and structurally unrelated compounds. P-gp overexpression in cancer cells confers multidrug resistance (MDR) by preventing sufficient accumulation of anticancer drugs within the cell, thus avoiding their cytotoxic effects. P-gp harnesses the energy from ATP hydrolysis to translocate substrates across the plasma membrane against a concentration gradient. Biochemical and structural investigations have identified the presence of a large aqueous central cavity which is likely the location for the drug binding sites (DBSs). The substrate polyspecificity displayed by P-gp is imparted by the existence of at least four pharmacologically distinct DBSs located within the transmembrane domain (TMD). However, whether these sites are spatially distinct from each other was not clear. The current investigation has identified several key contact residues of four pharmacologically distinct substrates/modulators of P-gp (nicardipine, vinblastine, rhodamine 123, and paclitaxel), known to bind at the four identified sites. Seven residues in various TMDs were mutated to a cysteine. Biochemical assays using purified, reconstituted P-gp expressing each mutant isoform was used to identify which contact residues were implicated in the binding of each drug. For rhodamine 123 binding, the identified contact residues were located within the central cavity of P-gp. However, for vinblastine, paclitaxel, and nicardipine, the implicated contact residues were located at the lipid-protein interface rather than the central cavity. A key residue (F978) located within the central cavity is believed to be involved in the interdomain communication between the TMDs and the nucleotide binding domains (NBD; site of ATP hydrolysis). Collectively, data presented here suggests the existence of at least four spatially distinct drug binding sites that are connected by a single translocation pore in the central cavity.

Table of Contents

DECLARATIONS 2

ACKNOWLEDGEMENTS 3

ABSTRACT 4

Chapter 1: INTRODUCTION 9

1.1 Multidrug Resistance (MDR) 10

1.1.1 Mechanisms of drug resistance in cancer 10

1.1.2 P-glycoprotein causes MDR 12

1.1.3 The physiological role of P-gp 13

1.2 P-gp is an ABC transporter 14

1.2.1 Structural organization of ABC transporters 14

1.2.2 P-gp structure and the biochemical mechanism of drug transport 17

1.2.3 The challenges of inhibiting P-gp function to overcome MDR 23

1.3 Photoaffinity labelling (PAL) 26

1.3.1 Identification of drug binding sites using PAL 28

1.3.2 PAL following proteolytic digestion of P-gp into domain fragments 29

1.3.3 PAL enhanced by MALDI-TOF 31

1.4 Cysteine-scanning mutagenesis 32

1.4.1 Understanding the structure of P-gp and NBD-TMD communication 33

1.4.2 Covalent modifications at cysteine residues 34

1.4.3 TM6 and TM12 are direct links to the NBD 37

1.5 Nature of drug binding: Does one size fit all? 39

1.5.1 A substrate-induced fit model for drug binding 39

1.5.2 Evidence for multiple drug binding sites on P-gp 42

1.6 Summary and Project Outline 52

1.6.1 Where we stand 52

1.6.2 Where we are headed 53

Chapter 2: MATERIALS AND METHODS 55

2.1 Materials 56

2.1.1 Tissue culture and protein expression 56

2.1.2 Protein purification 56

2.1.3 Reagents used for functional analysis of purified protein 57

2.1.4 SDS-PAGE and western immunoblotting 57

2.2 Methods 58

2.2.1 Tissue culture – cell maintenance 58

2.2.2 Viral amplification in Sf900 cells 58

2.2.3 Large scale expression of P-gp in Hi-5 cells 60

2.2.4 Preparation of crude membranes using nitrogen cavitation 61

2.2.5 Western immunoblotting 61

2.2.6 Protein purification from crude membranes 62

2.2.7 SDS-PAGE analysis of purification 64

2.2.8 Colorimetric assay to measure the ATPase activity of P-gp 65

2.2.9 Tryptophan fluorescence assay 67

2.2.10 Statistical analysis 69

Chapter 3: RESULTS 70
3.1 Expression, purification and reconstitution of mutant P-gp isoforms 71
3.1.1 Expression in insect cells and isolation of crude membranes 71
3.1.2 Purification and reconstitution of P-gp from crude membrane preparations 73
3.1.3 Yield of mutant P-gp isoforms 74
3.2 Assessing the functional integrity of mutant P-gp isoforms 77
3.2.1 Measuring ATPase activity 77
3.3 Assessing molecular interactions between mutant P-gp isoform and each drug 82
3.3.1 Measuring drug potency (EC_{50}) 82
3.3.2 Measuring binding affinity (K_{App}) 84
3.4 Identification of contact residues 94
3.4.1 Contact residues involved in the binding of nicardipine 95
3.4.2 Contact residues involved in the binding of vinblastine 98
3.4.3 Contact residues involved in the binding of rhodamine 123 100
3.4.4 Contact residues involved in the binding of paclitaxel 103
3.5 Summary of Results 105
Chapter 4: DISCUSSION 108
4.1 Findings of current investigation 109
4.2 Experimental approach of current investigation 110
4.3 Scope of current investigation 113

4.4 Evidence of drug binding site within the central cavity 115

4.5 Evidence of drug binding sites outside the central cavity 120

4.5.1 Drugs can access P-gp through ‘gates’ 121

4.5.2 Is P-gp a hydrophobic ‘vacuum cleaner’ or a drug ‘flippase’? 123

4.5.3 The four pharmacologically distinct drug binding sites are also spatially distinct..... 127

4.6 The importance of residue F978 in P-gp drug translocation..... 132

4.7 Scientific impact of the current investigation 135

REFERENCES 138

Chapter 1:
INTRODUCTION

1.1 Multidrug Resistance (MDR)

Clinical management of most cancers today depend on chemotherapy outcome. Successful chemotherapy treatment depends on acquiring a real understanding of the factors that limit it. The 170kDa plasma membrane glycoprotein, P-glycoprotein (P-gp), encoded by the *MDR1* gene, plays a major role in the acquisition of a drug resistant phenotype in many cancer cells. Initially identified in 1976 in Chinese hamster ovary cells cultured in the presence of the antimitotic agent colchicine, P-gp also significantly reduced the cellular accumulation of several chemically, structurally, and functionally distinct anticancer agents [1, 2]. When cancer cells acquire simultaneous resistance to a broad spectrum of chemotherapeutic agents, the phenotype is termed multidrug resistance (MDR) and significantly reduces positive outcomes following chemotherapy [3].

1.1.1 Mechanisms of drug resistance in cancer

Cancer results from the uncontrolled growth of abnormal cells which have undergone a dynamic alteration in their genome. Cancer progression impairs the biological process of normal healthy cells through invasion into neighbouring tissues, and metastasis to distant sites within the body. Current treatments include surgery, radiation, chemotherapy, combination therapy, and targeted therapies which exploit biological and molecular targets specific to types of cancers. Despite these, 90% of failures in chemotherapy are associated with cancers becoming resistant to drugs [4, 5]. There are several different resistance mechanisms.

Many chemotherapeutic agents must first undergo metabolic activation *in vivo* to acquire clinical efficacy. Cancer cells can develop resistance to treatments by decreasing drug activation. One mechanism of drug activation and inactivation is

through the cytochrome P450 (CYP system). Polymorphisms in CYP may alter these proteins' metabolic capabilities such as increasing the breakdown of drugs or promoting their secretion by the kidneys [6, 7]. The glutathione-*S*-transferase (GST) family of detoxifying enzymes may contribute to drug resistance through direct detoxification of cellular macromolecules from electrophilic compounds generated to damage DNA in cancer cells, resulting in decreased cytotoxic damage to cancer cells, as well as through inhibiting the MAPK (mitogen-activated protein kinase) pathway [8].

Changes in apoptosis-related proteins such as the tumour suppressor protein p53 (*TP53*) in response to chemotherapy can also promote drug resistance. *TP53* is mutated in 50% of cancers and can impair the connection between DNA damage (caused by chemotherapeutic agents) and activation of the apoptosis pathway [9]. Inactivation of P53 regulators (including caspase-9 and its cofactor Apaf-1) can also result in drug resistance [10].

Additionally, the efficacy of a drug is also influenced by alterations in its molecular targets through mutations and expression levels in cancer cells, leading to resistance. For example, 30% of breast cancer patients overexpress the human epidermal growth factor receptor 2 (HER2) receptor tyrosine kinase [11], and long-term use of drugs that inhibit this kinase can result in drug resistance [12]. Use of trastuzumab for the treatment of HER2+ breast cancer has shown high levels of efficacy in combination chemotherapy, but many patients eventually stop responding and the mechanism of resistance is thought to be achieved by alteration in the signal transduction process that mediates drug activation [13].

Repair of damaged DNA also plays a key role in anticancer drug resistance. Chemotherapeutic agents can directly or indirectly damage DNA and DNA damage response (DDR) mechanisms can reverse the drug-induced damage in cancer cells. This is evident in the use of platinum-containing chemotherapy drugs such as Cisplatin which leads to apoptosis following formation of damaging DNA crosslinks. Increased nucleotide excision repair and homologous recombination are ways that cancer cells overcome these damages, thus reducing the efficacy of DNA-damaging, cytotoxic drugs [14, 15].

1.1.2 P-glycoprotein causes MDR

A key mechanism of drug resistance is through increased transport of anticancer drugs out of the cancer cells. The overexpression of P-gp in cancer cells was either inherent or acquired (generated following exposure to multiple anticancer drugs). P-gp mediates drug translocation across the plasma membrane against considerable concentration gradients in an ATP-dependent manner. Though it is one of many resistance mechanisms, there is strong evidence in support of the clinical relevance of P-gp expression and its association with drug resistance and poor prognosis [16-18]. The list of compounds known to interact with P-gp are in excess of 300 and include many of the new generation targeted therapies (e.g. kinase inhibitors) [19]. There continues to be a pressing need to address the unwanted effects of P-gp by generating compounds and strategies that can overcome MDR to increase effectiveness of chemotherapy in cancer, as well as to influence the pharmacokinetic profile of a vast number of clinically prescribed drugs [20, 21]. To do this, a better understanding the drug-protein interactions at the molecular level is required, including studying the drug binding site(s) and their physicochemical environment.

This will further comprehension of the polyspecific nature of P-gp and hopefully aid in rational drug design of compounds that are able to inhibit or evade P-gp function.

The next few sections cover the background of P-gp structure, function and pharmacology, and key techniques and findings over the past several decades that have helped answer the question, *"are there multiple drug binding sites in P-gp?"*. The current investigation identifies the location of four spatially and pharmacologically distinct drug binding sites, providing support for the existence of multiple drug binding sites to help address how P-gp is polyspecific and thus capable of recognising and binding a vast variety of chemically unrelated substrates.

1.1.3 The physiological role of P-gp

P-gp is expressed at low levels across most human and rodent tissues but found at much higher amounts at the apical surface of epithelial cells lining the gastro-intestinal tract, proximal tubules of the kidneys, and the biliary face of hepatocytes in livers [22, 23]. This localization suggests that P-gp is involved in an excretory role, preventing the entry of potentially toxic compounds from the gut into the blood, and removing endogenous metabolites into bile and urine [24]. P-gp is also expressed in the placenta, where it protects the developing foetus from toxicity of various endogenous and exogenous molecules, and in the adrenal gland, suggesting an involvement in the secretion of steroids or in the protection of the plasma membranes of steroid-secreting cells from high concentrations of steroids [25]. High expression is also observed on the apical surface of endothelial cells that line the capillaries in the brain [26]. These capillary endothelial cells comprise a continuous monolayer forming a major component of the blood-brain barrier that limits the entry of blood components into the central nervous system. The orientation of P-gp at the blood-brain barrier facilitates transport of substrates out of the CNS and into the blood [27].

This is a major limiting factor when administering chemotherapeutic drugs for the treatment of brain cancers that are substrates of P-gp. P-gp has known effects on the disposition of several clinically administered drugs, including many antibiotics, HIV protease inhibitors and immunosuppressive agents, affecting their bioavailability by altering the tissue absorption and distribution [28]. Transgenic mice lacking P-gp display significantly increased sensitivity to certain administered drugs, as well as a disrupted blood-brain barrier [29].

1.2 P-gp is an ABC transporter

P-gp is a member of the ATP binding cassette (ABC) transporter family of integral membrane proteins. ABC transporters are found across all species and play a critical role in biological processes by actively transporting ligands across biological membranes following ATP hydrolysis [30]. ABC transporters are involved in the uptake of nutrients, elimination of waste products, in cell signalling and energy generation. There are 48 human ABC transporters which are involved in most aspects of cell physiology [31]. Mutations in these transporters are associated with several genetic disorders including those of the eye [32] and liver [33], as well as cystic fibrosis and Tangier disease [34].

1.2.1 Structural organization of ABC transporters

In general, the core structure of an ABC transporter protein is comprised of two transmembrane domains (TMDs) and two nucleotide binding domains (NBDs). ABC transporters vary in their modular composition. Sequence analysis indicates that the majority of TMDs are composed of two sets of six hydrophobic transmembrane (TM) helices, although this varies across members of the superfamily [35]. The four domains may be comprised of two or four polypeptide chains (encoded by different

genes), assembled into monomers, hetero- or homodimers, or tetramers [35]. For example, the *E. Coli* ribose transporter, RbsA has two NBDs fused in a single polypeptide and forms a complex with two separate TMD polypeptides. The histidine permease from *Salmonella enterica* serotype Typhimurium is comprised of a core of four polypeptides with two NBDs and two TMDs. In some cases, two half-transporters, each comprised of one NBD and one TMD per polypeptide, may homodimerize (such as in the case of LmrA, a bacterial multidrug transporter), or heterodimerize (as in the case of TAP1/TAP2, the antigen presenting mammalian transporter) [36, 37].

The TMDs form the transmembrane core which contains the cytosolic and membrane spanning regions and the substrate-binding sites. The cytosolic NBDs are the sites of ATP binding and hydrolysis, providing the 'power' needed for active substrate translocation [38]. There is little sequence homology between TMDs in ABC proteins. This is related to their role in the recognition and binding of diverse substrates. Unlike TMDs, NBDs are homologous throughout the family and have several characteristic motifs (figure 1) [31]. The high degree of sequence homology in NBDs reflects the commonality of the ATP hydrolysis mechanism. The NBDs typically contain seven conserved motifs. Structurally, each NBD is L-shaped, comprised of two lobes. Lobe I, the larger of the two, is the ATP-binding 'core' sub-domain containing the Walker A and B motifs. The first of the two binds the nucleotide, and the latter provides the conserved glutamate residue responsible for the nucleophilic attack on ATP via a

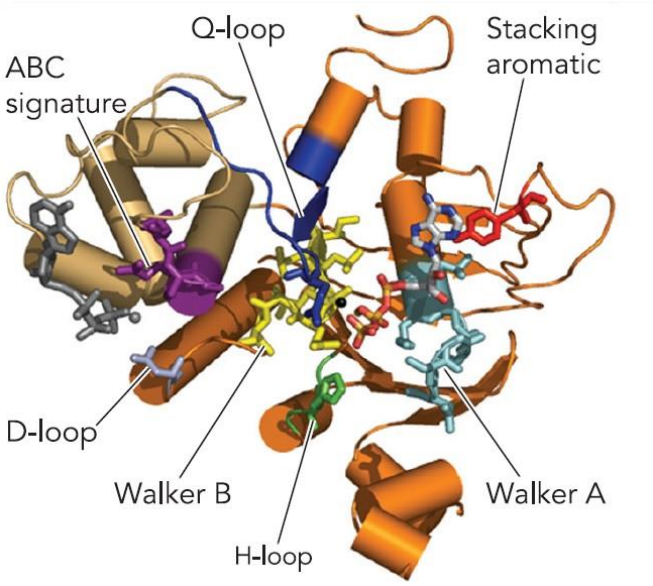

Figure 1: Schematic representation of one NBD. Lobe I (core subdomain; gold colour) is comprised of the elementally coloured ATP which is cradled between the Walker A (cyan) and Walker B (yellow) motifs, as well as the H-loop (green), Q-loop (blue), and the stacking aromatic (red). Lobe II (α-helical subdomain; pale brown colour) contains the main ABC signature in contact with the gray-coloured ATP which is bound with high affinity following the reciprocal arrangement of the other NBD (not shown). The D-loop hydrogen bonds with the other NBD. *(figure abstracted from Linton, 2007)*

water molecule. Lobe I also contains the highly conserved A-, Q-, D-, and H-loops [30]. The A-loop contains an aromatic side chain residue postulated to play a role in the formation of π-π stacking bonds to interact with the adenine moiety of the bound ATP nucleotide [36, 39]. The Q-loop forms the central flexion point and is thought to be involved in the contact interface with the TMD where it senses the ɣ-phosphate moiety of the nucleotide. The D-loop is largely involved in the contact interface between the two NBDs, and the 'switch motif' H-loop contains a histidine side chain thought to contribute to the overall catalytic reaction [40, 41].

The smaller lobe II α-helical sub-domain contains the highly conserved LSGGQ consensus sequence motif (also called the 'ABC signature motif' or the C-loop). The LSGGQ signature of one NBD monomer contacts the nucleotide sandwiched between the Walker A and B motifs of the other monomer, resulting in a head-to-tail

NBD dimer formation in the ATP-bound state [30, 38]. There are two ATP-binding sites formed between the NBD-NBD interface, providing the structural basis of the co-operativity observed in ATP binding and hydrolysis supported by sequence analysis and biochemical studies [42]. There currently exist several crystal structures of full-length ABC transporters (all are of bacterial origin), including Sav1866, a drug exporter from *Staphylococcus aureus* [43], BtuCD, a vitamin B12 transporter from *E. Coli* [44], and HI1470/1 from *Haemophilus influenzae*, a metal-chelate transporter [45]. Though many of the structures have some overlapping similarities, they are not identical in their structural organisation, but each have a plausible TMD-TMD interface, with an aqueous central chamber, and NBD-NBD interface capable of coordinating nucleotide binding.

1.2.2 P-gp structure and the biochemical mechanism of drug transport

Due to its role in clinical resistance to chemotherapy, P-gp (also known as ABCB1) is one of the most investigated human ABC transporters. P-gp is encoded by the *mdr1* gene and is a tandemly duplicated molecular sequence that encodes a protein of molecular mass 170kDa with 1280 amino acids [2, 46]. Each half of P-gp consists of

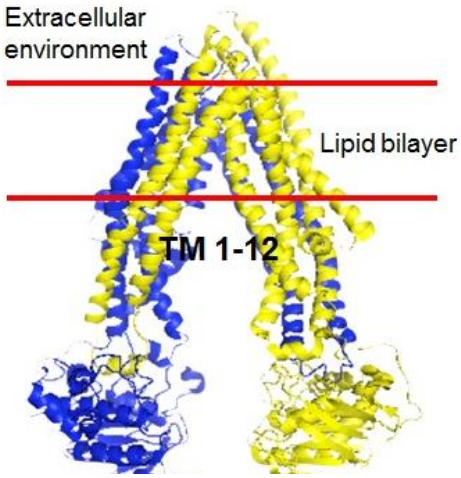

Figure 2: X-ray crystal structure of mouse P-gp. The N-terminal and C-terminal halves are coloured in yellow and blue respectively; TMs 1-12 are labelled and the two NBDs as shown in the cytosolic side of the lipid membrane bilayer represented by the red horizontal lines *(Aller et al., 2009)*.

a NBD and six TM helices forming a TMD. The 12 TM helices of the two TMDs associate together to form a cavity that contains drug binding sites and a conduit for passage to the extracellular environment (figure 2) [3, 47].

One of the first reported structures of P-gp was by single particle image analysis and electron crystallography of 2D crystals [48]. These low to medium resolution projection maps trapped P-gp at different stages of the hydrolytic cycle and suggested that the TM helices formed a central chamber within the membrane, open to the extracellular environment. It also suggested accessibility of substrates from the lipid bilayer at the interfaces between two TM segments [49].

Several mouse P-gp structures have since been obtained, however also at relatively low resolutions due to the intrinsic flexibility of P-gp [50-52]. Mouse P-gp bears 87% sequence homology to human P-gp [53]. In 2009, the first mouse P-gp X-ray structure was reported in the absence of a nucleotide and with or without inhibitors at a resolution of 3.8-4.4Å. A striking feature is the large internal cavity of ~6000Å^3 open to both the cytoplasm and the membrane inner leaflet. In this orientation the two NBDs showed a wide separation of ~38Å, measured between the cysteine residues of the Walker A motifs [47]. It is postulated that hydrophobic drugs may bind at several different locations within this cavity. This is supported by the co-crystallization data of mouse P-gp with two stereo-isomers of cyclic hexapeptide inhibitors (QZ59-RRR and QZ59-SSS) bound to the central cavity of P-gp at different sites [50, 52], consistent with previous biochemical studies that demonstrated binding of at least two molecules of the same compound at the same time [41]. The slight differences in the physicochemical features of the two inhibitors (their optical properties) was sufficient to be differentiated in terms of binding sites. Biochemical studies have also identified that the cavity is lined by several transmembrane segments from both

halves of the P-gp; in particular TM helices 4, 5, 6, 10, 11, and 12. The internal cavity has also been posited to contain two portals for entry of substrates from the inner bilayer leaflet [24, 54].

A later near-atomic resolution cryo-EM structure of P-gp with a bound small-molecule inhibitor, zosuquidar, was resolved by Alam et al., [55] and showed the transporter in an occluded conformation with all TM helices lining the central, enclosed inhibitor-binding pocket. The structure was trapped by an engineered disulfide cross-link between the NBDs and bound to the antigen-binding fragment of the human-specific inhibitory antibody (UIC2). The investigation revealed additional cryo-EM structures which shed light on a dual mode of inhibitor binding, with movement of TM helices from both halves of P-gp associating to close the gap between the NBDs and facilitate binding of antibodies and small molecules. The investigation provided insight into the modulation of P-gp and the chemistry of the underlying specific ligand cuccinteractions (thus facilitating development of more potent antibody and small-molecule P-gp inhibitors) and ruled out the existence of an outward-open P-gp conformation.

The current understanding of how interactions between protein and substrate at the NBDs and TMDs is coupled to bring about drug transport, is formed around three distinct properties of transport proteins required to mediate substrate translocation [41]. First, they must contain a cavity large enough to accommodate the solute/ligand. Second, it must undergo conformational changes to adopt inward- and outward-facing configurations so that the cavity is alternately open to either side of the membrane. Finally, the cavity should contain binding sites for the ligands which must alternate between high and low affinity for the substrate depending on the orientation of the site [56, 57].

The earlier crystal structures of P-gp (mouse, *C. elegans* and *C. merolae*) all exhibited an inward-facing conformation with the two NBDs separated, and provided insights into the mechanism of P-gp transport [50, 53, 58, 59]. There currently exist multiple P-gp X-ray diffraction derived structures of murine P-gp in the basal states, the PDB codes of which are *3G5U* [50], *4M1M* [52], *4KSB, 4KSC, DKSD* [51], and *5KPD* [53]. These structures represent inward facing conformations and likely approximate the drug and nucleotide free state with high affinity drug binding sites. Two cryo-EM structures, one containing a bound modulator (*6FN1*) and the other a human-mouse chimera (*6C0V*) with bound ATP, are trapped in inward-occluded and outward-facing conformations, respectively [55]. Each model shows a variety of differences in activity and specificity and were obtained in different conformations with or without bound modulators. Thus, they represent numerous differences in the topography and organization of P-gp. Additionally, the complexity associated with removing P-gp from its native bilayer environment to obtain the X-ray crystallography structures could have compromised its function [60].

The present investigation utilised the refined *4M1M* mouse P-gp structure (resolved to 3.8 Å). This model was chosen because of its ~87% sequence homology to human P-gp, as well as its refinement resulting in ~95% of residues in the favourable Ramachandran region, and therefore a significant improvement in protein geometry compared to other models [61]. Since the drug translocation pathway (enriched in aromatic residues) of mouse P-gp is 96% identical to human P-gp, the model allows for identification of key residues involved in substrate recognition [52].

The proposed mechanism of transport by P-gp involves two distinct, yet coupled, events. The catalytic step involves ATP hydrolysis to generate energy for transport. It comprises ATP binding and subsequent formation of an “NBD sandwich dimer” that

ensures high affinity substrate binding. This is followed by hydrolysis of ATP, dissociation of inorganic phosphate (P_i) and ADP. The energy derived from this process is coupled to the movement of substrates across the membrane [41, 56]. More recently an outward-facing structure of human P-gp was resolved by cryo-EM at a resolution of 3.4Å. This structure provided further support of the conformational changes that enable substrate translocation prior to ATP hydrolysis [62]. Two models have been hypothesized to describe the role of ATP binding and hydrolysis on substrate translocation (figure 3).

The ‘ATP switch model’ proposed by Higgins and Linton (figure 3A) suggested that drug binds to P-gp, lowering the activation energy required for formation of the closed “NBD sandwich dimer”, and increasing the affinity of the catalytic sites for ATP [57, 63]. ATP binding leads to structural changes in the TMDs that affects the affinity for substrate binding. It is assumed that conformational changes reorientate the drug-binding site to the extracellular environment and an associated switch from high- to low-affinity for drug binding at the site ensures dissociation of the drug from P-gp [31]. ATP hydrolysis initiates a resetting of the transporter to its basal, open dimer state. The closed sandwich dimer is destabilized due to the electrostatic repulsion between P_i (coordinated with the signature motif of one NBD) and the ADP coordinated with the Walker A motif of the other NBD). P_i and ADP are sequentially released, restoring the protein to its basal state and ready for another transport cycle. This process requires intricate communication between the drug binding sites and the NBDs containing the catalytic sites [23, 63].

The ‘alternating site model’ (figure 3B) proposes two hydrolysis events, wherein one powers drug efflux and the other resets the protein. Biochemical data suggested that both catalytic sites are required for drug transport [64]. It was proposed that only one of the two NBD catalytic sites hydrolyse ATP at any given time and the other must be in the transition state [65]. The two sites hydrolyse ATP in an alternating cycle, and it is hypothesized that the energy of ATP hydrolysis is essential in driving the NBD sandwich dimer apart and resetting the protein to its basal state, ready for another transport cycle [66, 67].

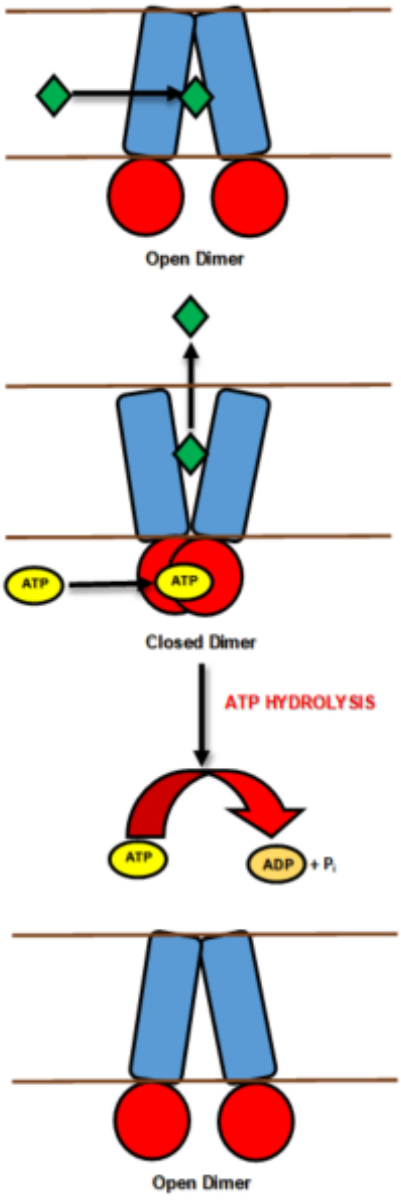

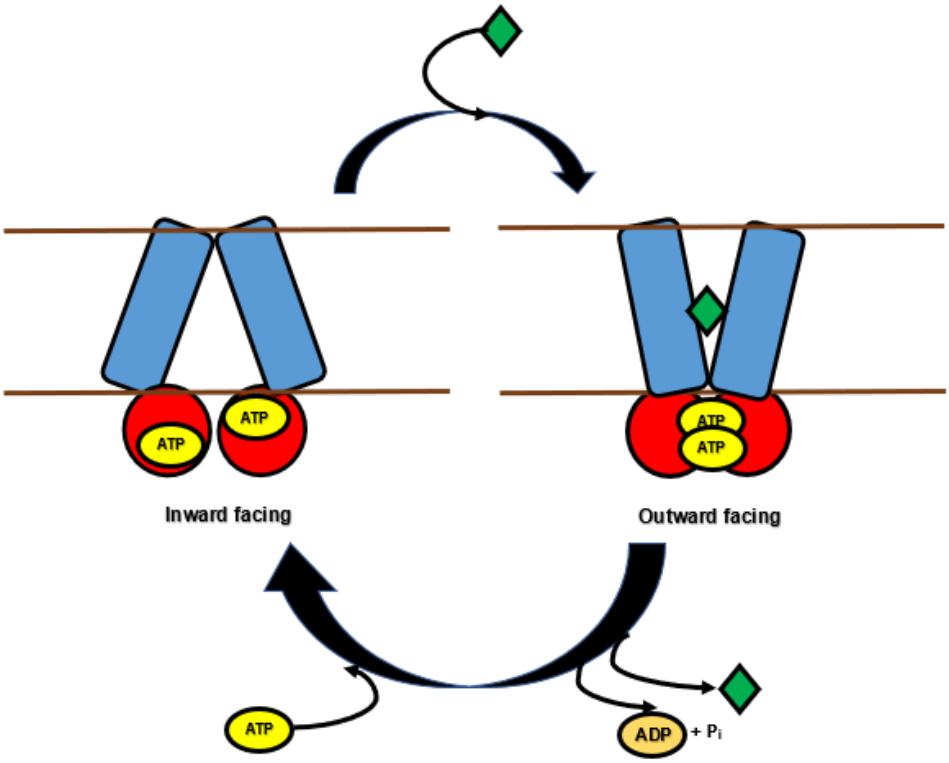

Figure 3: The two models of ATP binding and hydrolysis. Substrate is shown as green diamond, the blue rectangles show the two TMDs of P-gp, the red circles represent that two NBDs, and ATP molecules are shown as yellow labelled ovals. **(A) The ATP switch model** shows that substrate binds to a high-affinity pocket formed by the TMDs, which causes a conformational change in the NBDs, resulting in a change from the open to the closed dimer and a higher affinity for ATP binding at the NBDs. ATP molecules bind to the NBDs and the energy released following the formation of the closed dimer results in the conformational changes in the TMD which transitions into a low-affinity state and extrudes the substrate into the extracellular environment. Following ATP hydrolysis and the subsequent release of ADP and phosphate resets the transporter back to the open dimer conformation ready for the next cycle. **(B) The alternating site model** shows TMDs in an outward open conformation, switching to an inward facing conformation following substrate binding and ATP hydrolysis at the NBDs. The protein is then reset following the two hydrolysis events.

1.2.3 The challenges of inhibiting P-gp function to overcome MDR

One of the mysteries surrounding P-gp is how a single protein can interact with over 300 structurally and functionally unrelated compounds including chemotherapeutic drugs, steroids, fluorescent dyes, natural products, and linear and cyclic peptides [22]. The compounds recognised by P-gp are generally hydrophobic, weakly amphipathic, and sometimes contain planar aromatic rings usually with a positively

charged N atom [68]. Screening studies of a hundred chemically diverse P-gp substrates showed that the existence of two electron donor groups with a spatial separation of 2.5 ± 0.3Å was a common feature [69]. Knowledge of the factors that determine substrate specificity is vital in rational design of drugs for successful targeting.

The overexpression of P-gp and resistant phenotype has been well established in several leukemias including acute myeloid leukemia (AML) and acute lymphoblastic leukemia (ALL). It also plays a role in poor treatment outcome in tumours of the breast and colon [70-72] . Both animal and patient models showed improved intratumour distribution of chemotherapeutic agents following inhibition of P-gp, thus the development of potent inhibitors is highly beneficial in improving chemotherapeutic outcomes [73-75]. The general strategy has been to co-administer inhibitors of P-gp with anticancer drugs aimed at reducing the efflux function of P-gp and resulting in subsequent increased accumulation of the anticancer agent and increased cell cytotoxicity.

Verapamil, a calcium channel blocker, was the first compound used to inhibit P-gp in 1982. However, clinical trials showed that it had poor potency for P-gp (micromolar range) compared to its potent inhibition of L-type calcium channels, and the higher concentrations used to block P-gp resulted in cardiotoxicity [76-78]. Verapamil was considered a ‘first generation’ inhibitor, and other examples had unrelated pharmacological actions and relied on the polyspecificity of P-gp to compete for transport with the anticancer agents [79, 80]. All displayed poor potency for inhibition and led to unacceptable levels of systemic toxicity [81, 82].

The second generation of P-gp inhibitors were designed based on chemical modifications of the first-generation compounds, aimed at removing or dampening the intended activity while improving on their potency of interaction with P-gp. The third generation of compounds were a result of combinatorial chemistry approaches based on structure-activity relationships (SAR) for interaction with P-gp [20]. These third-generation compounds were often associated with adverse drug reactions due to the overlapping substrate specificity between the drug metabolizing enzyme cytochrome P450 (CYP3A4 isoform), and P-gp. Co-administration of an anticancer drug with one that had an overlapping specificity for both P-gp and CYP3A4 led to unwanted pharmacokinetic parameters and a range of toxicities, requiring a significant dose reduction of the anticancer agent [83]. Of all the inhibitors trialled thus far, of note are tariquidar (XR9576) [74, 84] and valspodar (PSC833) [85], which progressed to late stage clinical trials but still failed to clinically restore sensitivity to chemotherapy.

The overall reasons for clinical failure in the development of successful P-gp inhibitors so far can be attributed to several factors including: (i) poor selectivity and low affinity for P-gp resulting in the need for higher plasma concentrations thus leading to unwanted actions and toxic side-effects; (ii) overlapping specificity for cytochrome P450 leading to inhibition of its metabolic function and thus increased systemic concentration of the co-administered chemotherapeutic agent (requiring a reduction in dose levels); (iii) interaction with other ABC transporters that affected their physiological functions; and (iv) nonspecific inhibition of ABC transporters at physiological sites which reduced elimination of anticancer drugs [86].

As chemotherapeutic development begins to focus more on nongenotoxic agents that are generally cytotoxic, many of these novel anticancer agents are also targets

of P-gp [87, 88]. So far, chemical inhibitors of P-gp have been unable to distinguish between P-gp found in cancerous tissue and those expressed at normal sites in the body. This has led to unwanted side effects including increased permeability of the blood-brain barrier and subsequent increased absorption and distribution of cytotoxic drugs into the brain, necessitating a dose reduction. Thus, the problem of P-gp mediated MDR still needs to be addressed through novel approaches, many of which are discussed in the review by Callaghan et al. [20]. This is possible as we extend our understanding of the molecular architecture of the drug binding sites of P-gp and identify their location and total number. This will advance comprehension of how both inhibitors of P-gp and cytotoxic agents interact with the protein, thus guiding rational drug design towards compounds that circumvent or block P-gp function. The aim of the current research presented in this thesis has been to identify the location of the drug binding sites in P-gp.

Several different approaches have been previously used in identifying the location of the drug binding site(s). The following sections outline some of these approaches and key findings obtained to date.

1.3 Photoaffinity labelling (PAL)

Photoaffinity labelling (PAL) is a widely used technique for studying the interactions between ligands and their target proteins. It identifies unknown targets of ligands, assisting in the elucidation of protein structures, functions and conformation changes, as well as in identifying novel drug binding sites in proteins [89]. Initially developed in the 1960s, the basic principles of the technique remain unchanged and is outlined in figure 4 [90]. In this technique, a reversible complex is formed between the protein acceptor or target and the photoactivating probe. Following binding and incubation of the photoactive probe with the protein, it is irradiated with UV-light. Photolysis results

in the creation of highly reactive carbene and nitrene intermediates which form covalent bonds with the receptor protein [91-93].

A critical part of the experimental design is the choice of the photoactive group, which should display chemical stability in both darkness and ambient light at a range of pH levels. Additionally, it should have a similar activity and affinity level to the parent compound and be activated at wavelengths that do not cause photolytic damage to biological molecules but still lead to the creation of highly reactive intermediates. Ideally, the photophore should react with many different types of bonds (especially C-H and X-H bonds) and form a stable adduct so that the bond remains intact throughout the subsequent detection and isolation methodologies [94, 95]. Therefore, significant experimental planning in choosing the correct photoactive probe is a substantial task required for the success of this technique. Preserving the known pharmacophore for interaction with a given protein structural family can also result in identification of other proteins within the same class [89, 96].

PAL has successfully enabled identification of amino acids involved in interactions with the ligand in the binding pocket of P-gp, aiding understanding of the polyspecificity of P-gp.

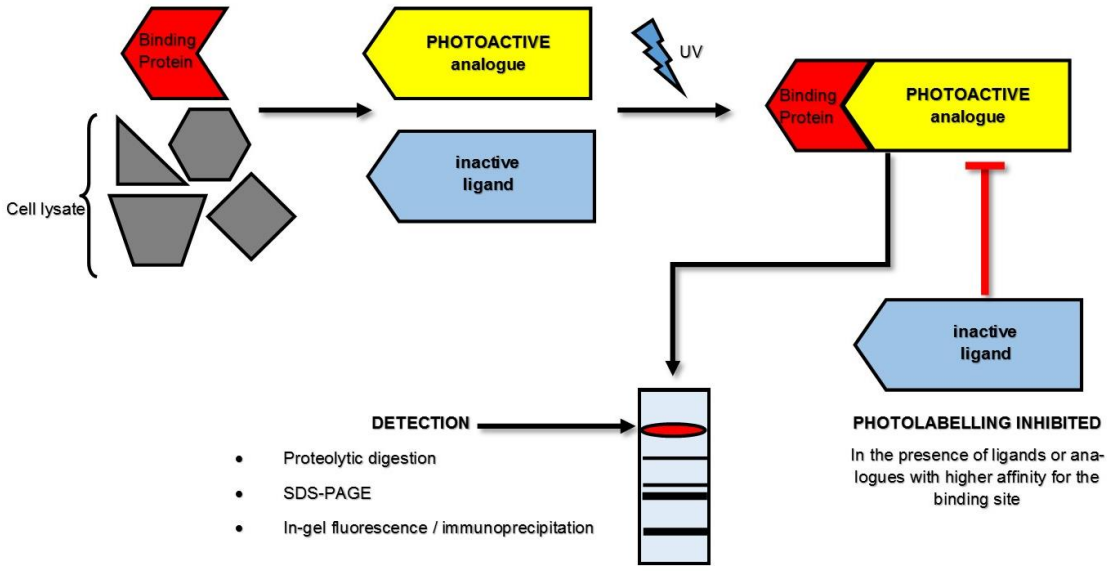

Figure 4: Schematic of photoaffinity labelling method. Basic schematic diagram identifying the general concept of photoaffinity labelling in identifying the binding site of a ligand using its photoactive analogue.

1.3.1 Identification of drug binding sites using PAL

The *Vinca* alkaloid, vinblastine, is a substrate of P-gp, and MDR cells expressing P-gp are resistant to this drug. Two of the initial photoaffinity analogues generated to explore P-gp function were those of vinblastine, known as [^{3}H]NABV and [^{125}I]NASV [97]. PAL experiments with these two analogues have shed light on the nature of the binding site. For example, photolabeling of P-gp with [^{125}I]NASV in a human neuroblastoma cell line that was 1400-fold resistant to vincristine, was inhibited in the presence of vinblastine, actinomycin D, or doxorubicin by 94, 79, and 74%, respectively. In the presence of methotrexate which is not affected by MDR, vinblastine photolabeling of P-gp by [^{125}I]NASV was unaffected. Colchicine, whose cytotoxicity is affected by P-gp also failed to block [^{125}I]NASV binding, suggesting that it likely binds to a separate site to vinblastine or has a lower affinity than [^{125}I]NASV for the site in P-gp [95, 98, 99].

Multiple analogues of other MDR-related drugs have also been used to study the binding sites of P-gp, including the anticancer drug, paclitaxel, a known P-gp substrate. [^{125}I]NAST was used to identify and characterize the paclitaxel binding site by photolabeling P-gp expressed in an MDR cell line. [^{125}I]NAST photolabeling was inhibited in the presence of paclitaxel, vincristine and actinomycin D, but not doxorubicin, suggesting that doxorubicin and paclitaxel bound to separate sites [100, 101]. Similarly, the labelling of P-gp by the photoaffinity analogue of the fluorescent dye rhodamine 123, another P-gp substrate, was inhibited by vinblastine and verapamil, suggesting overlapping or common drug binding sites on P-gp. Labelling was not affected in the presence of colchicine, suggesting that it binds to a distinct site on P-gp to rhodamine 123 [102].

PAL studies have been able to identify that the compounds vinblastine, paclitaxel, and rhodamine 123, three of the four compounds explored in the current investigation, bound to separate sites on P-gp. However, the actual location of photo-incorporation remained unknown.

1.3.2 PAL following proteolytic digestion of P-gp into domain fragments

Over the last three decades, photoaffinity analogues of known P-gp substrates have been used to locate the drug binding sites of P-gp following proteolytic digestion into large fragments and then labelling by the photoactive probe. The results have shown that both halves of the protein are photolabeled, indicating multiple binding sites for a single ligand [103]. Tamai and Safa conducted numerous photoaffinity labelling studies followed by kinetic analysis [104, 105]. They showed that azidopine (a dihydropyridine calcium blocker) had a distinct binding site to verapamil (a phenylalkylamine calcium channel blocker). Cyclosporin A (a MDR modulator), which was previously reported to interact competitively with P-gp at the *vinca* alkaloid

binding site, also inhibited azidopine binding in a non-competitive manner [104]. Together these investigations indicated the presence of at least two distinct drug binding sites in P-gp which were kinetically differentiable – one for *vinca* alkaloids, cyclosporin A and verapamil; and one for azidopine. This was one of the earliest supporting evidence for the existence of multiple and discrete drug-binding sites on P-gp, and that the substrates were interacting non-competitively [95, 105]. Greenberger et al. [106] also explored whether P-gp substrates and modulators shared a common binding site by labelling peptide fragment maps of P-gp with [^{3}H]azidopine and [^{125}I]IAAP. The two major photolabeled fragments attained after complete proteolytic digestion of P-gp was 5- and 4-kDa in size and located within or immediately C-terminal to TM6 and 12, respectively. Analysis of the peptide segments showed that both [^{3}H]azidopine and [^{125}I]IAAP bound to similar domains of P-gp despite their chemical dissimilarity [106, 107].

An investigation by Dey et al. provided support for multiple drug binding sites using [I^{125}]IAAP and *cis(*Z)-flupentixol, a modulator of P-gp [108]. Following photoaffinity labelling of P-gp, the molecule was proteolytically cleaved in the linker region and resolved by SDS-PAGE. The labelling of [I^{125}]IAAP was distributed in a 2:3 ratio between the N- and C-terminal halves. Upon addition of *cis(*Z)-flupentixol, the effect of [I^{125}]IAAP labelling of P-gp was examined. Flupentixol specifically enhanced the photolabeling of P-gp by [I^{125}]IAAP at the C-terminus, with no alteration of labelling at the N-terminus. This observation supported the existence of two non-equivalent labelling sites and a possible allostery between the sites for IAAP and flupentixol binding.

1.3.3 PAL enhanced by MALDI-TOF

Propafenone and its analogues have the advantage of being intrinsically photoactivatable, thus avoiding unnecessary chemical modifications of the parent drug. Moreover, propafenones are known to inhibit transport of P-gp substrates including vinblastine, rhodamine 123, mitoxantrone and doxorubicin [109-111]. The radioactive propafenone analog [^{3}H]GPV51 was used to label plasma membrane vesicles expressing P-gp and following photolabeling, proteins were separated by SDS-PAGE. The core-glycosylated 140 kDa P-gp band was excised and proteolytically degraded sequentially by chymotrypsin and trypsin. Trypsin digestion provides approximately 50% sequence coverage, whereas 60% was covered by chymotrypsin digestion. This combination enabled greater than 80% of the P-gp protein sequence to be recovered. The labelled fragments were identified using matrix-assisted laser desorption/ionization time-of-flight (MALDI-TOF) mass spectrometry fingerprinting. This technique allowed sensitive identification of ligand and associated amino acid residues. Results characterized eight protein regions associated with binding of propafenone analogues, including TM5 (304-316), TM6 (327-343), TM8 (755-784), TM12 (976-994), cytoplasmic loops 2 and 3, as well as extracellular loop 6. This provided further support that the binding site is comprised of multiple segments of the protein [109, 111, 112].

In a subsequent follow up study, the group utilized a homology model of P-gp which was generated using *Vibrio cholera* MsbA lipid transporter as a template [113]. This allowed the labelling pattern of [^{3}H]propafenone to be projected onto a three-dimensional atomic-detail model of P-gp. Continuing the increased sophistication of this process, the labelled fragments were analysed by MALDI-TOF, identifying TM helices 3, 5, 8, and 11 as regions of P-gp that were labelled. The locations of these TM helices were predicted to be at the interfacial regions between two TMDs of P-gp. One of the interfaces is comprised of TM3/11 and the other by TM5/8 (figure 5). It was postulated that substrates access the central binding cavity of P-gp through these two interfaces, which were termed 'binding gates' [113, 114].

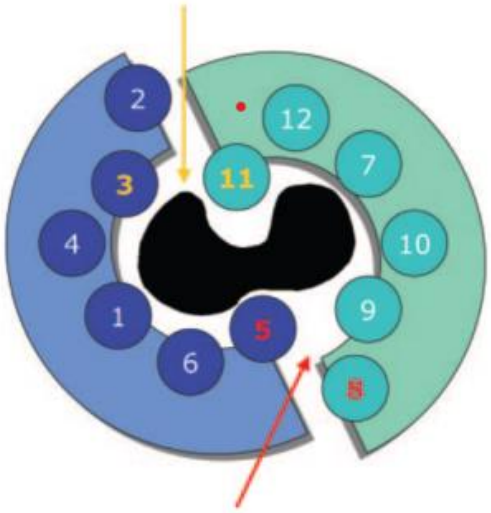

Figure 5: Schematic representation of the 'binding gates' of P-gp. The N- and C-terminal halves are symbolised as dark blue, and cyan arches, respectively. Circles and numbers show the TM segments of P-gp. The yellow and red labelled TMs are located at the two TMD/TMD interfaces. The arrows show the path along which substrates are postulated to gain access to the central binding cavity of P-gp. (*Figure abstracted from Pleban, K. et al. 2005.*)

1.4 Cysteine-scanning mutagenesis

Another widely used technique to refine the points of drug interactions on P-gp is cysteine-scanning mutagenesis. P-gp is amenable to this process because it contains only seven endogenous cysteines (at positions 137, 431, 717, 956, 1074, 1125, 1288, and 1304) and mutating all of them to alanine resulted in a Cys-less P-

gp that was functionally active [115, 116]. This section covers key studies that have revealed the structure of and binding residues on P-gp using cysteine-scanning mutagenesis, a technique that is used in the present investigation.

1.4.1 Understanding the structure of P-gp and NBD-TMD communication

Site-directed mutagenesis has provided considerable insight into the structure and mechanism of P-gp. The cys-less P-gp mutant provided supporting evidence for the primary structure of P-gp predicted to contain six TM segments in each of the two TMDs [117]. Single cysteine mutations in the predicted extracellular and intracellular loops of the TM segments also helped determine the topology of cys-less P-gp at the cell surface [118]. In addition, the importance of the two ATP-binding sites in the NBDs were examined by cysteine mutagenesis at the two Walker A sites followed by incubation with the thiol-reactive probe, NEM (*N*-ethylmaleimide), which forms covalent bonds with the cysteines, and subsequent measurement of drug-stimulated ATPase activity. The mutants when treated with NEM had little effect on the cys-less P-gp but inactivated both Walker A cysteine mutants. The presence of ATP protected the mutants from being labelled with NEM. Thus, both sites were required for activity of P-gp [119].

Another investigation provided support for the NBD “sandwich dimer” (head-to-tail structure) of P-gp formed when two ATP molecules bind at the interface of the LSGGQ signature sequence of one NBD and Walker A motif of another. Pairs of cysteines were introduced at these locations in cys-less P-gp and mutants were subjected to cross-linking analysis using an oxidant, and the cross-linked products detected by SDS-PAGE analysis. Cross-linking of the mutants was prevented in the presence of ATP and affected by drug substrates and modulators that bound to P-gp [120]. This provided evidence of communication between the TMDs where drugs

bound, and the NBDs where the mutations were inserted [121-123]. Binding of ATP to P-gp mutants lacking the ability to hydrolyse ATP also resulted in conformational changes in the TMDs, showing that the communication between TMDs and NBDs was bidirectional [124, 125].

Disulfide cross-linking studies identified TM segments that were important in forming the drug translocation pathway, as well as in facilitating NBD-TMD communication. Cross-linking studies between TM6 in TMD1 and TM12 in TMD2 of P-gp showed that cysteines at positions 332 (TM6) and 975 (TM12) in cys-less P-gp could be cross-linked when exposed to the oxidant [126]. However, in the absence of ATP, even in the presence of the oxidant, the two mutants (Cys332 in TM6/Cys975 in TM12) did not cross-link. TMs 4-6 (in TMD1) and TMs 10-12 (in TMD2) form the drug translocation pathway through the membrane [127, 128], with the remaining TM segments thought to lie outside this pathway. Subsequent cross-linking investigations involving the introduction of mutants in TM 2, 5, 8, and 11, showed that TM5 directly cross-linked with cysteines in TM8, and TM2 could be cross-linked with cysteines in TM11 and the topological model amended accordingly [129, 130].

1.4.2 Covalent modifications at cysteine residues

Identification of drug binding sites in P-gp would also aid understanding of the mechanism of transport. Cysteine mutagenesis data using thiol-reactive drug substrates of P-gp (MTS-rhodamine [131], MTS-verapamil [132], and dibromobimane (dBBn)) have helped map the location of the binding sites on P-gp [133-135]. 252 single cysteine residue mutants were introduced into cys-less P-gp and each reacted with the thiol-reactive drug substrate and assayed for inhibition of ATPase activity after addition of the substrate. If a residue was involved in binding of the drug, covalent attachment of a large bulky group such as dBBn to the cysteine, significantly

disrupted drug-P-gp interactions and resulted in reduced ATPase activity. Mutants that showed inhibition of ATPase activity in the presence of the drug, following incubation with the thiol-reactive substrate, were then tested for protection of inhibition by the drug (figure 6). Of the 252 mutants, 15 mutants within TMs 4, 6, 10, and 12, showed significant reduction in ATPase activity after incubation with MTS-Verapamil. Addition of verapamil significantly protected residues S222C (TM4), L339C (TM6), A342C (TM6), and G984C (TM12) from inhibition by MTS-verapamil, indicating the proximity or involvement of these residues in the binding site of verapamil. In contrast, residues V118C and V125C (TM2), and V982C (TM12) were inhibited by both dBBn and MTS-verapamil, but less protected from inhibition by verapamil. The difference in the extent of inhibition by dBBn and MTS-verapamil may be explained through the assumption of a single ‘substrate-induced fit’ binding site, which suggests that the flexibility of P-gp allows for accommodation of structurally diverse substrates (discussed in the next section) [136].

Similarly, five mutants, I340C (TM6), A841C (TM9), L975C (TM12), V981C (TM12), and V982C (TM12), showed significant protection from MTS-rhodamine labelling after pre-treatment with the parent compound, rhodamine, thus implicating TMs 6, 9 and 12 in the binding of these rhodamine dyes [131]. Cross-linking studies determined that TM6 lies close to TMs 10, 11 and 12 and that TM12 in turn lies close to TMs 4, 5 and 6, with all six TMs postulated to line the drug-binding pocket since

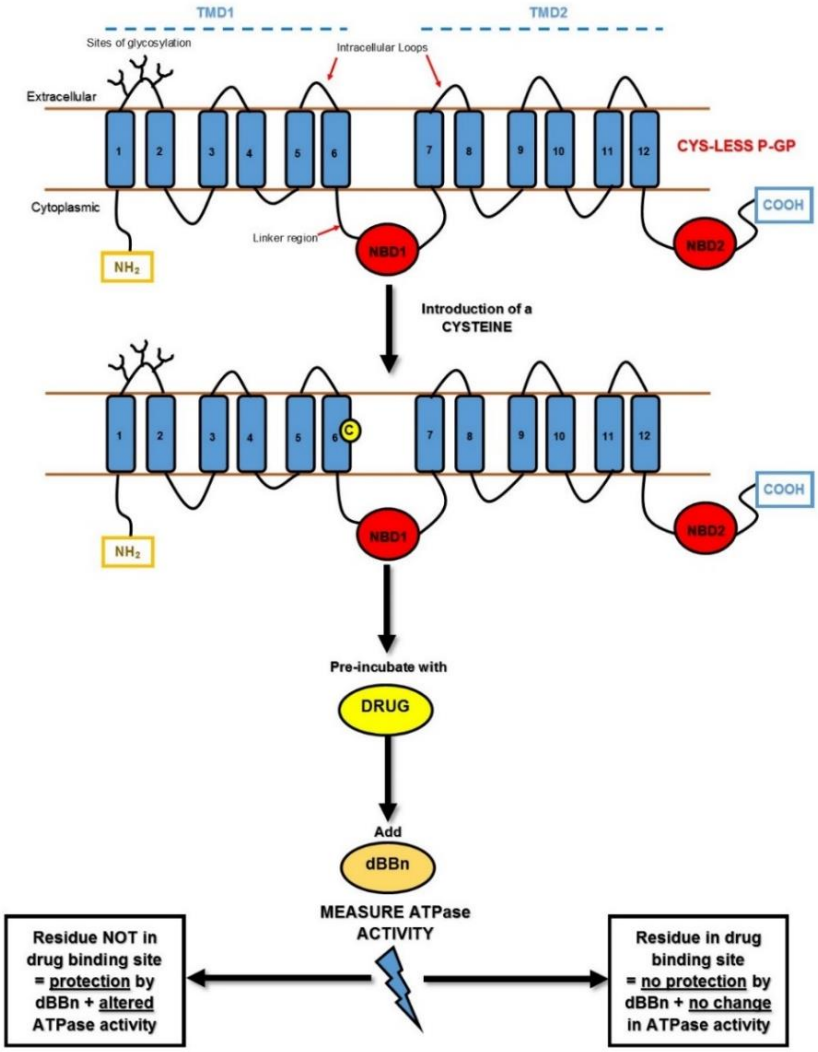

Figure 6: Cysteine-directed mutagenesis and dibromobimane (dBBn) protection assay. Seven endogenous cysteines in wild-type P-gp was mutated to alanine to construct a cys-less P-gp allowing site-directed insertion of cysteine residues. The schematic flow-diagram above outlines the dBBn protection assay. The thiol-reactive cross-linking agent, dBBn, covalently binds to the cysteine and causes inactivation of verapamil-stimulated activity. If the residue mutated to a cysteine is important in the binding of a particular drug, then pre-incubation with that drug prior to addition of dBBn should protect from inactivation and identify the residue as important in drug binding.

the presence of drug substrates inhibited the formation of cross-links between two sulfhydryl residues in separate TMs [137].

1.4.3 TM6 and TM12 are direct links to the NBD

Numerous cysteine scanning mutagenesis studies employing a thiol-labelling approach have been used to focus on the key role of TM6 and TM12 in ATP-dependent conformational changes. Previous mutational studies [138-141] had shown that site-directed mutagenesis of TM6 resulted in significant alteration in the drug-stimulated ATPase activity of P-gp, as well as in an alteration in the drug resistance profile. TM6 was also implicated in drug binding by photolabeling of P-gp with drug analogs followed by mass spectrometry [111]. Similarly, TM12 was also implicated in playing a key role in the progression of the ATP hydrolysis cycle and mediating communication between the TMDs and NBDs using cysteine mutagenesis [142, 143].

ATP-dependent changes of TM6 have been monitored using various protein chemistry approaches in conjunction with cysteine mutagenesis, including use of thiol-reactive probes that are hydrophobic (coumarin maleimide), hydrophilic (fluorescein maleimide), or amphipathic (BODIPY-maleimide) [144]. Labelling of seven cysteines (V331C, T333C, F335C, S337C, L339C, G341C, F343C) in TM6 in the presence or absence of AMP-PNP or after vanadate trapping showed that depending on the stage of the catalytic cycle or in the presence of nucleotides, the labelling patterns varied. Flourescein maleimide only resulted in significant labelling of mutant F343C in the absence of nucleotide, but not in the presence of AMP-PMP or after vanadate trapping of nucleotide. For labelling with BODIPY-maleimide, patterns varied depending on the presence or absence of AMP-PNP, nucleotide, or after vanadate trapping. Mutants L339C and V331C could only be labelled in the

absence of nucleotide or after vanadate trapping, but not in the presence of AMP-PNP. Coumarin maleimide labelled all seven mutants and the labelling was not significantly altered depending on the stage of the catalytic cycle. Together, these results indicated that TM6 underwent significant conformation changes or “tilting” in response to nucleotide binding or ATP-hydrolysis. In consensus with studies using cysteine-scanning mutagenesis and covalent cross-linking formation, the helical tilting hypothesis presented by Rothnie et al., [144, 145] provided a mechanism for interdomain communication during drug transport, especially since TM6 directly links to the N-terminal NBD. The observed nucleotide-driven tilting of TM6 also provides support for the demonstrated alterations in drug-binding site affinity during the catalytic cycle [144-146].

Further investigations by Crowley et al., [142] also provided evidence of the key role of TM12 in the progression of the ATP hydrolytic cycle in P-gp even in the absence of a transported substrate. Using cysteine mutagenesis at various locations in TM12, the group showed that several mutations significantly reduced the maximal ATPase activity of P-gp due to a reduced basal rate (drug-free state) of hydrolysis of the nucleotide. Mutants L976C and L978C reduced binding of [ɣ-^{32}P]-azido-ATP to P-gp by 4- and 15-fold, respectively, whereas A980C showed a 1.8-fold increase in binding of [ɣ-^{32}P]-azido-ATP at the same concentration. The increased rate was attributed to modified basal activity.

Comparison between the effects of site-directed mutagenesis in TM6 versus TM12 and homology modelling revealed that TM12 is more ‘rigid’ than TM6, rendering it more sensitive to site-directed mutagenesis and consequently, a greater number of functional perturbations. This suggests that the communication between TM6 and TM12 to NBD1 and NBD2 is asymmetrical, even though the ultimate outcome of the

communication is the same, i.e., to control hydrolysis and facilitate effective drug translocation [142]. A subsequent investigation [143] further implicated the role of TM12 in mediating progression of the ATP hydrolytic cycle through communication between the TMDs and NBDs. Using cysteine-directed mutagenesis and thiol-reactive fluorescent probes with differing physiochemical properties, each isoform was analysed at the different catalytic stages of the ATP cycle. This identified TM12 to be in a predominantly hydrophobic environment and the importance of the carboxy region to nucleotide binding and hydrolysis at the NBDs, and its direct involvement in interdomain communication.

Thus, cysteine mutagenesis studies have provided significant information on the structure of P-gp, as well as in identifying key TM segments that comprise the drug translocation pathway. It has implicated TM6 and TM12 in playing key roles in the communication between TMD-NBD during the catalytic cycle.

1.5 Nature of drug binding: Does one size fit all?

The identification of the drug binding site(s) in P-gp has remained a major goal of many investigations, demonstrating that binding takes place in the TMDs of P-gp [147]. Numerous structural and biochemical studies have made attempts to identify the specific sites. The following sub-sections will present evidence in support of a substrate-induced fit model of drug binding and those in support of a multiple drug binding site model.

1.5.1 A substrate-induced fit model for drug binding

The data collected by Loo and Clarke's mutagenesis studies strongly implicate the role of multiple helices lining the central cavity in forming the drug translocation pathway. Studies identified numerous residues located in these TM segments that

directly interacted with distinct substrates of P-gp. Certain residues were also involved in the binding of specific classes of P-gp substrates [148, 149]. The TM helices surround the central cavity which contains the drug binding sites. The ‘substrate-induced fit’ model of drug binding proposes a common binding site for all drugs regardless of its class or whether it is a substrate or modulator. This binding site is formed for individual drugs following localised conformational changes to specific TM segments, driven by the energetics of substrate interactions [150]. This is supported by cross-linking studies that show that the helices lining the cavity are mobile and that P-gp displays structural flexibility that enables it to accommodate binding of chemically diverse substrates. Drug binding therefore results in re-arrangement of the TM segments lining the drug translocation pathway, producing an ‘induced-fit’ substrate binding site [151]. According to this model, substrates of P-gp share a common drug binding site with a substantial overlap of drug-binding residues, and that only one drug can bind in the binding pocket at a time.

One such study supporting this model, involved introduction of pairs of cysteine mutants into cys-less P-gp followed by treatment with an oxidant (copper phenanthroline) to promote formation of disulphide bonds. Cross-linking occurred if the two cysteines were close enough in the tertiary structure. The cross-linking was measured in the absence or presence of various drugs including progesterone, cyclosporin A, vinblastine, and verapamil, to determine the rearrangement of the TM segments. Figure 7 shows a schematic of progesterone-induced conformational changes in the TM segments. The ‘substrate- induced fit’ model of drug binding helps facilitate the polyspecificity demonstrated by P-gp by reducing the number of individual drug binding sites needed for recognising and binding over 300 known substrates. The study [149] identified that mutants P350C (TM6) and S993C (TM12)

could be cross-linked, but cross-linking was inhibited (and ATPase activity restored) in the presence of a thiol-reducing agent. 143 double mutants, each containing P350C (TM6) and another cysteine on the cytoplasmic half of TMs 7 – 12, or those containing S993C (TM12) and a corresponding mutant in the cytoplasmic half of TMs 1 – 6, were generated. The extent of crosslinking was determined by SDS-PAGE. Most mutants did not cross-link in the presence of substrates. In the absence of any drug substrate, P350C (TM6) and S993C (TM12) could be cross-linked. Cross-linking patterns differed in the presence of progesterone, cyclosporin A, vinblastine, and verapamil.

The ability of a substrate to change the pattern of cross-linking suggests that TM segments undergo conformational change as well as re-orientate or 'tilt' themselves to accommodate different substrates. Multiple other studies [137, 148, 149, 152, 153] support the re-packing of TM segments to form a substrate-induced drug binding pocket, leading to the identification of residues that are involved in the binding of multiple structurally different substrates, and thus explaining the polyspecificity demonstrated by P-gp.

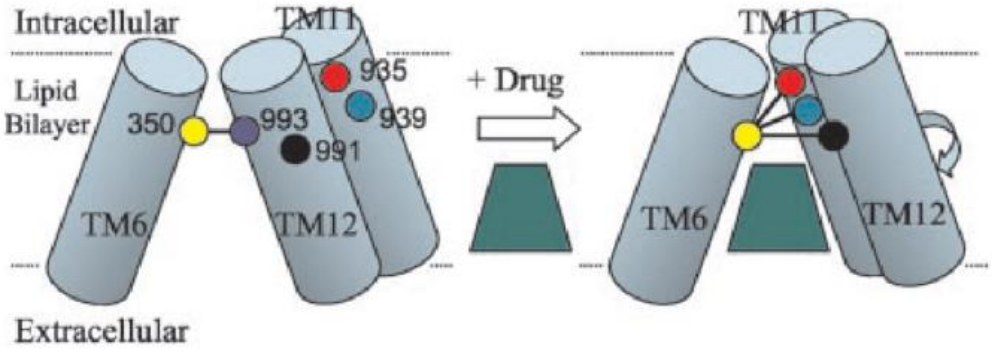

Figure 7: Model of progesterone-induced conformational changes in the TM segments of P-gp. TM6, 11, and 12 are shown as cylinders. In the absence of a drug substrate, disulfide cross-linking occurs between P350 (yellow ball) and S993C (purple ball). In the presence of progesterone, TM11 and12 undergo tilting and lateral movements to allow cross-linking between P350C and V991C (black ball) in TM12 and with A935C (red ball) and G939C (turquoise ball) in TM11. *Figure extracted from Loo et al., 2003*.

1.5.2 Evidence for multiple drug binding sites on P-gp

Though the ‘substrate-induced fit’ model for drug binding can provide an explanation for how one transporter is capable of identifying and binding such a broad range of compounds, it does not justify evidence presented by numerous studies [108, 136, 137, 148, 154] showing simultaneous binding of two compounds in the drug binding pocket P-gp. Directly contradicting the ‘substrate-induced fit’ model is the ‘multisite’ drug binding model. This model first proposed that P-gp contains at least two distinct transport active sites, the R-site which binds rhodamine 123 and anthracyclines, and the H-site which shows specificity for Hoechst 33342 and colchicine [155]. A third site, the P-site has also been reported to preferentially bind progesterone and prazosin and demonstrates allosteric properties [156]. Radioligand studies support the existence of more than two distinct drug binding sites [157], with up to seven different sites being proposed using competition binding experiments [95]. Studies have also proposed the existence of primary and secondary binding sites in P-gp which demonstrate substrate overlap, explaining the polyspecificity of P-gp [158].

Together, the evidence points towards the existence of multiple drug binding sites in P-gp for a range of chemically and structurally distinct compounds. Results obtained from the current investigation provides support of a multi-site model of drug binding.

1.5.2.1 Identification of the location of H- and R-sites

Shapiro and Ling proposed three drug binding sites in P-gp, designated as the H-site, R-site, and P-site, based on fluorescence kinetic studies [155, 156, 159, 160] of drug transport by purified and functionally reconstituted P-gp-rich plasma membrane vesicles from $CH^{R}B30$ cells (Chinese Hamster Ovary cells). Continuous fluorescence monitoring was used to measure P-gp mediated transport of Hoechst 33342, a blue

fluorescent DNA dye, and rhodamine 123, a known fluorescent substrate of P-gp. Transport of Hoechst 33342 to the extracellular environment by P-gp was monitored as loss of fluorescence [161]. The fluorescence spectra of Hoechst 33342 and rhodamine 123 do not overlap, which enabled continuous fluorescence monitoring of each dye in the presence of the other. It was observed that the presence of one dye stimulated the transport of the other in a concentration-dependent manner, suggesting the presence of two co-operative drug transport sites. The R-site preferentially interacts with rhodamine 123 and anthracyclines (including doxorubicin and daunorubicin); the H-site preferentially binds Hoechst 33342, quercetin, and colchicine. The observation that both dyes are transported simultaneously and co-operatively can be explained by the presence of at least two transport-competent drug-binding sites [155, 161, 162]. Both sites displayed similar affinity for vinblastine, etoposide, and actinomycin D, consistent with previous results [163]. Studies showed that one compound could bind to two sites with different affinities and that depending on the concentration, the affinity of binding of a second compound was influenced at both sites. This showed an overlap in substrate specificity at two distinct binding sites on P-gp [164]. These results agree with the observation that at lower concentrations, the anthracyclines preferentially bound at the R-site, stimulating Hoechst 33342 transport, but at higher concentrations the anthracyclines competed for binding at the H-site, causing inhibition of Hoechst 33342 transport [165]. Additionally, a third allosteric site, the P-site was identified to preferentially bind prazosin and progesterone, classified as weak substrates or modulators of P-gp. Binding at the P-site had a positive allosteric effect on drug transport by the H- and R-sites, stimulating transport of both rhodamine 123 and Hoechst 33342, separately [156].

Mutagenesis data from Loo and Clarke identified residues (I340, A841, L975, V981, and V982) that formed part of the rhodamine B binding site, as discussed in section 1.4.2. These residues were protected by rhodamine B from inhibition of ATPase activity by MTS-rhodamine following mutagenesis to a cysteine [131]. These observations suggested that these residues were a part of the proposed R-site. Homology models of human P-gp based on the refined X-ray structures of mouse P-gp showed that residues I340 (TM6), L975, V981, and V982 (all on TM12) were close enough (an estimated 11Å between the side chain of I340 and the other three residues) to accommodate a substrate and form a drug-binding site specifically for the rhodamine dyes [115, 151]. In contrast, residue A841 is thought to be a point of interaction for rhodamine upon entry into the central P-gp cavity from the cytoplasmic leaflet, as it is located at a distance from the proposed R-site.

The mouse P-gp crystal structure resolved in the presence of two cyclic peptides, QZ59-*RRR* and QZ59-*SSS* at the central cavity, has been used to further refine the location of the H- and R-sites [50]. Martinez et al., [166] measured the effects of both cyclic peptides on the transport of daunorubicin (for the R-site) and Hoechst 33342 (for the H-site) using a NIH3T3 cell line transfected with wild-type *MDR1* (ABCB1). Results revealed distinct inhibitory mechanisms for each compound, suggesting localisation of these substrate binding sites within the transporter's binding cavity. Following docking simulations, they proposed that the R-site lies deep in the cavity. The location of the R-site was predicted to overlap that of the *SSS* enantiomer molecule most embedded in the structure, but only slightly overlapping the binding site of the *RRR* enantiomer (figure 8). This location agrees with that of rhodamine B and other molecules that showed binding deeper in the cavity carried out in previous modelling studies [167, 168]. They also identified residues F303, Y307, and Y310 to

be a part of the H-site, proposed to line the central cavity. Crystal structure analysis suggested that the H-site overlapped both locations of the bound *SSS* enantiomers [166].

These results were further corroborated by another study [169] which proposed approximate locations of the H- and R-sites. The study measured the effects of the potent inhibitors elacridar (GF120918) and tariquidar (XR9576) on the accumulation of rhodamine 123 and Hoechst 33342. They identified that the binding site for both inhibitors overlapped with the H- and R-sites.

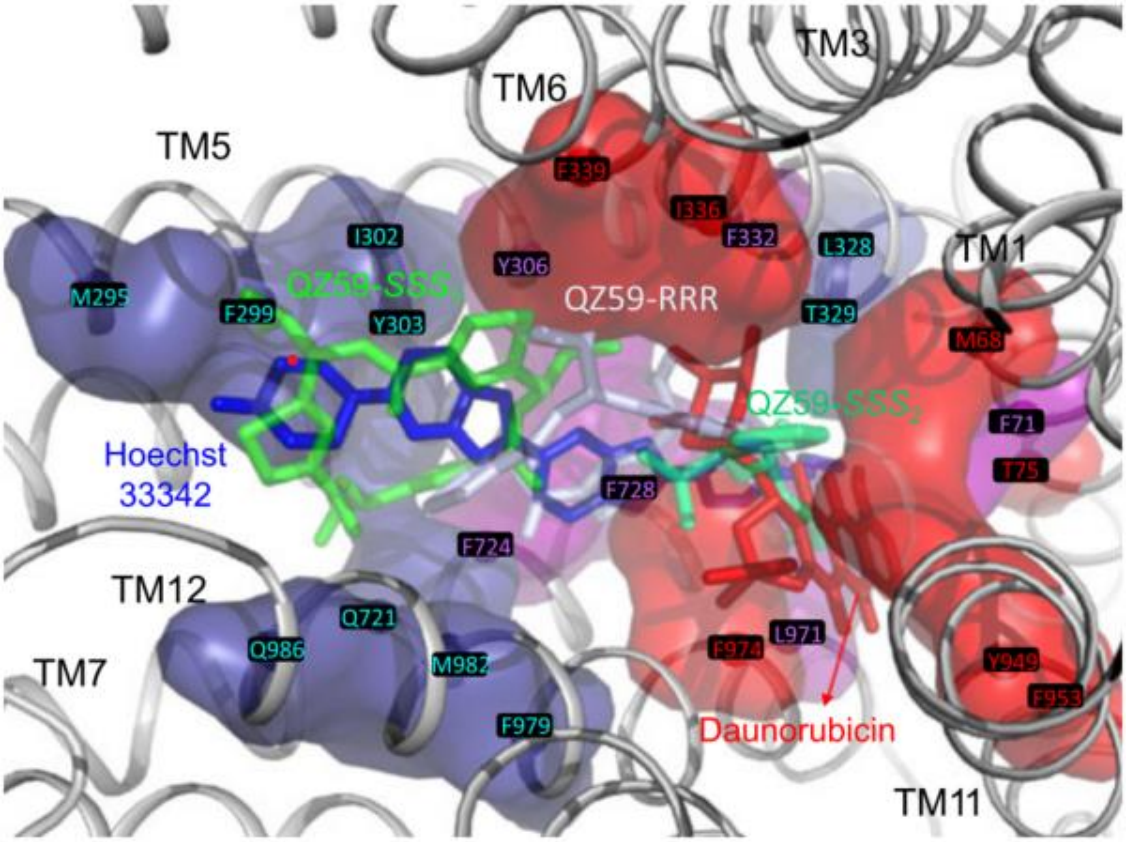

Figure 8: Docking simulation identifying the H and R-sites in mouse P-gp (PDB ID: 4LSG). The two QZ59-*SSS* enantiomers are shown in green and teal, the *RRR* enantiomer shown in pale white. The binding locations of the compounds daunorubicin (red) and Hoechst 33342 (blue) are shown following independent docking simulations. Residues that interact with or form the H- and R-sites are shown in the surface and labelled. Residues corresponding to the H-site are shown in blue, those to the R-site in raspberry, and those residues that are common to both sites, shown in purple. (This figure was extracted from *Martinez et al., 2014*.)

1.5.2.2 Chemical characterisation of the H- and R-sites using fluorescence spectroscopy

Support for the existence of a H-site and R-site is also provided by fluorescence spectroscopy studies by Lugo and Sharom [170] using the fluorescent DNA dye LDS-751, which along with rhodamine 123, is a substrate of the R-site. P-gp contains seven tryptophan residues in the N-terminal half and four in the C-terminal, which give it an inherent fluorescence spectrum. The role of these tryptophan residues in substrate recognition can be exploited in determining substrate binding [171]. Binding of modulators, nucleotides, and hydrophobic peptides to P-gp alter its conformation and physicochemical environment, resulting in a quenching of the tryptophan fluorescence emission spectrum in a saturable fashion with increasing substrate concentration [172, 173]. The high degree of tryptophan quenching following binding of certain drugs to P-gp suggests that these aromatic residues may be directly involved in substrate binding, possibly through π-π stacking interactions. Studies [172] have suggested the involvement of aromatic residues in substrate recognition

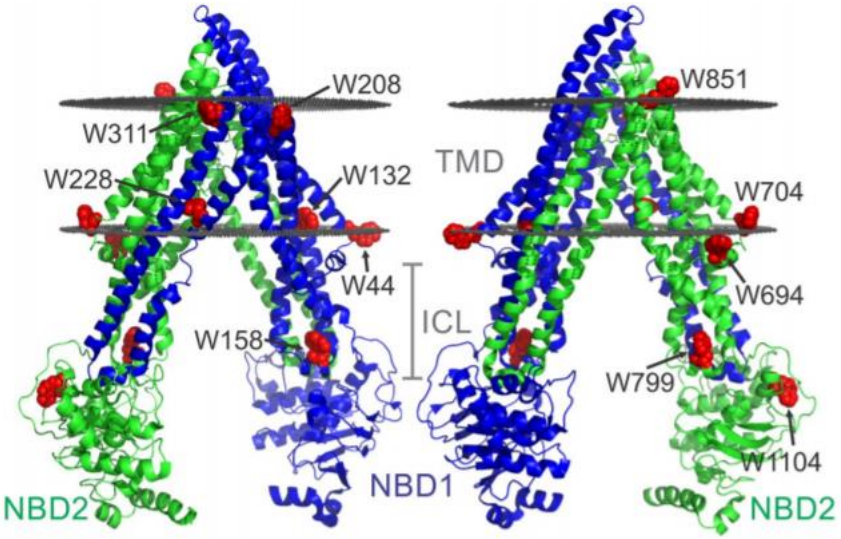

Figure 9: Locations of the eleven native tryptophan residues in P-gp (PDB ID: 4QH9). The N-terminal (blue) and C-terminal (green) halves are shown, with eight Trp residues in the TMDs, and three in the cytoplasmic domains (shown as red spheres and labelled with residue numbers). (*Figure extracted from Swartz et al., 2020*)

and binding due to their over-representation in the TM regions of P-gp. Figure 9 shows the distribution of Trp (W) residues in a homology model of P-gp.

Using FRET (fluorescence Resonance Energy Transfer) the H-site was mapped to the regions of P-gp within the cytoplasmic leaflet [174]. FRET involves the energy transfer from a fluorescent donor to the excited state of an acceptor fluorophore, i.e., between a tryptophan residue and a fluorescent bound drug such as Hoechst 33342 or rhodamine 123 [175]. Using purified P-gp and LDS-751, which interacts with the R-site, a 50-fold enhancement in its fluorescence was measured. The binding of LDS-751 produced a concentration-dependent saturable quenching of tryptophan fluorescence (40%). The LDS acceptor was estimated to be located within the cytoplasmic region of the membrane, closer to the interfacial region of the lipid bilayer than the H-site. The chemical properties of the fluorescent bound compounds characterised both binding sites (H and R) to be of very hydrophobic and non-polar nature [176]. This contradicts the concept of drug binding sites being open to a large aqueous chamber [150]. Additionally, these FRET studies also mapped the putative R-site to 18-25Å from the line connecting the Walker A cysteines to the NBDs. No mutagenesis studies were done to validate the proposed location in the NBD-ICL (intracellular loop) interdomain region [176].

Further biochemical characterisation of the R-site with respect to its two fluorescent substrates, LDS-751 and rhodamine 123, indicated that both bound at the same site, forming a ternary complex, and competed for transport. This contrasts with the expected mutual exclusion for two R-site drugs. LDS-751 showed a large fluorescence enhancement following binding at the R-site, allowing estimation of the K_d value, which is sub-micromolar (0.75µM). In the presence of rhodamine 123, this K_d value for LDS-751 was altered, showing a non-competition model of binding.

Single and sequential dual fluorescence titrations of purified P-gp using both drugs showed that rhodamine 123 reduces the affinity of LDS-751 binding to P-gp by 5-fold and vice versa [154, 177]. It is possible that the putative R-site may be large enough to accommodate two compounds simultaneously. Alternatively, the locations of the binding sites for LDS-751 and rhodamine 123 may be adjacent to, or overlapping with each other, and possibly exist within a common hydrophobic pocket [154]. These results concluded that the existing two-site model previously described by Shapiro and Ling required modification in acceptance of a multi-site model [170].

Fluorescent approaches have been invaluable in demonstrating direct interaction between P-gp and multiple drugs, as well as in quantifying their binding affinity. The present investigation employs tryptophan fluorescence assays to identify multiple drug binding sites in support of the multi-site model.

1.5.2.3 Evidence of a primary and secondary binding site

Additionally, a study using QZ59-S-SSS, which is an analog of the cyclic peptide QZ59-*SSS*, which binds to mouse P-gp [52], identified residues I306-Y307-F343-Q725-F728 as forming a part of the H-site in human P-gp. Residues F978-V982 were found to be common to both R-site and H-site. These residues are also known to bind tariquidar, cyclosporin A, valinomycin, and FBSA. The data suggested that these four compounds bound P-gp at both the R- and H-sites, supporting the concept of overlapping binding sites for chemically unrelated compounds. The key finding supports the existence of a primary binding site (also known as the site where drugs bind to P-gp and inhibit photolabeling by [^{125}I]IAAP), and a secondary binding site, which is revealed upon site-directed mutagenesis of residues in the primary binding site, interrupting their binding [158].

This ability to bind a molecule after chemical modification of residues at the primary binding site reveals information on the topology of P-gp. The central drug binding cavity contains several drug-binding sites with many common residues involved in the binding and transport of chemically unrelated compounds. This generates multiple possibilities for binding and supports the molecular or chemical flexibility of P-gp leading to its polyspecificity. This model further supports the existence of multiple drug binding sites for each drug, thus making P-gp a very efficient transporter [151, 158].

1.5.2.4 Evidence of at least four distinct drug binding sites and communication between them

Another investigative approach used to support the existence of multiple drug binding sites rather than a common drug binding pocket, is the use of classical equilibrium binding studies and kinetic radioligand saturation and displacement assays. The first has been used for a few drugs and allowed quantification of their affinity and capacity for P-gp [178]. The latter two assays have revealed reversible competitive and non-competitive interactions on P-gp [157, 179]. This information was crucial in supporting the polyspecific nature of P-gp as it showed binding of multiple drugs at one time, something that cannot be supported in a ‘substrate-induced fit’ model. These studies not only identified at least four distinct drug binding sites, but also allowed establishment of allosteric interactions between drug combinations, therefore indicating communication between the binding sites. The investigations supported that binding of a drug to at least one of these sites was dependent on their physical and chemical properties and that depending on where the drug bound, the outcome of the interaction (i.e., transport or inhibition) differed. Therefore, a chemical class of

drugs could share a common yet distinct drug binding site, explaining the ability of P-gp to identify such a vast number of compounds.

The investigations used radioligand assays to determine the binding affinities of ligands (K_d), their binding capacity (B_{max}), and the inhibition constant (K_i) of modulators, provided by Languir Adsorption (Saturation) Isotherms [180]. Schild plots demonstrated the nature of interaction between two drugs by the effects on the K_d/B_{max}. Kinetic assays can also be used to determine the association and dissociation rate constants (k_{off}) to provide evidence of allosteric interactions. A key study [178] demonstrated that the B_{max} for [^{3}H]-vinblastine was reduced by XR9051, XR9576 (tariquidar), GF120918 (elacridar), Hoechst 33342 and rhodamine 123. In the absence of any alteration in the K_d for [^{3}H]-vinblastine, a decrease in the B_{max} was indicative of non-competitive interaction. This interaction was a negative allosteric heterotropic interaction as demonstrated by the increase in the dissociation rate constant (k_{off}) for [^{3}H]-vinblastine. The data indicated that these other transported substrates and modulators bound at sites distinct to the vinblastine binding site of P-gp, providing evidence for multiple ‘distinct’ sites depending on the physical and chemical properties of the examined compounds.

Similarly, tariquidar ([^{3}H]-XR9576) (shown to inhibit ATPase activity of P-gp but not transported [181]), resulted in a non-competitive interaction in the presence of [^{3}H]-vinblastine, but a competitive interaction in the presence of Hoechst 33342. Indicating that tariquidar interacts with P-gp at the same location as the transported substrate, Hoechst 33342, but at a distinct site to vinblastine. The shared site was therefore capable of transport even though it also bound a non-transported modulator such as tariquidar (i.e., it was not a ‘distinct’ site), further supporting the polyspecific nature of P-gp substrate recognition. Why then is [^{3}H]-XR9576 not transported? The

dissociation rate (k_{off}) of [^{3}H]-XR9576 was found to be considerably lower than that of vinblastine or paclitaxel and rapid dissociation from the external facing binding site is essential for efficient transport [157, 178].

Nicardipine and XR9501 increased the K_d of [^{3}H]-XR9576 without altering the B_{max}, indicating a competitive interaction. Additionally, nicardipine interaction increased the dissociation rate, indicating a non-competitive allosteric interaction. Nicardipine therefore bound at a distinct site separate from that of XR9051, XR9576, and Hoechst 33342. A significant dose-dependent decrease in the B_{max} of [^{3}H]-XR9576 and [^{3}H]-vinblastine in the presence of Elacridar was observed, indicating that it binds to a site distinct from both [157].

Collectively, these investigations [157, 178] provide evidence for the existence of at least four distinct binding sites on P-gp and highlights complex allosteric communications between them (figure 10). It also demonstrates that substrates and modulators can bind at equivalent sites, thus it is the nature of the interaction at the site rather than the properties of the site that determines whether a drug is transported. Additionally, previous investigations [182, 183] using ATP hydrolysis assays also supported the presence of distinct drug binding sites on P-gp with evidence of interaction between them. Some of these identified sites interacted and generated synergistic stimulation of hydrolysis.

Thus, the complex nature of the distinct drug binding sites, their physicochemical preferences in substrate recognition, and the evident inter-communication, all play a key role in determining the polyspecificity of P-gp. However, these investigations did not provide information on the spatial relationship between the distinct drug binding sites. The current investigation aimed at building on the existing multiple drug binding

site model described here by refining the location of these sites in P-gp, as well as investigating the molecular interactions that govern binding.

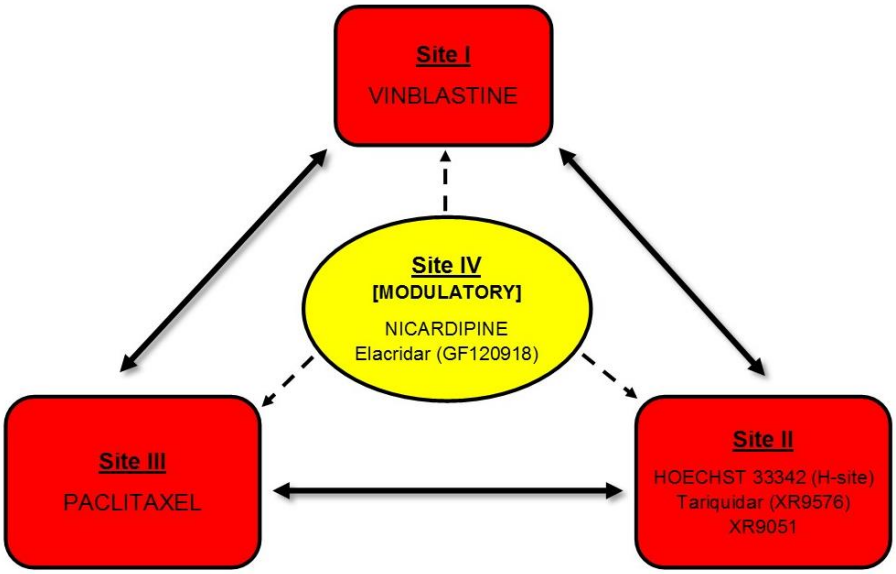

Figure 10: Classification of four drug binding sites on P-gp. The diagram above shows the existence of at least four distinct drug binding sites. Sites I, II and III are classified as sites of transport; site IV is a modulatory site and bound non-transported modulators/inhibitors of P-gp. Site II is not a distinct site as it binds both Hoechst 33342 and tariquidar (a non-transported inhibitor of P-gp), showing evidence of both transport and regulatory functions. Rhodamine 123 could not be assigned a specific site but may bind to any of the sites other than site II (in support of Shapiro and Ling's work), or at an non-identified independent site. The arrows demonstrate the communication between the different sites. The four binding sites can allosterically communicate in a negative heterotropic manner. *Figure adapted from Martin et al., 2000.*

1.6 Summary and Project Outline

1.6.1 Where we stand

Biochemical, pharmacological, structural, and bioinformatic approaches over the last few decades have attempted to localise the drug binding sites on P-gp and elucidate its molecular interactions with a vast number of structurally and chemically distinct compounds. Collective evidence demonstrates the existence of a large central cavity in P-gp lined by multiple helices that contain the drug binding domain. It is thought that the binding domain comprises multiple binding sites that have specific

interactions with different classes of drugs. The drug-protein interactions involve a combination of hydrogen bonds and π-π stacking interactions with aromatic amino acids in the transmembrane segments.

The individual residues mediating drug-protein interactions at the individual sites within the domain remain to be elucidated. Photoaffinity labelling, transport studies, equilibrium binding assays, and investigation of P-gp mutants, have provided valuable information on the location of these binding sites and how they interact with each other. High-resolution structural data would immensely aid in determining the location and architecture of the binding sites. In fact, the combination of structural data with powerful biochemical and pharmacological approaches have revealed several putative sites and residues involved in drug binding. The possibility of elucidating the drug-binding site structure along with the pharmacophore of its substrates would engender renewed interest in P-gp being considered as a promising pharmacological target in overcoming multidrug resistance.

1.6.2 Where we are headed

The overall aim of this project is to contribute further evidence in support of multiple distinct drug binding sites and to identify their spatial relationship. This will be achieved through extensive biochemical characterisation of seven mutant P-gp isoforms, selected based on biochemical and structural data described in this chapter. A cysteine has been substituted at specific residues in various TM helices for each of the mutants (figure 11). The effects of these mutations on the interactions of four pharmacologically distinct compounds, vinblastine, nicardipine, paclitaxel, and rhodamine 123, will be determined through functional assays such as ATP hydrolysis assays as well as binding assays involving measurement of tryptophan fluorescence. Systematic analysis of each ‘contact residue’ of these chemically distinct classes of

drugs will open doors for further refinement of any identified putative binding sites using more site-directed mutagenesis in the future.

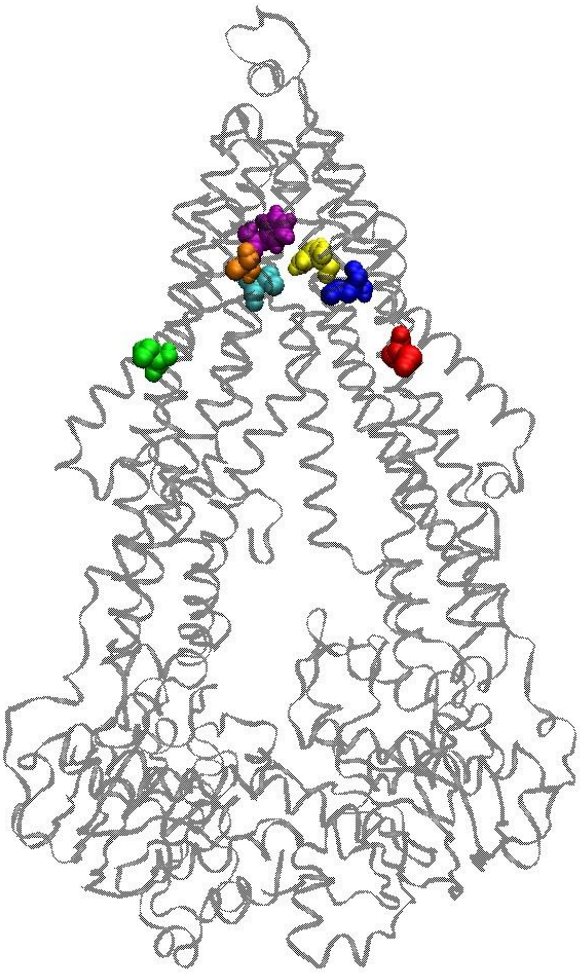

Figure 11: P-gp homology model (side view). A structural model of mouse P-gp (PDB: 4M1M) showing the distribution of the different residues in TM1 (**L65**), TM3 (**M197**), TM5 (**A311**), TM6 (**F336**), TM8 (**T769**), and TM12 (**F978** & **V982**) that were mutated to cysteines in the present investigation.

Chapter 2:

MATERIALS AND METHODS

2.1 Materials

2.1.1 Tissue culture and protein expression

Spodoptera frugiperda (Sf9) and *Trichoplusia ni* (Hi-5) cells were used for viral amplification and protein expression, respectively. Both were purchased from Invitrogen Ltd. (Paisley, U.K.). The low titre (P1) recombinant baculoviruses were provided by Dr Ian Kerr of the University of Nottingham, U.K. Hi-5 cells were grown in Excell 405 cell culture medium purchased from Sigma Aldrich Fine Chemicals (SAFC; NSW, Australia); Sf9 cells were grown in Insect Xpress cell culture media sourced from Lonza Australia (Victoria, Australia). Foetal Calf Serum (FCS) was added to the Insect Xpress media and sourced from Bovogen Biologicals Ltd. (Victoria, Australia). In addition, penicillin-streptomycin (Pen/Strep) was also added to both culture media and obtained from ThermoFisher (Victoria, Australia). The round-bottom tissue culture glass flasks used for maintaining and bulking insect cells were manufactured by Pyrex. The large scale (>300ml) infections were carried out in 2.8L Fernbach-style Nalgene polycarbonate flasks (Thermofisher, Leicestershire, U.K.). Nitrogen cavitation device used for membrane preparation was obtained from Parr Instrument (Illinois, U.S.). The protease inhibitor cocktail (EDTA-free) tablets were sourced from Sigma Aldrich (NSW, Australia).

2.1.2 Protein purification

n-Dodecyl-β-D-maltopyranoside (DDM), the detergent used in solubilisation of purified P-gp, was purchased from Anatrace (Ohio, U.S.). Total *E. coli* lipid extract was purchased from Avanti Polar Lipids Inc. (Alabama, U.S.) and cholesterol (>99% purity) was purchased from Sigma Aldrich (NSW, Australia). Ni-NTA His-bind Resin was sourced from EMD Chemicals (NSW, Australia). Protease Inhibitor Cocktail (in DMSO) and Imidazole (powder) were purchased from Sigma Aldrich (NSW,

Australia). The immobilised metal ion chromatography 10ml HisTrap Econo columns were sourced from GE Healthcare Biosciences (Buckinghamshire, U.K.). The PD-10 disposable gel permeation (desalting) columns used for buffer exchange were purchased from GE Healthcare (NSW, Australia). SM2 adsorbent polystyrene BioBeads were obtained from BioRad Laboratories (Victoria, Australia).

2.1.3 Reagents used for functional analysis of purified protein

Nicardipine hydrochloride, vinblastine sulfate salt, paclitaxel, rhodamine 123, Adenosine 5'-triphosphate disodium salt hydrate, and phosphorus standard solution were all purchased from Sigma Aldrich (NSW, Australia). The 1ml quartz cuvette used for fluorescence measurements was purchased from Hellma Analytics, Germany. Ascorbic acid was obtained from Ajax Finechem (subsidiary of Thermo Fisher Scientific, Victoria, Australia). The Detergent Compatible (DC) Protein Assay Kit was purchased from BioRad Laboratories (Victoria, Australia).

2.1.4 SDS-PAGE and western immunoblotting

N,N,N',N'-Tetramethylethylenediamine (TEMED) and 2-Mercaptoethanol were purchased from Sigma Aldrich (NSW, Australia). BioRad Laboratories (NSW, Australia) provided 40% Acrylamide/Bis Solution. The Hybond ECL nitrocellulose membrane and the Amersham ECL western blotting detection reagent (chemiluminescent reagents and photographic film) were obtained from GE Healthcare Life Sciences (NSW, Australia). Monoclonal mouse IgG_1 HRP-conjugated anti-His antibody was supplied by R&D Systems (Oxfordshire, U.K.). The skim milk powder was purchased from Coles (Canberra, Australia) and the Tween-20 from Sigma Aldrich (NSW, Australia). Bovine Albumin Serum (BSA) was purchased from Santa Cruz Biotechnology and distributed by Thermo Fisher Scientific (Victoria, Australia). The pre-stained protein ladder used as a molecular marker on gels, as

well as the PageBlue Protein Staining Solution used for gel staining, were both purchased from Thermo Fisher Scientific (Victoria, Australia).

2.2 Methods

2.2.1 Tissue culture – cell maintenance

Hi-5 and Sf9 cells were cultured and maintained in suspension at 140rpm as previously described [144, 184], in round-bottomed glass flasks at 27°C in an incubator separate to baculovirus infected cell cultures. Hi-5 cells have a log phase of ~$1x10^6$ – $6x10^6$ cells/ml and a doubling time of 18 – 24 hours. They were subcultured to a density of 3 – $5x10^5$ cells/ml and maintained at 0.5 – $5x10^6$ cells/ml in Excell 405 media supplemented with 1% (v/v) Pen/Strep in an orbital shaker for approximately 72 hours or until reaching a cell density ≥$3x10^6$ cells/ml. The cells were passaged a maximum of 25 times. Sf9 cells were readily converted to Sf900 cells by removal of FCS in the initial Insect Xpress media (containing 10% (v/v) heat-inactivated Foetal Calf Serum) used. The Insect Xpress media was also supplemented with 1% (v/v) Pen/Strep. These cells were cultured at a calculated density of 6 – $8x10^5$ cells/ml and maintained at 10^6-10^7 cells/ml. The Hi-5 cells were concurrently subcultured as monolayers in T75 flasks to maintain a backup. To generate a new subculture, an aliquot of cells was added to fresh Excell medium at a calculated density of $5x10^5$ cells/ml.

2.2.2 Viral amplification in Sf900 cells

Dr Ian Kerr (University of Nottingham, U.K.) provided the initial low-titre (P1) recombinant baculovirus stocks frozen at -80°C. Using site-directed mutagenesis of the C-terminal hexa-histidine tagged cys-less P-gp construct, each of the seven mutant P-gp isoforms studied were generated as previously described [144, 184,

185]. High-titre recombinant baculovirus stocks were then generated following two rounds of amplification in Sf900 cells. To make a P2 stock, Sf900 cells were cultured at a density of $1x10^6$ cells/ml on the day prior to infection in a total medium volume of at least 10ml. On the day of infection, the cell density was confirmed to be at least $2x10^6$ cells/ml before direct infection with the P1 baculovirus stock at a multiplicity of infection (M.O.I.) of 0.1, if the baculovirus titre was $1x10^8$ p.f.u./ml (p.f.u. = plaque forming units). This allowed calculation of the volume of low-titre P1 needed to infect the Sf900 cells:

$$\frac{Cell\ density\ (cells/ml)\ x\ M.O.I.x\ Culture\ volume\ (ml)}{1x\ 10^8\ (pfu/ml)}$$

Equation 1: Calculating the volume of low-titre baculovirus needed for the amplification of baculovirus stock in Sf900 cells. The cell density calculated as the number of Sf900 cells per ml of culture was multiplied by the M.O.I. and the total culture volume (ml), and divided by $1x10^8$ (the assumed baculovirus titre at p.f.u./ml)

Following infection, the cells were incubated (shaking at 140rpm at 27°C) for 6 days, prior to counting in the presence of Trypan Blue. The ideal percentage of total cell death (≥60% but ≤90%) or cell-permeability, was calculated before harvesting the infection. The culture was centrifuged (4000g, 10 min) under sterile conditions and the pelleted cells removed. The supernatant, consisting of the culture medium and the secreted virus was retained in a new, sterile container. The P2 baculovirus was filter-sterilised (0.22µm syringe filter), supplemented with FCS (3% (v/v)), chloroform (10µl/100ml of virus), and stored at 4°C.

P2 baculovirus stock was then used (as described above for P1→P2) to further amplify the baculovirus stock to generate the higher-titre, larger volume, P3 baculovirus working stock, which was then used to infect Hi-5 cells.

Expression of His-tagged P-gp (cys-less and mutants) was confirmed by Western immunoblot using the HRP-conjugated anti-His IgG_1 mouse monoclonal antibody (refer to 2.2.5). Working stocks of virus were routinely tested for expression of the target protein by small-scale infection in Hi-5 cells.

2.2.3 Large scale expression of P-gp in Hi-5 cells

Using the previously established methods by Callaghan et al. [142, 146, 184], all P-gp mutants were expressed in Hi-5 cells using the high-titre P3 working stock recombinant baculovirus. Prior to the day of infection, Hi-5 cells were subcultured to a density of $1.5x10^6$ cells/ml in culture volumes ranging from 200 – 400ml. On the day of the infection, cells were infected by direct addition of the P3 recombinant baculovirus, provided that the Hi-5 cell density was ~$3x10^6$ cells/ml; if not, the cells were left incubating for longer. The P3 baculovirus was added at a M.O.I. of at least 2 (refer to 2.2.2), and the Hi-5/baculovirus culture incubated at 27°C for 1 hour statically. The cell suspension was then diluted to a final density of $1.5x10^6$ cells/ml by addition of Excell 405 medium and incubated for at least 72 hours at 140rpm at 27°C.

Using Trypan Blue cells were visually inspected for signs of infection. Cell death due to lysis was established by counting the blue-stained cells and a cell permeability of at least 30% resulted in the harvesting of the infection. Harvesting was done similarly to Sf900 cells (refer to 2.2.2), but the Hi-5 cell pellet, instead of the supernatant, was collected and stored at -80°C. Similarly, expression of the His-tagged P-gp isoforms were confirmed using Western immunoblotting (refer to 2.2.5).

2.2.4 Preparation of crude membranes using nitrogen cavitation

The frozen (stored at -80°C) Hi-5 pellets were rapidly thawed in a 37°C water bath and resuspended using a Dounce homogeniser in a mixture of membrane isolation buffer (20mM MOPS pH 7.4, 200mM NaCl, 0.2mM $CaCl_2$, 0.25M sucrose) and EDTA free protease inhibitor (10x concentrated stock). The volume of resuspension buffer used was at least ten times the volume of the pellet, and 0.5ml of protease inhibitor was used per ml of pellet. Cells were disrupted by high pressure nitrogen (1200 p.s.i.) in four cycles of 20 minutes at 4°C, cells being released to atmospheric pressure in between each cycle. Cell debris was removed by differential centrifugation (2000g, 10mins, 4°C) and the pelleted crude membrane fraction was isolated from the retained supernatant containing the burst cells by ultracentrifugation (100,000g, 45mins, 4°C). The membrane was then resuspended in an ice-cold $CaCl_2$-free resuspension buffer (20mM MOPS pH 7.4, 200mM NaCl, 250mM sucrose) and supplemented with EDTA-free protease inhibitor (in DMSO) [184]. The total protein concentration of membranes was determined using the DC BioRad Protein Assay Kit as per manufacturer's instructions. Immunoblotting using the anti-His monoclonal antibody (refer to 2.2.5) was used to detect P-gp expression in the membrane fractions, as well as to determine the efficacy of the membrane isolation procedure. The prepared crude membranes were stored in 1ml aliquots at -80°C till purification or up to a year.

2.2.5 Western immunoblotting

Samples of known total protein concentration (20µg) were mixed with 5x Laemmli Sample Buffer (LSB; 0.25M Tris pH 6.8, 50% (v/v) glycerol, 10% (w/v) SDS, 6% (v/v) 2-mercaptoethanol, 0.01% (w/v) bromophenol blue), and resolved by SDS-PAGE gel with 7% (w/v) acrylamide before being transferred to a nitrocellulose membrane by

Western blotting (90V, 60mins, ≤250mA). The nitrocellulose membrane was then washed using a blocking buffer comprised of 5% (w/v) skim milk dissolved in PBS-T (135mM NaCl, 2.5mM KCl, 10mM Na_2HPO_4, 1.75mN KH_2PO_4, pH 7.4, containing 0.1% (v/v) Tween-20), for 1 hour to reduce non-specific binding. It was then incubated overnight (at 4°C) or for at least 2 hours in room temperature (22°C) with the anti-6x-His mouse IgG_1 HRP-conjugated antibody (diluted 1:10,000 in blocking buffer). Proteins with the bound antibody were detected using chemiluminescent reagents (Amersham ECL™ Western Blotting Detection Reagent) as per the manufacturer's instructions and digitised using the GelDoc Vilber Fusion SL Chemiluminescence system for quantification and analysis.

2.2.6 Protein purification from crude membranes

Crude membranes expressing the P-gp mutants were purified by virtue of their C-terminal poly-histidine tag using nickel-NTA immobilised affinity chromatography (IMAC). The purification procedure was adapted from methods employed previously by Callaghan et al. [143, 144, 146, 184].

2.2.6.1 Solubilisation and purification of crude membranes using IMAC

Protein was solubilised in a lipid-detergent micelle suspension comprised of a lipid film made of *E. coli* lipid extract and cholesterol in a 4:1 (w/w) ratio, dissolved in a solvent consisting of chloroform and methanol in a 2:1 (v/v) ratio, and resuspended in solubilisation buffer (20mM Tris, 150mM NaCl, 20mM MOPS, 20% glycerol) containing 2% (w/v) of DDM at pH 6.8, to achieve a final lipid concentration of 0.4% (w/v). The crude Hi-5 membranes were isolated using ultracentrifugation (100,000g, 45mins) and resuspended in the solubilisation buffer for a final concentration of 5mg/ml total protein. This mixture was then solubilised by constant stirring at 4°C for

up to 90 minutes before separation of the insoluble protein material by ultracentrifugation (100,000g, 60mins, 4°C).

The resultant supernatant containing the solubilised protein was then incubated with His-bind Resin (800µg per 100mg of crude membrane) for 1 hour at 4°C on a windmill rotor, ensuring continuous agitation of the resin and promoting binding of the poly-histidine tag of the P-gp protein to the nickel in the resin. Imidazole (10mM) was also added to the solubilised protein-resin mixture to reduce non-specific binding. As described previously, gravity chromatography was used to purify the protein from the resin-packed solubilisation mixture [184]. After collecting the initial flow through (FT) fraction which contained contaminants that did not bind to the nickel in the resin, the column was washed in five bed volumes (bv) of chromatography buffers with increasing concentrations of imidazole (20, 40, and 80mM) to remove weakly bound contaminants. At the highest imidazole concentration buffer (500mM imidazole, 0.1% (w/v) *E.Coli* lipid/cholesterol (4:1), 0.1% (w/v) DDM, 150mM NaCl, 1.5mM $MgSO_4$, 10mM MOPS, 10% glycerol; pH 6.8), P-gp was eluted. Fractions were collected at each wash and elute step and purification of P-gp was confirmed using SDS-PAGE electrophoresis followed by PageBlue staining (refer to 2.2.7).

2.2.6.2 Buffer exchange

Purified protein was used in tryptophan fluorescence assays to measure the binding of drugs through the fluorescence quenching of the intrinsic tryptophan residues in P-gp [186]. Prior to this, the imidazole in the solution containing purified P-gp was removed by buffer exchange (200mM NACl, 20mM MOPS, pH 7.4, 5% (v/v) glycerol, 0.1% (w/v) DDM, and 0.1% (w/v) lipid mixture) before reconstitution into proteoliposomes (refer to 2.2.6.3). This was necessary since high imidazole

concentrations interfered with the fluorescence emission spectrum signal of the endogenous tryptophan residues.

2.2.6.3 Reconstitution of purified P-gp into proteoliposomes

The eluted pure P-gp was reconstituted into proteoliposomes from the mixed lipid-detergent micelles. The detergent was removed from the micelle suspension by adsorption using SM2 BioBeads (225mg/ml of purified protein), and gentle agitation for 2 hours at room temperature (22°C). Prior to use, the BioBeads were washed in solutions of: (i) 100% H_2O, (ii) 50% (v/v) methanol, (iii) 100% methanol, (iv) 50% (v/v) methanol, and (v) four times in 100% H_2O, as per the manufacturer's instructions. Successful reconstitution was confirmed as previously described using a sucrose density centrifugation gradient followed by western blotting or SDS-PAGE analysis (section 2.2.5 and 2.2.7), of the fractions collected from each density gradient. Efficient reconstitution resulted in a signal/band in the 5-10% sucrose gradient fraction [184, 187].

2.2.7 SDS-PAGE analysis of purification

2.2.7.1 Purification gel

To ascertain that the purification was successful, a SDS-PAGE gel with 7% (w/v) acrylamide was resolved using the BioRad mini-PROTEAN Tetra system. The gel was loaded with fractions collected during chromatography (accounting for 0.8 – 1.6% of total fraction volume) mixed with 5x Laemmli Sample Buffer (LSB: 30mM Tris HCl (pH 6.8), 50mM DTT, 1% (w/v) SDS, 6% (v/v) glycerol). The SDS-PAGE gel was stained using PageBlue, and following de-staining (as per manufacturer's instructions), proteins were detected as blue bands on the clear gel. The pre-stained protein ladder loaded on each gel allowed verification of the molecular weight of the

purified protein which was a visible band at ~140kDa. The gels were imaged using the GelDoc BioRad XR+ system.

2.2.7.2 Determination of protein concentration and densitometry analysis

Due to the composition of the buffer containing purified P-gp, and the consequent interference in the absorption spectra caused by imidazole or lipids, the concentration of purified reconstituted P-gp was not measured using the commercial BioRad DC^{TM} Total Protein Assay kit as in the case of samples of crude membranes (refer to 2.2.4). Instead, P-gp concentration was determined using SDS-PAGE analysis of a standard curve of known concentrations of BSA (ranging between 0.1 – 2.0 µg), against known volumes (10, 20, and 40µl) of loaded protein. The gels were analysed using the ImageJ programme (NIH, U.S.) to determine the densitometry of each visible band (i.e. the number of pixels or Optical Density per band). Linear regression resulted in a BSA standard curve which allowed interpolation between the optical density (OD) and the amount of protein in each lane [184].

2.2.8 Colorimetric assay to measure the ATPase activity of P-gp

The ATPase activity of purified P-gp in reconstituted liposomes was measured using a colorimetric assay that allowed detection of liberated inorganic phosphate (P_i), adapted from the Chifflet assay and previously described by the members of the Callaghan laboratory [184, 188]. The assay, carried out in a 96-well plate, included an inorganic phosphate standard curve with P_i ranging from 0 - 20nmol in a total volume of 50µl. Each sample well contained 200 - 400ng of purified reconstituted P-gp, also in a total volume of 50µl.

Two separate types of ATPase activity measurements were taken for each P-gp mutant analysed. The first assay was undertaken to determine the Michaelis-Menten

parameters (V_{max} and K_m) of the purified protein (equation 2). In this case, the activity of purified P-gp was measured in the absence or presence of 10µM of nicardipine added to each well, over a range of disodium ATP concentrations (0 – 1.75 mM); final volume in each well was made up to 50µl using ATPase buffer (50mM Tris at pH 7.4, 150mM NH_4Cl, 5mM $MgSO_4$, 0.02% (w/v) NaN_3).

$$V = \frac{Vmax\ [S]}{Km + [S]}$$

Equation 2: Michaelis-Menten parameters were determined by non-linear regression of the resultant hyperbolic relationship between the rate of ATP hydrolysis versus concentration of ATP (using GraphPad Prism software). The ATPase activity (V) was calculated as the moles of P_i liberated per unit of time for a unit of pure protein (nmol P_i min^{-1} mg^{-1}), where V_{max} refers to the maximal rate of ATP hydrolysis, K_m is the affinity of ATP in P-gp, and [S] is the ATP concentration.

The second type of ATPase activity assay undertaken obtained the potency (EC_{50}) of each of the four compounds, nicardipine, vinblastine, rhodamine 123 and paclitaxel, to stimulate ATPase activity in each P-gp mutant. In this case, the concentration of disodium ATP was kept constant (2mM), but varying concentrations of the four drugs were used. Consequently, the ATPase activity was plotted as a function of increasing concentration of each compound on a logarithmic scale (equation 3). For nicardipine and vinblastine the concentrations ranged from $7.5x10^{-8}$ to $2.5x10^{-3}$ M, and for paclitaxel and rhodamine 123 it was between $7.5x10^{-9}$ to $2.5x10^{-4}$ M. All drug stocks were made in DMSO and the total solvent concentration did not exceed 1% (v/v) to avoid adverse effects on P-gp function.

$$V = V_{initial} + \frac{V_{final} - V_{initial}}{(1 + 10^{(log_{10}EC_{50} - [D])})}$$

Equation 3: Dose-response relationship. The EC_{50} (potency) of each compound to stimulate ATPase activity (V) was estimated using non-linear regression of the general dose response equation, where [D] is the drug concentration (M), and $V_{initial}$ and V_{final} are the measured activities in the absence, or presence of drug, respectively.

Following addition of all relevant reagents, the plate was incubated at 37°C for 40 minutes. The reaction was then stopped upon addition of 40µl of 12% (w/v) SDS, followed by 100µl of a solution containing ammonium molybdate (6% (w/v) ascorbate, 0.5% (w/v) ammonium molybdate, 0.5M HCl). The inorganic phosphate was then measured after allowing completion of the colour-changing reaction resulting from the formation of a complex with molybdate, as previously detailed [188]. The plate was then read using the UV/Vis spectrophotometer, Imark™ plate reader, at 750nm absorbance. The P_i standard curve (0-20 nmol) allowed extrapolation of the amount of liberated phosphate in each well and this was converted to nmol of P_i/min/mg of protein. The data was then analysed using GraphPad Prism® Software (California, U.S.) as described above.

2.2.9 Tryptophan fluorescence assay

To measure the intrinsic tryptophan fluorescence of purified, reconstituted P-gp, the imidazole in the buffer was removed (refer to 2.2.6.2), since high imidazole concentrations interfere with the fluorescence signal of the endogenous tryptophan residues. The protein was then reconstituted in imidazole-free buffer and the final protein concentration determined (refer to 2.2.7.2). A protein concentration of at least 50µg/ml was required for sufficient signal intensity [189]. Purified reconstituted protein (1ml) in buffer (200mM NaCl, 20mM MOPS, pH 6.8) was added to a 1ml quartz-silica cuvette to measure the tryptophan fluorescence in the absence and

presence of drug. DMSO did not exceed 1% (v/v) of the total solvent concentration in the drug stocks used. Spectrophotometer was used to measure the fluorescence spectrum. The excitation and emission wavelengths were set to 295 ± 5nm and 300-500nm, respectively, and the scan speed was set to 120nm per minute.

The fluorescence emission spectrum was measured in the absence of drug (control buffer alone with 1% DMSO), and then repeated following sequential addition of each drug. Nicardipine, vinblastine, and paclitaxel, were added at a range of 2 - 35µM, whereas rhodamine 123 concentrations were between 5 - 50µM. A five-minute incubation period was used prior to scanning. The fluorescence intensity was plotted against drug concentration and the maximum intensity of the spectrum in the absence of drug was used as a reference point. Upon addition of vinblastine, there was an alternative spectral effect of drug addition with a shift in the wavelength (λ_{max}) producing the maximum intensity. The changes in fluorescence emission intensity or wavelength maximum was plotted as a secondary curve against the drug concentration. Both effects produced a hyperbolic curve when fitted by non-linear regression using the one-site binding equation (equation 4). This was used to determine the apparent binding affinity (K_{App}) of each drug to the protein.

$$\mathbf{B} = \frac{(\boldsymbol{B_{max}}[\mathbf{D}])}{(\boldsymbol{K_{App}} + [\mathbf{D}])}$$

Equation 4: Measuring drug binding to protein, where [D] is the drug concentration, and the two measured parameters are the K_{App} (apparent binding affinity) and B_{max} (maximal binding capacity) of each drug in each P-gp mutant.

2.2.10 Statistical analysis

Curve-fitting and statistical analysis of all data was done using the GraphPad Prism® Software, version 6.0. All results obtained were presented as mean ± SEM (standard error of mean), collected from at least three independent purifications from separate membrane preparations. Comparison of all values from different P-gp isoforms was achieved using the ANOVA (analysis of variance) function and applying the Dunnett post-hoc test. A significant result was determined by a *p value* <0.05.

Chapter 3:
RESULTS

The aim of this investigation was to locate the pharmacologically distinct drug binding site(s) in P-gp of four compounds, nicardipine, vinblastine, rhodamine 123 and paclitaxel. Seven residues in various transmembrane helices were mutated to cysteines, namely L65C (TM1), M197C (TM5), F336C (TM6), T769C (TM8), F978C, and V982C (both in TM12). The effects of these mutations on the interaction between P-gp and the four drugs was assessed using purified, reconstituted protein. Each P-gp mutant was expressed in High-Five insect cells with recombinant baculovirus. Functional assays including ATP hydrolysis assays, and the fluorescence of endogenous tryptophan residues, was used to identify residues that affected drug-protein interactions.

3.1 Expression, purification, and reconstitution of mutant P-gp isoforms

3.1.1 Expression in insect cells and isolation of crude membranes

As described previously, expression of human P-gp was achieved in High-Five insect cells following infection with recombinant baculovirus [184, 190]. The High-Five cells were subjected to nitrogen cavitation and differential centrifugation to isolate crude membranes containing P-gp mutant expressing cells (methods 2.2.4). Figure 12 shows a representative western immunoblot of the membrane preparation from High-Five cells expressing the P-gp mutant V982C. All P-gp mutant constructs were engineered with a poly-histidine tag at the C-terminal to allow for purification using affinity chromatography and ease of detection by western blotting. Crude cell membrane (lane v) shows a strong signal for P-gp expression, comparable to the P-gp expression in the Wild-type membrane used as a positive control (lane vi). The comparatively low P-gp signal in lanes (iii) and (iv) demonstrate that the majority of the P-gp containing cellular fraction was successfully isolated as crude membrane.

Successful expression of all seven P-gp mutants and the cys-less P-gp construct was achieved as shown in figure 13. The comparative expression levels for the seven isoforms showed no major difference. All membrane preparations were routinely analysed for their P-gp expression. Two additional P-gp mutants were also initially generated for analysis, but despite multiple attempts, expression of mutants was entirely unsuccessful for F343C and F951C, failing to yield any detectable amount of protein (data not shown).

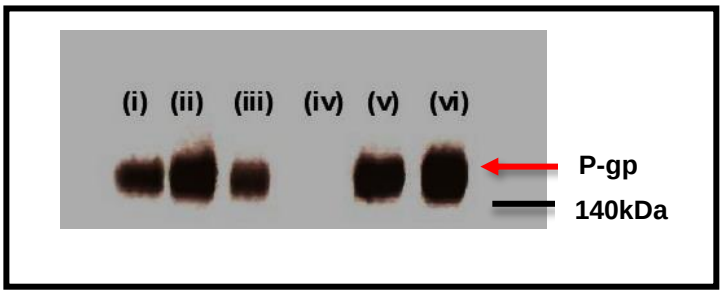

Figure 12: Preparation of crude P-gp mutant (V982C) membrane from High-Five cells. Immunoblot analysis of fractions obtained during the isolation of membranes from High-Five cells. The protein samples (20µg) were resolved by 7% (w/v) acrylamide SDS-PAGE. Lane assignments are as follows: (i) the resuspended High-Five cell pellet; (ii) and (iii) the supernatant and pellet, respectively, following centrifugation at 2000g; (iv) and (v) the supernatant and pellet, respectively, following centrifugation at 100,000g, and (vi) the wild-type P-gp positive control. P-gp was detected by the anti-His antibody using chemiluminescence.

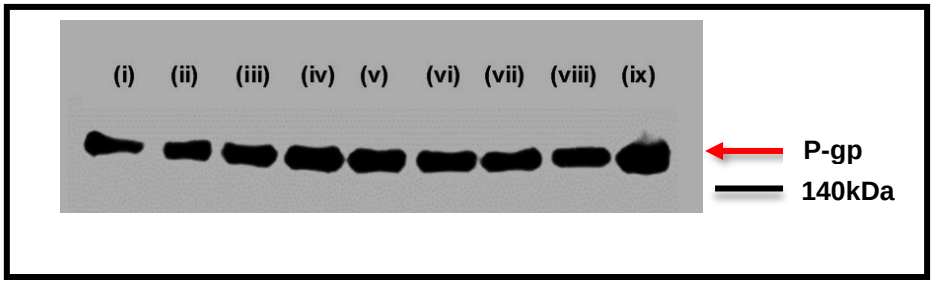

Figure 13: Immunoblot analysis of the level of P-gp expression for each mutant isolated from crude insect cell membranes. Crude membrane protein samples (20µg) of each P-gp mutant and both cys-less and Wild-type P-gp controls were resolved by 7% (w/v) acrylamide SDS-PAGE. Following transfer to nitrocellulose membrane and incubation with anti-His antibody, P-gp expression was detected using chemiluminescence. Lane assignment is as follows: (i) L65C, (ii) M197C, (iii) A311C, (iv) F336C, (v) T769C, (vi) F978C, (vii) V982C, (viii) cys-less P-gp construct, and (ix) the Wild-Type P-gp positive control.

3.1.2 Purification and reconstitution of P-gp from crude membrane preparations

All seven mutants and cys-less P-gp were successfully purified using immobilised metal affinity chromatography (IMAC) by virtue of their C-terminal poly-histidine tag. The mutants were solubilised from crude insect cell membranes using DDM in the presence of excess lipids and cholesterol. Figure 14 shows a representative SDS-PAGE gel of the fractions collected at each step of the chromatography process for purification of cys-less P-gp. Proteins that did not bind to the nickel containing resin of the IMAC column were lost in the flow-through (FT). Further protein contaminants were removed during the wash steps (lanes 1-6) in buffer containing increasing concentrations of imidazole.

The dodeca-poly-histidine tag in P-gp provided high affinity binding with the nickel during the wash steps with lower concentrations of imidazole. At the highest concentration of imidazole (500mM), the cys-less P-gp was eluted (lanes 7-8) as the imidazole outcompeted the P-gp poly-histidine tag for binding to the nickel. The band at approximately 140kDa in lane 7 shows cys-less P-gp protein of high purity, estimated by densitometric analysis to be >90% of total protein in the sample. The eluted P-gp was then reconstituted into proteoliposomes after removal of the detergent by selective adsorption using BioBeads. Reconstitution of pure P-gp into a lipid bilayer environment enabled functional analysis using standard biochemical assays (section 3.2).

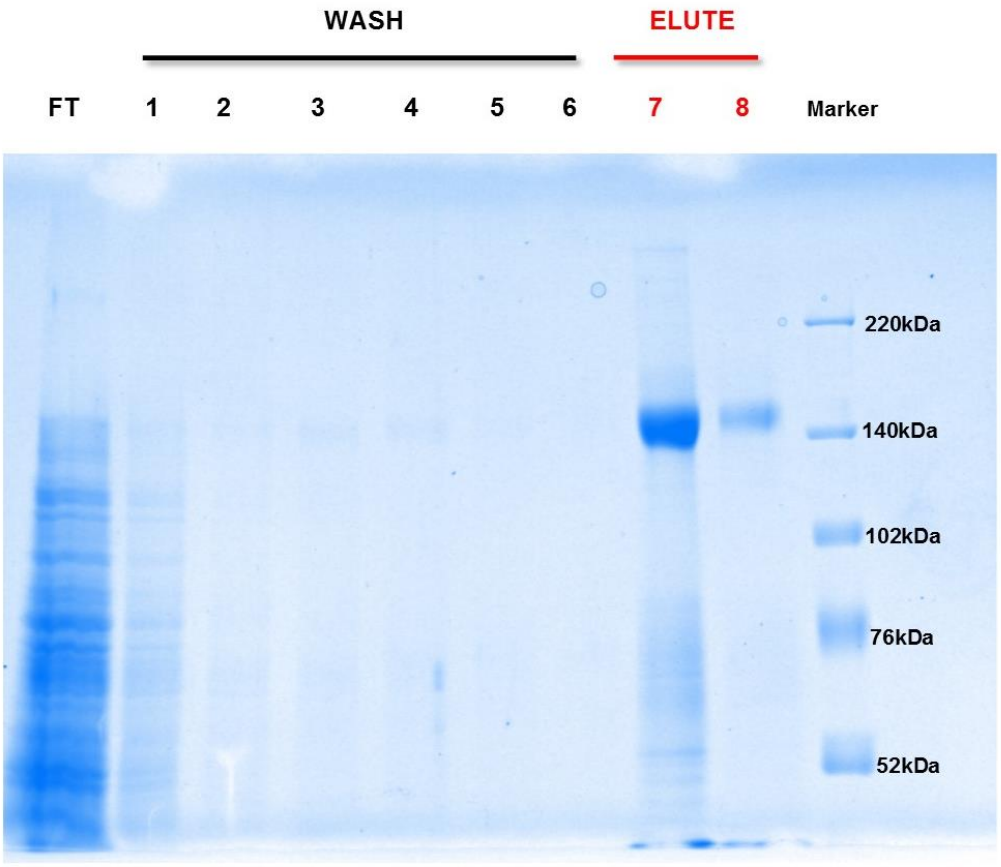

Figure 14: Purification of poly-histidine tagged cys-less P-gp using IMAC. Cys-less P-gp was solubilised in DDM and purified using IMAC. Fractions (40µl) were collected at each stage of IMAC and mixed with 10µl of 5x LSB and resolved by 7% (w/v) SDS-PAGE. Protein was detected using PageBlue stain. FT contains unbound material. Lanes 1-6 corresponds to washes in imidazole containing buffer. The first wash (1-2) was 20mM imidazole buffer (pH 8.0), the second wash (3-4) 40mM imidazole buffer (pH 8.0), and the last wash (5-6) using 2mM imidazole buffer (pH 6.8). P-gp was eluted (7-8) using buffer containing 500mM imidazole (pH 6.8). Lane 7 shows the eluted pure cys-less P-gp as a prominent band at ~140kDa.

3.1.3 Yield of mutant P-gp isoforms

The protein yield following purification and reconstitution of the 12His-3C-P-gp mutants is summarised in table 1. The values represent the amount of protein in the final purified sample, determined by densitometric analysis of SDS-PAGE which contained internal BSA standards (figure 15). Known volumes (unknown concentrations) of purified and reconstituted P-gp mutants were loaded alongside the known concentrations of BSA protein. Linear regression was used to determine the relationship between BSA

concentration and the optical density of the bands, allowing estimation of the concentration of the P-gp samples by interpolation (figure 16). It was not possible to determine P-gp concentration using conventional colorimetric assays due to the considerable interference by lipids, glycerol, imidazole and other buffer components present in the samples.

The yield of cys-less P-gp was 0.36 ± 0.07 mg L^{-1} cell culture, which equates to an expression level of P-gp as 0.13% of total crude membrane protein. Table 1 summarises the individual yields of each of the purified mutant P-gp isoforms. The overall yield of purified protein per litre of culture ranged between 0.36 – 0.57 milligrams, approximately 0.1 – 0.2% of the total amount of crude membrane per litre of culture. These yields for membrane proteins reflect on the high expression system of the baculovirus in insect cells and were within the range of previous observations [184, 185]. There were no significant differences between the yield of each mutant P-gp isoform purified.

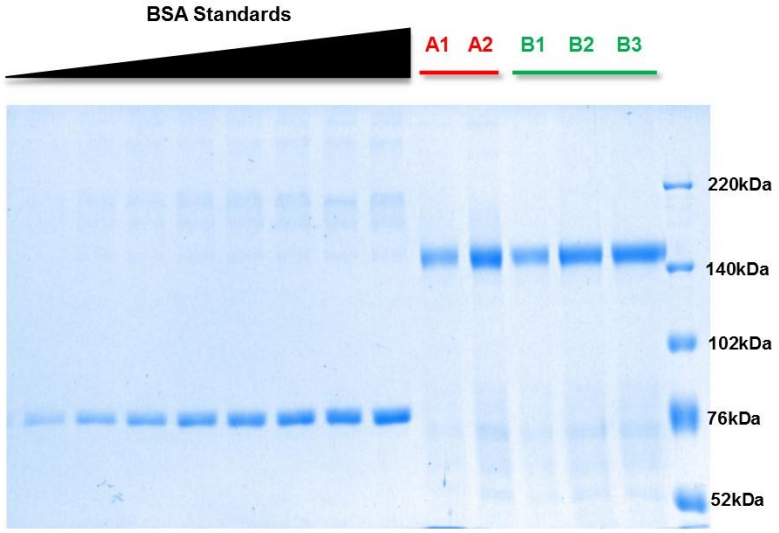

Figure 15: Representative densitometric analysis of P-gp concentration using SDS-PAGE. BSA standards (0.3 – 1.0µg of BSA) were used to provide a relationship between staining density and protein concentrations. 5µl and 10µl (lanes A1 and A2) samples of purified protein following elution using 500mM imidazole containing buffer was loaded alongside 10, 20 and 30µl (lanes B1-B3) of purified and reconstituted protein in buffer following removal of imidazole (buffer exchange). The protein was resolved by 7% (w/v) SDS-PAGE and detected using PageBlue stain.

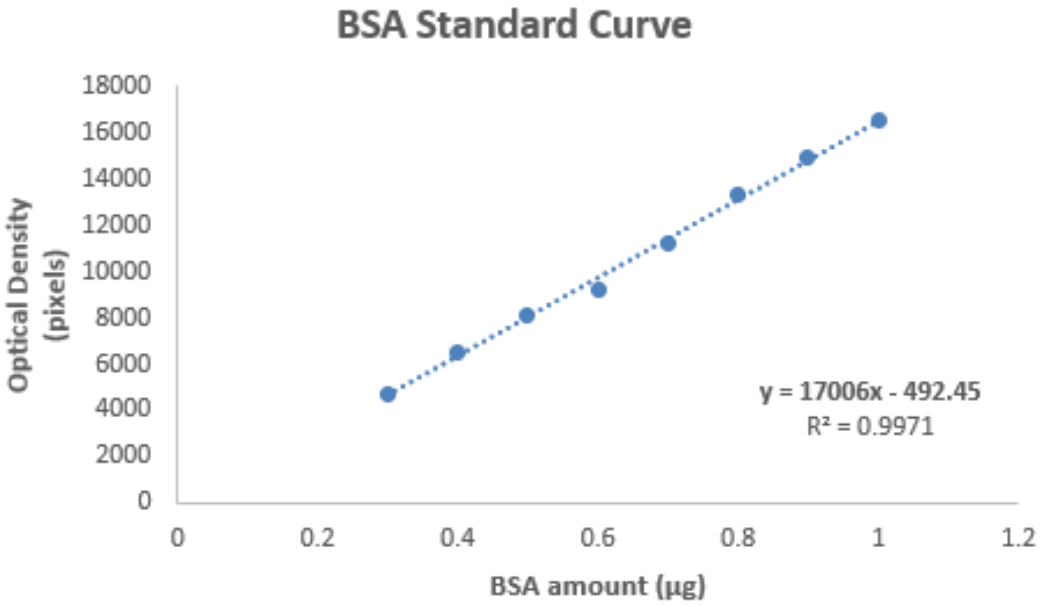

Figure 16: Quantitative analysis densitometric SDS-PAGE to determine unknown P-gp concentrations. The optical density of each of the BSA concentration bands was plotted as a function of BSA concentration (0.3 – 1.0µg) and linear regression used to determine concentration of unknown protein amounts loaded on the gel. Concentration of samples were determined using the linear equation by interpolation.

Table 1: Yield of purified P-gp mutants. The yields of crude membrane and purified protein was determined by recording the initial culture volume of the baculovirus-infected High-Five cells, the concentration of crude membrane isolated from the pellet, and the concentration of purified, reconstituted protein obtained from the membranes (normalised to per litre of cell culture). The percentage of expression of each mutant P-gp isoform in total crude membrane is also noted. The sample size was n≥5 independent membrane preparations and purifications and the values in parentheses indicate the number of independent membrane preparation per mutant P-gp isoform.

P-gp mutant	Crude membrane (mg L^{-1} culture)	Yield of purified protein		% of total crude membrane
		(µg mg^{-1})	(mg L^{-1})	
Cys-less	278 ± 10 (11)	2.1 ± 0.2	0.36 ± 0.07	0.13%
L65C	258 ± 8 (8)	1.9 ± 0.3	0.51 ± 0.10	0.20%
M197C	328 ± 7 (9)	0.9 ± 0.3	0.41 ± 0.04	0.13%
A311C	200 ± 25 (6)	2.0 ± 0.3	0.36 ± 0.03	0.18%
F336C	307 ± 8 (7)	1.7 ± 0.1	0.43 ± 0.02	0.14%
T769C	320 ± 40 (10)	1.7 ± 0.2	0.57 ± 0.13	0.18%
F978C	277 ± 43 (9)	1.8 ± 0.2	0.50 ± 0.10	0.18%
V982C	336 ± 83 (5)	1.2 ± 0.4	0.41 ± 0.07	0.12%

3.2 Assessing the functional integrity of mutant P-gp isoforms

The ATPase activity was measured to assess whether each P-gp isoform maintained functionality following expression, purification, and reconstitution. ATP is hydrolysed by the NBDs and the resultant energy is coupled to the transport of substrates across the membrane. Substrates of P-gp can stimulate ATP hydrolysis in the protein, and retention of this property indicates that the protein is also capable of binding drugs and maintaining inter-domain communication.

3.2.1 Measuring ATPase activity

The maximal rate of ATP hydrolysis for cys-less P-gp in the absence of drug was V_{max} (basal) = 386 ± 36 nmol Pi min^{-1} mg $protein^{-1}$. The substrate affinity constant for

ATP was K_m = 0.66 ± 0.06 mM (figure 17). In the presence of 10µM of nicardipine, the stimulated V_{max} was significantly (*p<0.05*) increased to 1048 ± 103 nmol Pi min^{-1} mg $protein^{-1}$; a 3.0 ± 0.4-fold increase in basal activity (table 2). The stimulated K_m (0.85 ± 0.28 mM) was not significantly different to the basal activity. These values are in agreement with those published in earlier studies [142, 144, 146, 184] which reported a V_{max} basal rate of 580 ± 160 Pi min^{-1} mg $protein^{-1}$, and a nicardipine stimulated ATPase activity of 1300 ± 130 Pi min^{-1} mg $protein^{-1}$. Nicardipine, a known modulator of P-gp, has been widely used across ATPase assays to assess P-gp function. In the present investigation, initially only nicardipine was used to establish that P-gp retained function following purification and reconstitution by measuring its drug-stimulated ATPase activity.

Additionally, The V_{max} basal rate was also comparable to that of wild-type (WT) P-gp (610 ± 50 Pi min^{-1} mg $protein^{-1}$). The V_{max} in the presence of 50µM of nicardipine in WT P-gp was reported to be significantly higher (2100 ± 170 Pi min^{-1} mg $protein^{-1}$) than in cys-less P-gp, suggesting that mutating cysteines to serines resulted in subtle changes in the drug-protein interactions following stimulation by nicardipine [184].

The cysteine containing P-gp mutants were also assessed for their ATPase activities and the parameters compared to those obtained for cys-less P-gp (table 2). The basal V_{max} was 231 ± 83 nmol Pi min^{-1} mg $protein^{-1}$ and the K_m was 1.01 ± 0.54 mM for the L65C mutant. In the presence of nicardipine, the V_{max} was stimulated 2.9 ± 0.9-fold to 1280 ± 161 nmol Pi min^{-1} mg $protein^{-1}$, and the K_m was not significantly altered at 2.24 ± 0.81 mM. For M197C, the basal V_{max} was 446 ± 112 nmol Pi min^{-1} mg $protein^{-1}$ (basal K_m = 0.48 ± 0.04 mM), which was stimulated 3.5 ± 0.4-fold in the presence of nicardipine to 1133 ± 270 (stimulated K_m = 0.93 ± 0.10 mM). The mutants A311C and F336C had basal V_{max} values of 524 ± 86 and 524 ± 86 nmol Pi

min^{-1} mg $protein^{-1}$, and K_m values of 1.38 ± 0.35 mM and 0.57 ± 0.08 mM, respectively. Addition of nicardipine resulted in stimulated V_{max} values of 1248 ± 159 nmol Pi min^{-1} mg $protein^{-1}$ (2.4 ± 0.1-fold stimulation) in A311C, and 1305 ± 100 nmol Pi min^{-1} mg $protein^{-1}$ (3.8 ± 1.0-fold stimulation) in F336C, with no significant changes in the stimulated K_m values which were 1.14 ± 0.27 (A311C) and 0.37 ± 0.05 mM (F336C).

The basal V_{max} (92 ± 19 nmol Pi min^{-1} mg $protein^{-1}$) for T769C was significantly lower (*p<0.05*) compared with the cys-less P-gp (basal V_{max} 386 ± 36 nmol Pi min^{-1} mg $protein^{-1}$). The isoform was associated with a 9.0 ± 1.6-fold increase in stimulation of ATP hydrolysis by nicardipine, to a V_{max} of 682 ± 66 nmol Pi min^{-1} mg $protein^{-1}$. Therefore, despite the significant reduction in basal activity, the maximal activity was not significantly different for T769C compared to cys-less P-gp, although the extent of stimulation was greater (*p<0.05*).

Lastly, the two mutants F978C and V982C had basal activities of 362 ± 155 nmol Pi min^{-1} mg $protein^{-1}$ (K_m = 0.68 ± 0.22 mM), and 273 ± 66 nmol Pi min^{-1} mg $protein^{-1}$ (K_m = 0.65 ± 0.10 mM). This was stimulated to 951 ± 47 nmol Pi min^{-1} mg $protein^{-1}$ (3.6 ± 1.2-fold) for F978C, and to 1614 ± 442 nmol Pi min^{-1} mg $protein^{-1}$ (6.1 ± 0.9-fold) for V982C.

As summarised in table 2, there were no significant differences in the maximal rate of ATP hydrolysis for any of the seven mutants compared to the cys-less P-gp. The introduction of cysteines at residue positions L65C, M197C, A311C, F336C, T769C, F978C, and V982C, did not significantly perturb the native rate of ATP hydrolysis in the presence of a saturating concentration of nicardipine. Moreover, the purified, reconstituted mutant proteins were all functionally competent and thus could be used

for further functional assays to determine the contribution of each residue in drug binding.

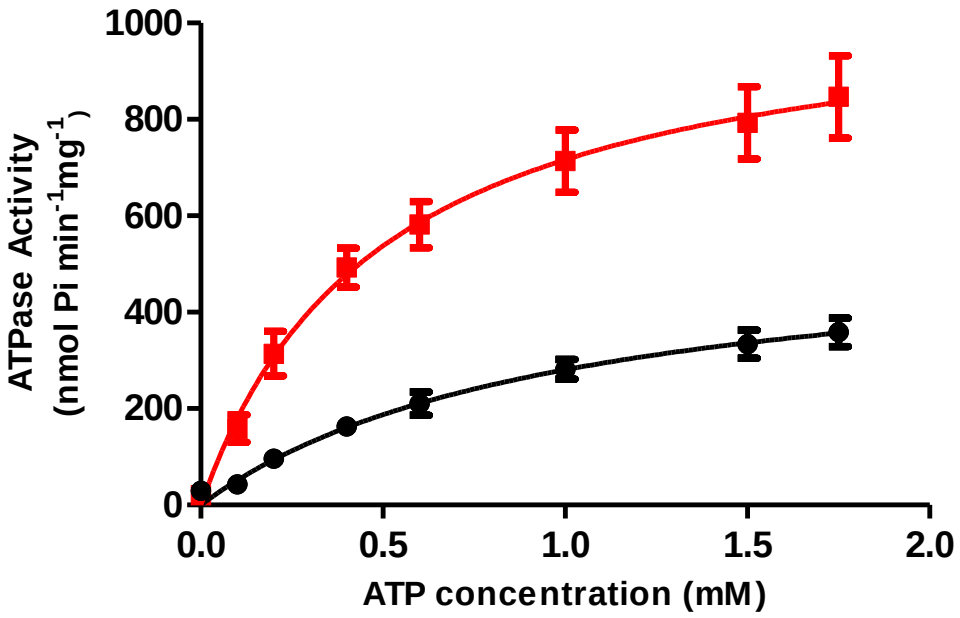

Figure 17: ATPase activity of purified and reconstituted cys-less P-gp. The Michaelis-Menten parameters of purified cys-less P-gp were determined in the presence of varying concentrations of ATP (0 – 1.75mM). The ATPase activity of 150µg of purified reconstituted P-gp protein was measured as the rate of liberation of inorganic phosphate (nmol Pi min^{-1} mg $protein^{-1}$), in the absence (basal activity – **black line**), or presence (stimulated activity – **red line**), of 10µM nicardipine. The data was analysed by non-linear regression of the Michaelis-Menten equation to obtain the parameters, V_{max} (maximal activity) and K_m (substrate affinity). Each point represents the mean ± SEM of nine independent protein purifications.

Table 2: Summary of Michaelis-Menten parameters for purified mutant P-gp isoforms. The parameters K_m (substrate affinity), V_{max} (maximal activity), and fold-stimulation of hydrolysis are presented as the mean ± SEM for cys-less P-gp and all mutants in the presence or absence of 10 µM of Nicardipine (n≥5 independent protein purifications, with individual values shown in parentheses next to each mutant). Fitting of the Michaelis-Menten equation was by non-linear least squares regression. One-way ANOVA was used to determine statistically significant differences in parameters between cys-less P-gp and each mutant, where a significant difference is indicated by ***** (*p<0.05*).

P-gp mutant	Substrate Affinity (K_m) (mM)		Maximal Activity (V_{max}) (Pi nmol min^{-1} mg $protein^{-1}$)		
	BASAL	STIMULATED	BASAL	STIMULATED	Fold Stimulation (stimulated/basal)
Cys-less (11)	0.66 ± 0.06	0.85 ± 0.28	386 ± 36	1048 ± 103	3.0 ± 0.4
L65C (5)	1.01 ± 0.54	2.24 ± 0.81	231 ± 83	1280 ± 161	2.9 ± 0.9
M197C (5)	0.48 ± 0.04	0.93 ± 0.10	446 ± 112	1133 ± 270	3.5 ± 0.4
A311C (6)	1.38 ± 0.35	1.14 ± 0.27	524 ± 86	1248 ± 159	2.4 ± 0.1
F336C (6)	0.57 ± 0.08	0.37 ± 0.05	524 ± 86	1305 ± 100	3.8 ± 1.0
T769C (6)	0.25 ± 0.12	0.68 ± 0.10	92 ± 19*****	682 ± 66	9.0 ± 1.6*
F978C (5)	0.68 ± 0.22	1.19 ± 0.41	362 ± 155	951 ± 47	3.6 ± 1.2
V982C (5)	0.65 ± 0.10	1.12 ± 0.52	273 ± 66	1614 ± 442	6.1 ± 0.9

3.3 Assessing molecular interactions between mutant P-gp isoform and each drug

3.3.1 Measuring drug potency (EC_{50})

The potency of nicardipine, vinblastine, rhodamine 123, and paclitaxel, to stimulate ATP hydrolysis in the seven mutant P-gp isoforms were compared with cys-less P-gp. Drug effects were determined in the presence of a fixed amount of ATP (2 mM) and varying concentrations of each compound (methods 2.2.8). The four compounds stimulated the ATPase activities of the P-gp mutants in a dose dependent manner and the potency of effect (EC_{50}) was estimated from the sigmoidal dose-response relationships. An altered potency compared to cys-less P-gp would implicate the residue in the binding of the drug in question.

Figure 18 (panels A-D) demonstrates the effects of each compound on ATP hydrolysis by cys-less P-gp. In panel A, the sigmoidal increase in ATPase activity was characterised by a potency for nicardipine of EC_{50} = 1.10 ± 0.41 µM with an associated 2.0 ± 0.3-fold stimulation of hydrolysis. For vinblastine, this was EC_{50}= 1.78 ± 0.22 µM (1.59 ± 0.14-fold stimulation) as shown in panel B. Rhodamine 123 and paclitaxel had potencies of 255 ± 56 µM (1.8 ± 0.2-fold stimulation), and 0.55 ± 0.09 µM (2.2 ± 0.3-fold stimulation), shown in panels C and D, respectively. These results fall within the range previously published [146, 184]

The dose-response analyses of each compound on ATP hydrolysis by the mutant P-gp T769C is shown in figure 19 (panels A-D). There was no significant difference in the observed potencies of vinblastine, rhodamine 123 and paclitaxel to stimulate ATP hydrolysis in T769C, compared to cys-less P-gp. However, the potency of nicardipine

to stimulate ATP hydrolysis in T769C was significantly reduced ($p<0.05$) to EC_{50} = 3.46 ± 0.97 µM (3.5 ± 0.4-fold stimulation).

Similar dose-response relationships were established in all other mutants for each of the four compounds and summarised in tables 3-6. The results from ATPase binding assays are comprehensively discussed in section 3.4.

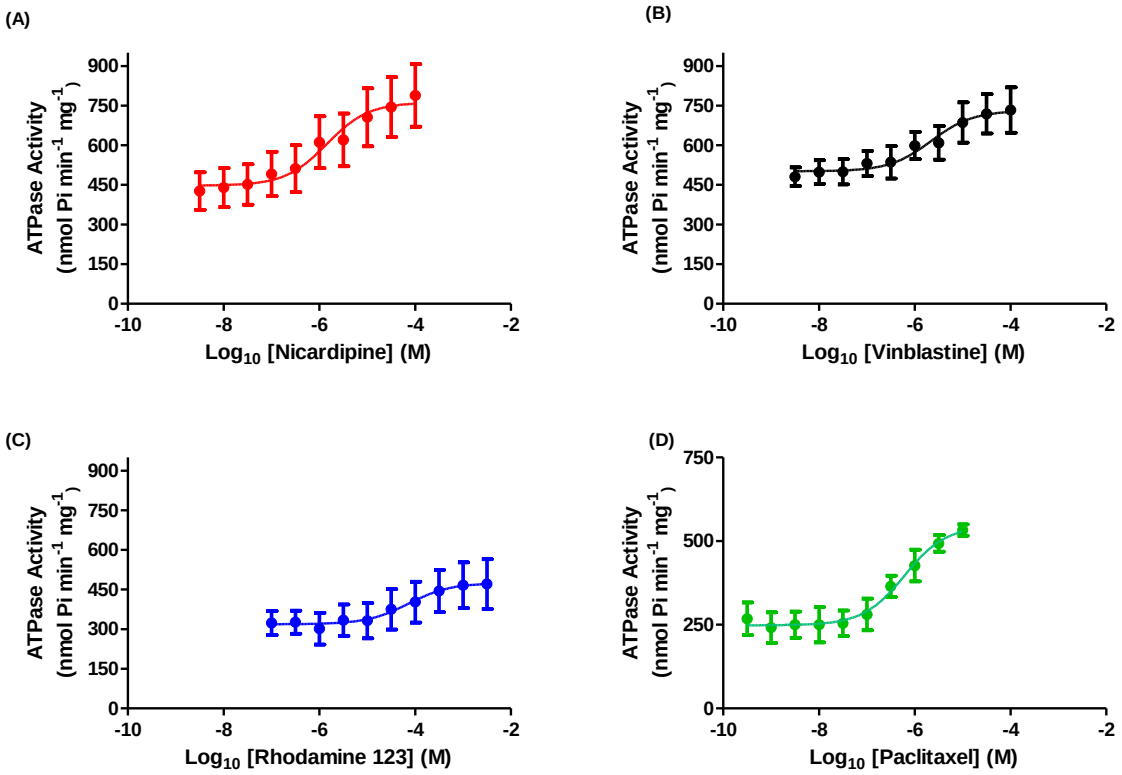

Figure 18: Drug stimulated ATPase activities of cys-less P-gp. Panels A-D show the dose response curves of **nicardipine**, **vinblastine**, **rhodamine 123**, and **paclitaxel**, respectively. The ATPase activities were measured using a colorimetric assay in the presence of a fixed ATP concentration (2mM) and varying concentrations of each drug. Data was fitted with a sigmoidal dose response curve using non-linear regression to obtain the effective concentration of drug required to stimulate 50% of maximal activity (potency or EC_{50}). Data presented was obtained from ≥4 independent purifications.

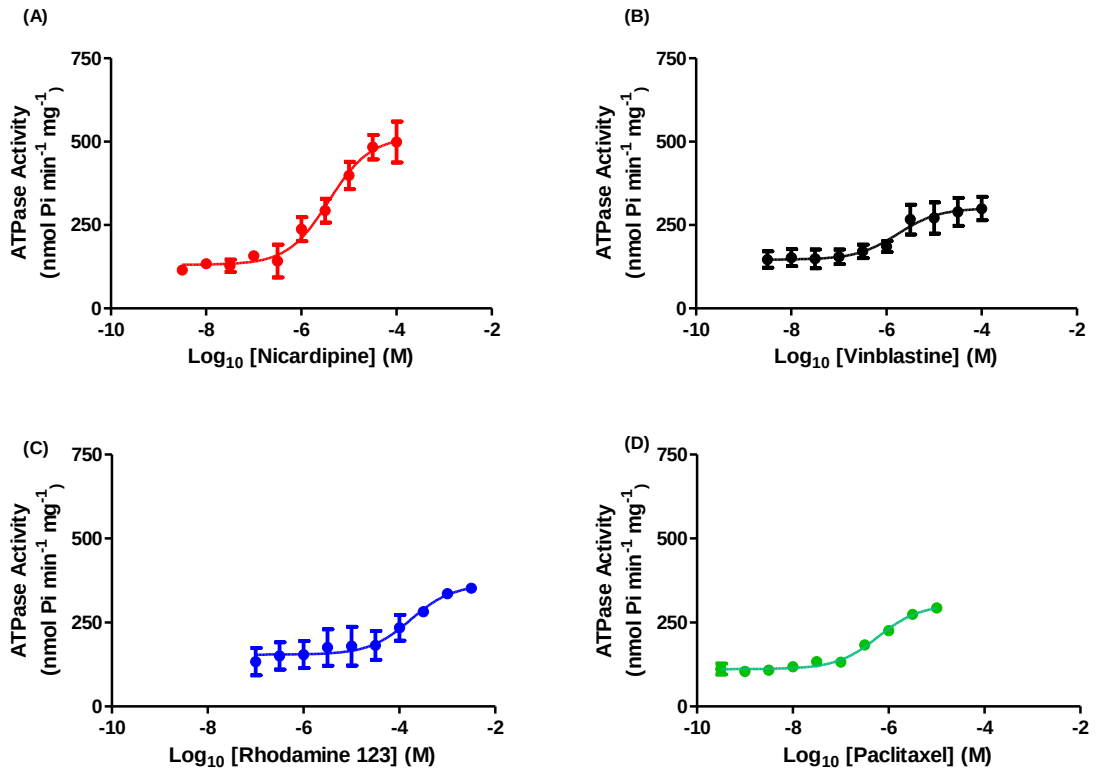

Figure 19: Drug stimulated ATPase activities of P-gp mutant T769C. Panels A-D show the dose response curves of **nicardipine**, **vinblastine**, **rhodamine 123**, and **paclitaxel**, respectively. The ATPase activities were measured using a colorimetric assay in the presence of a fixed ATP concentration (2nM) and varying concentrations of each drug. Data was fitted with a sigmoidal dose response curve using non-linear regression to obtain the effective concentration of drug required to stimulate 50% of maximal activity (potency or EC_{50}). Data presented was obtained from ≥4 independent purifications.

3.3.2 Measuring binding affinity (K_{App})

The fluorescence of the 11 intrinsic tryptophan residues in P-gp may be altered following the binding of substrates and modulators. Previous studies have used this assay to show that binding of drugs, nucleotides, hydrophobic peptides, and modulators of P-gp resulted in decreased intensity of the emission spectrum (i.e. quenching) in a saturable fashion, allowing estimations of dissociation constants [186]. This is likely a result of hydrophobic drugs undergoing π-π stacking with nearby tryptophan residues and thus interfering with the overall fluorescence emission spectrum. Alternatively, a change in the fluorescence spectrum can also

manifest as an alteration in wavelength, as drug binding to P-gp and the subsequent conformational change may alter the local environment of the tryptophan residue(s).

Prior to undertaking tryptophan fluorescence assays in P-gp, the fluorescence emission spectrum of 10µM of tryptophan was measured in the various buffer components and environments. Tryptophan has a wavelength of maximum absorption of 280nm and the emission peak ranges between 300-360nm depending on the polarity of the environment [173]. Figure 20 shows tryptophan in varying environments of increasing hydrophobicity from methanol, ethanol, to propanol. The dielectric constants of methanol: 33.3, ethanol: 25.1, and propanol: 20.1, have been established in 298 K, compared to water which has a dielectric constant of 80.2 [191]. The dielectric constant is an important physicochemical parameter as it is related to many important physical and biological applications. There is an associated shift in both the wavelength and the peak fluorescence emission intensity of the spectrum of tryptophan in increasingly hydrophobic environments. Tryptophan in all three hydrophobic solvents tested displayed wavelengths of <350nm compared to tryptophan in PBS only (>350nm). With increasing hydrophobicity (methanol < ethanol < propanol) there was an increase in the tryptophan fluorescence intensity, but the intensity of all three solvents was significantly reduced compared to PBS only (figure 20).

The presence of DDM did not interfere with the emission spectrum of tryptophan. In contrast, figure 21 shows that the fluorescence emission spectrum of tryptophan in the presence of imidazole (~330nm peak) differs from that in PBS (~357nm peak). The emission spectrum of imidazole strongly interferes with that of tryptophan. Tryptophan fluorescence assays were thus undertaken using purified reconstituted

P-gp following buffer exchange to remove the imidazole in the initial purification buffer (methods 2.2.9).

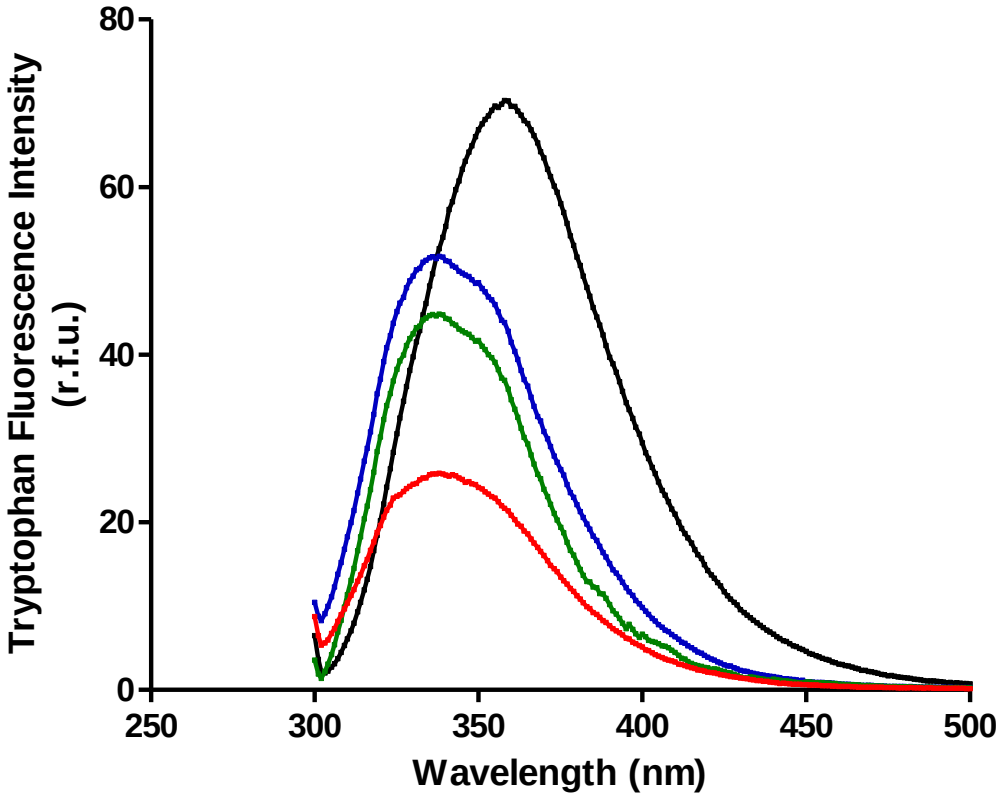

Figure 20: Fluorescence emission spectrum of tryptophan in various solvents. The fluorescence emission spectra (300-500nm) of 10µM L-tryptophan in **PBS**, and in increasingly hydrophobic solutions of **methanol**, **ethanol**, and **propanol**, was measured.

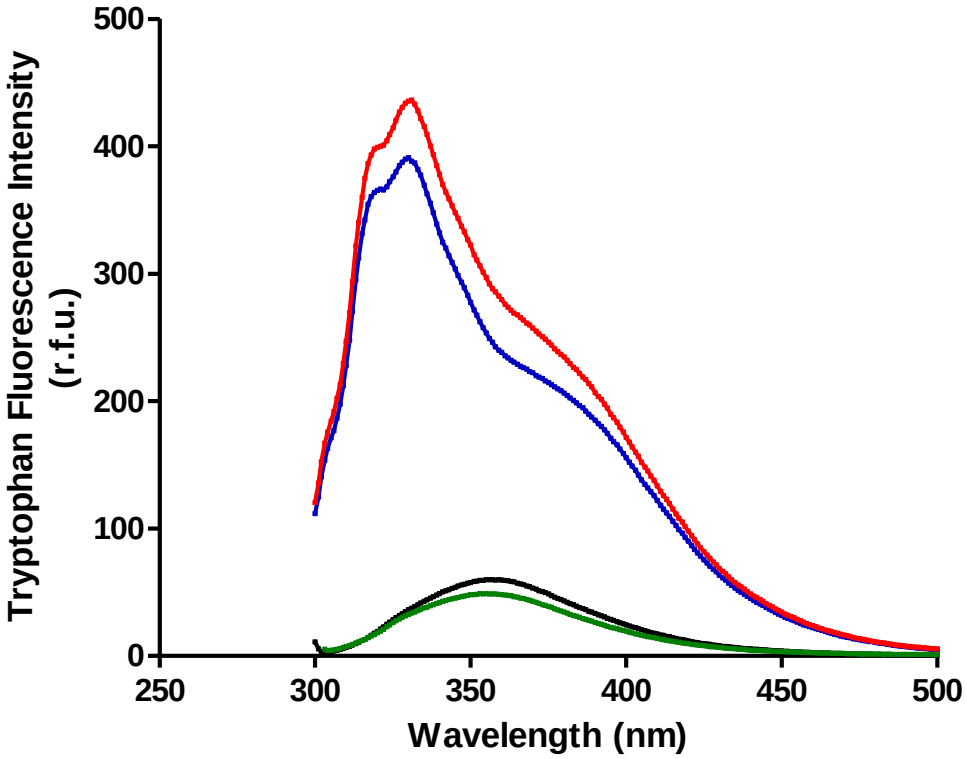

Figure 21: Tryptophan fluorescence emission spectra in various buffer components. The fluorescence emission spectra of 10µM L-tryptophan (**blue line**) was measured from λ_{em} 300-500nm. The individual spectra of various buffer components including PBS (**black line**), buffer supplemented with 2% DDM only (**green line**), and buffer supplemented with 100mM imidazole (**red line**) was also measured.

It was also essential to establish that none of the drugs could interfere with the intrinsic tryptophan fluorescence signal. Figure 22 shows the absorption spectrum of each compound over a wavelength scan range of 250 – 700nm and compared to tryptophan. The maximum absorption (λ_{max}) of nicardipine was 235nm. Vinblastine showed absorption maxima at 262, 284, and 290nm, and paclitaxel at a wavelength of 273nm. Rhodamine 123 had a pronounced maximum absorption at wavelength of 500nm, with a shoulder at approximately 475nm. The absorption maximum for tryptophan was 278nm therefore there was no overlap between the absorption

maxima (λ_{max}) of the four drugs and the tryptophan fluorescence emission λ_{max}. This indicates that no energy transfer between drug and tryptophan was possible.

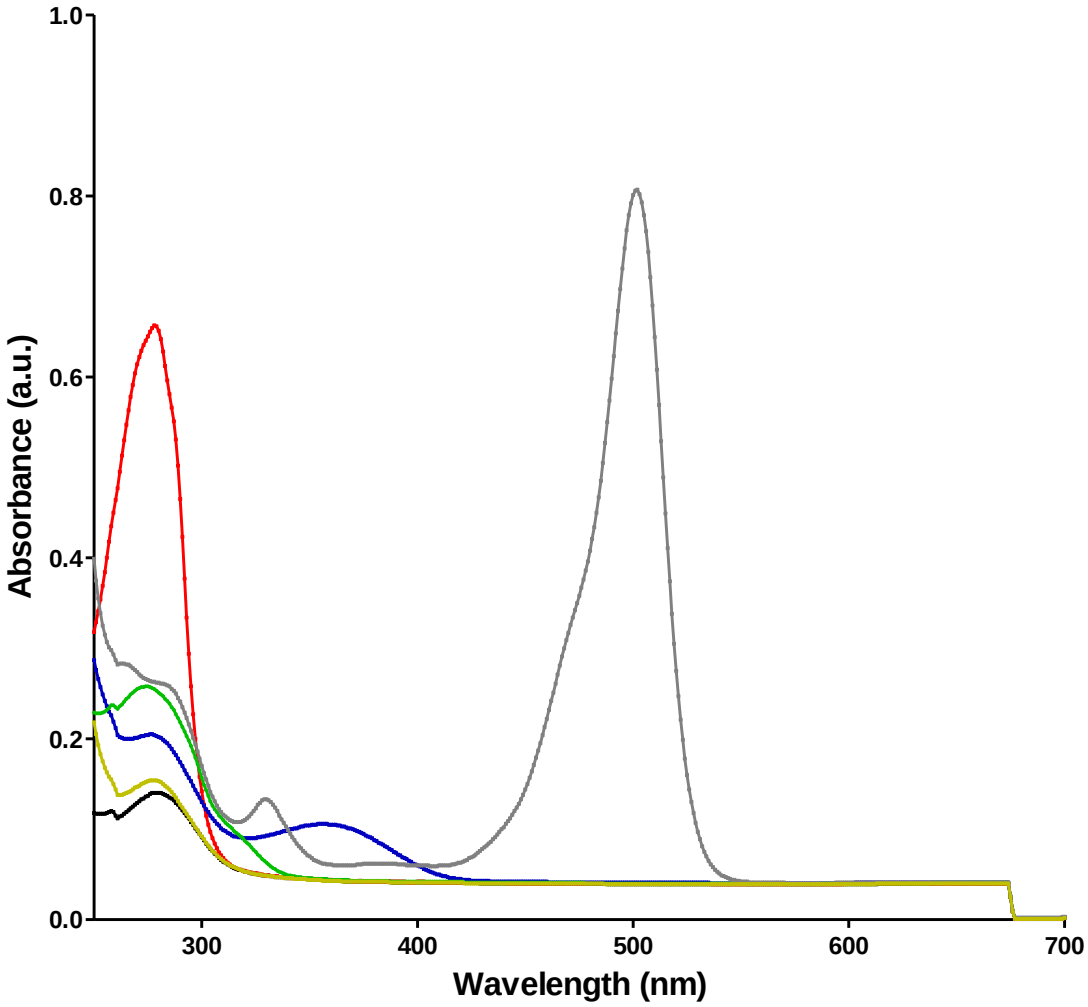

Figure 22: Wavelength scan of the different drug compounds used in the tryptophan fluorescence binding assay. The absorption spectra of **tryptophan**, **nicardipine**, **vinblastine**, **rhodamine 123**, and **paclitaxel** was measured. 10µM of all compounds was added to imidazole free purification buffer (absorption indicated by **black line**), and the absorption spectra measured over a range of 250-700nm.

Figures 23 (panel A) demonstrates the effect of nicardipine on the tryptophan fluorescence emission spectrum of cys-less P-gp. There was a dose-dependent reduction in the emission maximum intensity for tryptophan and indicates quenching of the fluorescence emission spectrum. Similar dose-dependent quenching of intensity was seen for both rhodamine 123 (figure 25, panel A), and paclitaxel (figure 26, panel A). However, the reduction in signal was to a less pronounced extent with sequential addition of paclitaxel. In contrast, addition of vinblastine (figure 24, panel A) caused a dose-dependent shift in the wavelength for maximal emission (λ_{max}), in addition to an associated increase in the intensity of the emission spectrum. In the case of all four compounds, the magnitude of the shift (I_{max} or λ_{max}) in response to increasing concentration of each drug was plotted to generate a one-site binding isotherm. No exogenous tryptophan was added to the drug samples when measuring emission quenching. Figure 23 (panel B) shows the hyperbolic binding isotherm for nicardipine interaction with cys-less P-gp, increasing to a B_{max} of 44 ± 4 (r.f.u.). This was defined by an apparent binding affinity of nicardipine for cys-less P-gp as K_{App} = 43 ± 4 µM. Similar binding isotherms were generated for vinblastine (figure 24, panel B), rhodamine 123 (figure 25, panel B), and paclitaxel (figure 26, panel B). The K_{App} for vinblastine was 6.8 ± 0.8 µM (B_{max} = 32.9 ± 4.2 r.f.u.), for rhodamine 123 it was 40 ± 3 µM (B_{max} = 30 ± 7 r.f.u.), and for paclitaxel K_{App} = 26 ± 6 µM (B_{max} = 6 ± 2 r.f.u.). Similar fluorescence emission spectra and binding isotherms were obtained for the interaction of each of the four compounds with the seven mutant P-gp isoforms and the data will be discussed later in conjunction with effects on ATPase activity (section 3.4; tables 3-4).

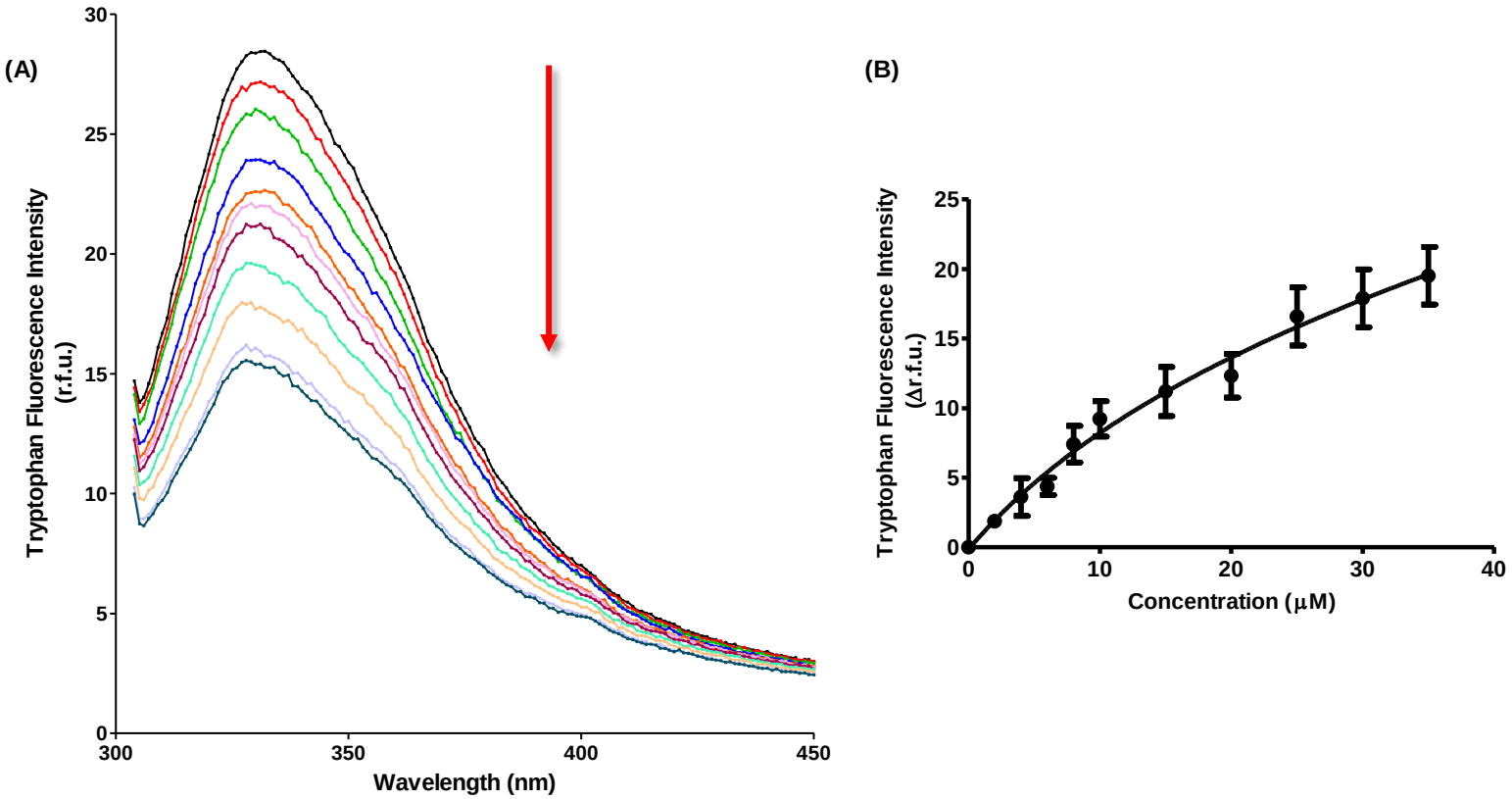

Figure 23: Binding of nicardipine to cys-less P-gp using tryptophan fluorescence assay. Panel A shows the fluorescence emission spectrum for cys-less P-gp (λ=305-450nm) in the absence (**black line**), and presence of increasing concentrations of nicardipine (**2**, **4**, **6**, **8**, **10**, **15**, **20**, **25**, **30**, **35**μM, in the direction of the red arrow). The change in fluorescence intensity (Δr.f.u.) was plotted as a hyperbolic binding isotherm (panel B), fitted using non-linear squares regression. Data represented was the mean ± SEM for 4 independent purifications.

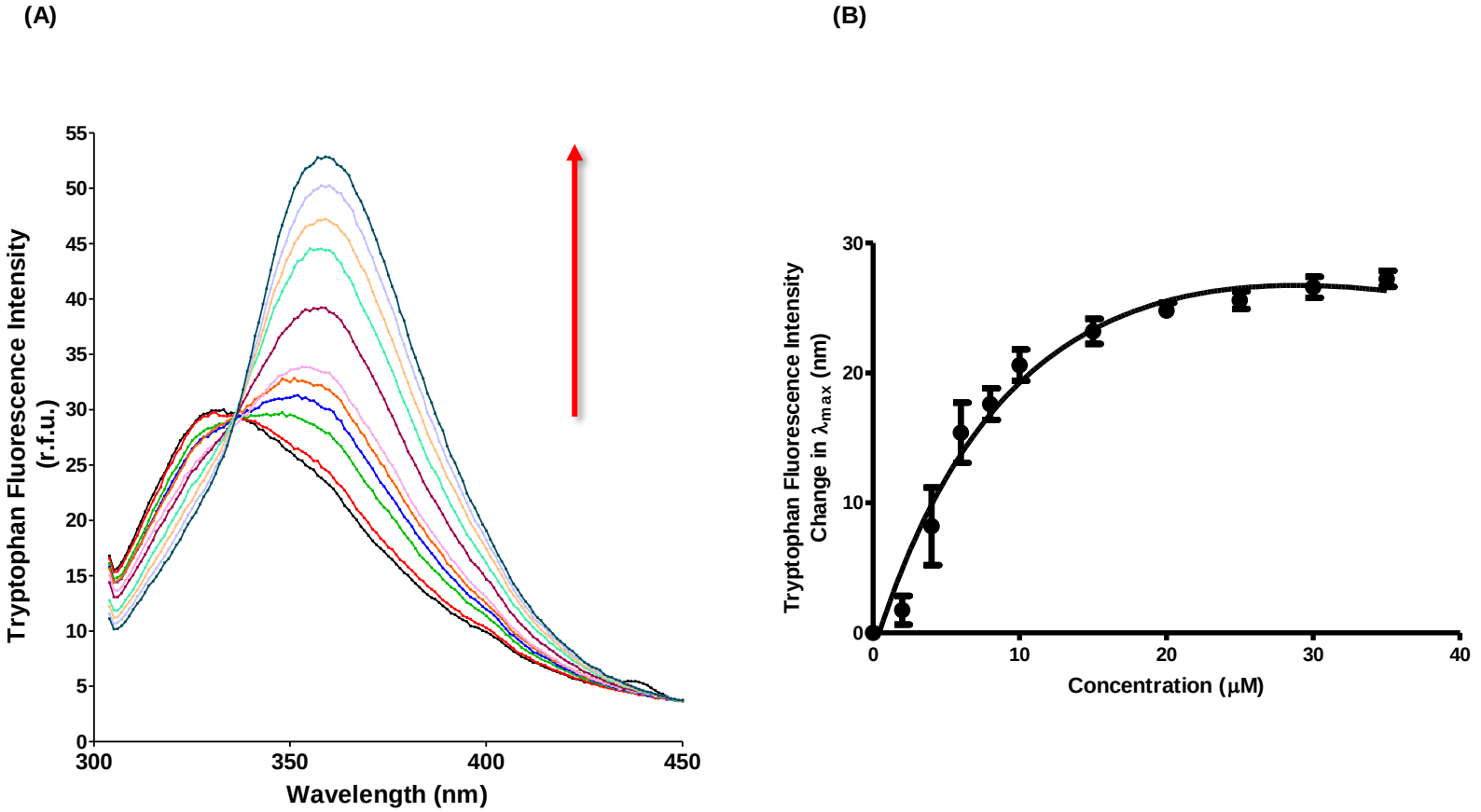

Figure 24: Binding of vinblastine to cys-less P-gp using tryptophan fluorescence assay. Panel A shows the fluorescence emission spectrum for cys-less P-gp (λ=305-450nm) in the absence (**black line**), and presence of increasing concentrations of vinblastine (**2**, **4**, **6**, **8**, **10**, **15**, **20**, **25**, **30**, **35**μM). The extent of shift in λ_{max} was plotted using a polynomial curve (panel B), fitted using non-linear squares regression. Data represented was the mean ± SEM for 5 independent purifications.

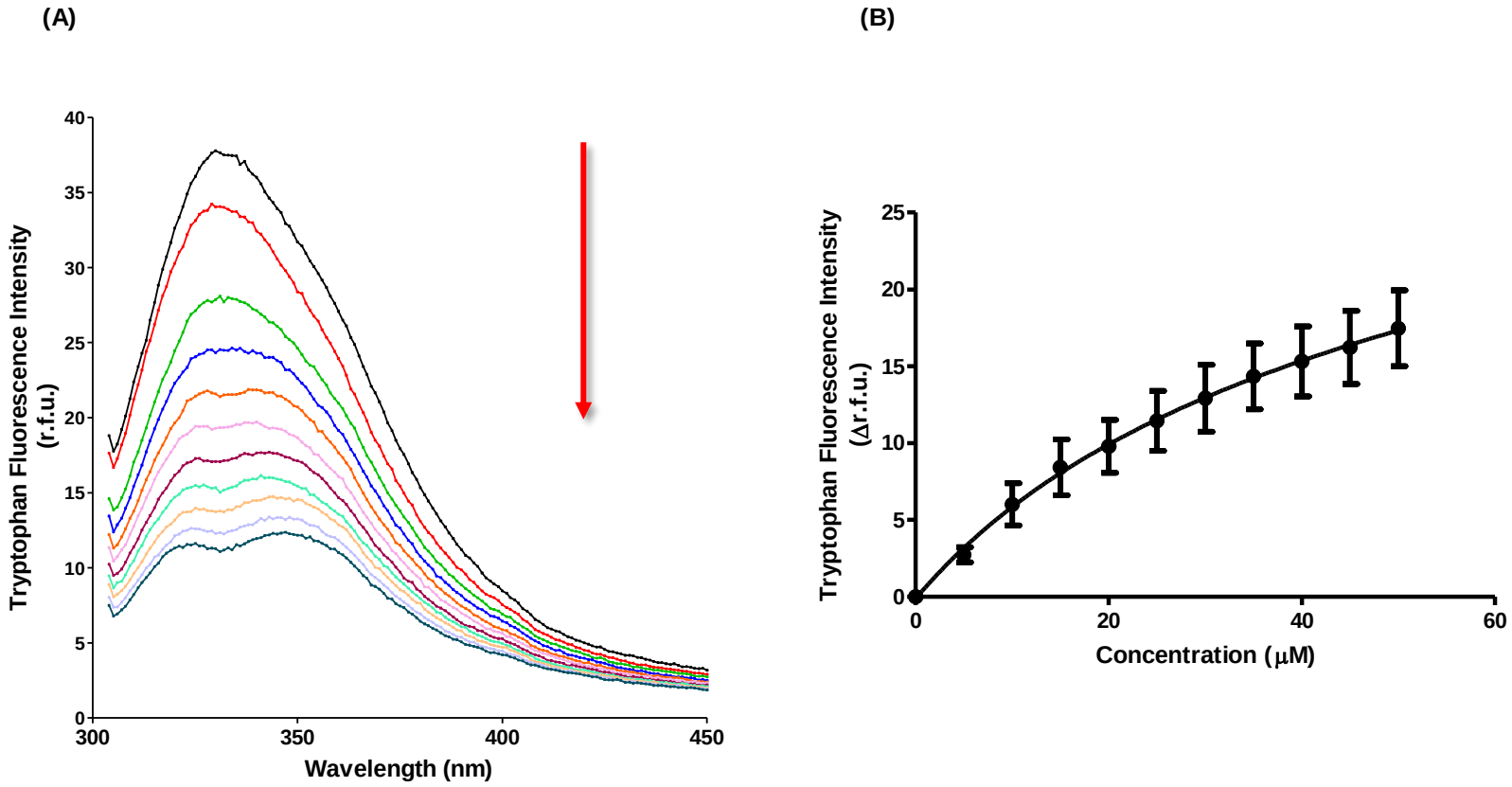

Figure 25: Binding of rhodamine 123 to cys-less P-gp using tryptophan fluorescence assay. Panel A shows the fluorescence emission spectrum for cys-less P-gp (λ=305-450nm) in the absence (**black line**), and presence of increasing concentrations of rhodamine 123 (**5**, **10**, **15**, **20**, 25, **30**, 35, 40, 45, **50**μM, in the direction of the red arrow). The change in fluorescence intensity (Δr.f.u.) was plotted as a hyperbolic binding isotherm (panel B), fitted using non-linear squares regression. Data represented was the mean ± SEM for 5 independent purifications.

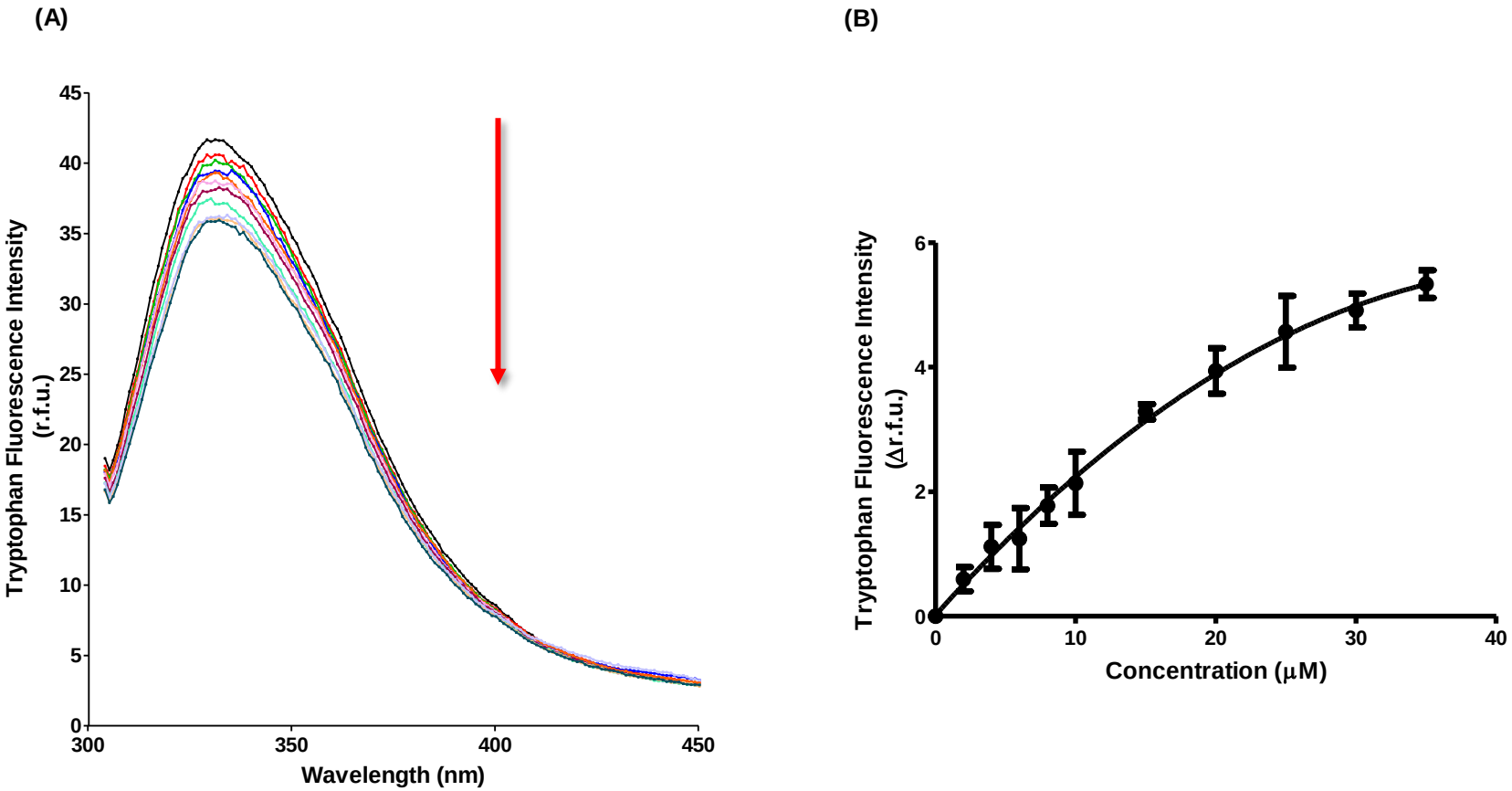

Figure 26: Binding of paclitaxel to cys-less P-gp using tryptophan fluorescence assay. Panel A shows the fluorescence emission spectrum for cys-less P-gp (λ=305-450nm) in the absence (**black line**), and presence of increasing concentrations of paclitaxel (**2**, **4**, **6**, **8**, **10**, **15**, **20**, **25**, **30**, **35**μM in the direction of the red arrow). The change in fluorescence intensity (Δr.f.u.) was plotted as a hyperbolic binding isotherm (panel B), fitted using non-linear squares regression. Data represented was the mean ± SEM for 3 independent purifications.

3.4 Identification of contact residues

Each P-gp mutant was assessed for the potency of nicardipine, vinblastine, rhodamine 123, and paclitaxel to stimulate ATP hydrolysis, compared to cys-less P-gp (section 3.3.1; figures 18 and 19). P-gp mutants that showed altered potency for any of the four compounds to stimulate ATP hydrolysis were further examined using the tryptophan fluorescence assay which allowed measurement of direct binding of drug to P-gp. Establishing a reduced potency to stimulate ATP hydrolysis alone was not indicative of the involvement of a residue in drug binding since it could be a result of impaired interdomain communication alone. To establish a contact residue for a compound, the mutations identified as resulting in reduced EC_{50} (potency to stimulate ATP hydrolysis) for a compound, would also result in an altered apparent binding affinity (K_{App}) of the compound to P-gp, as measured by the tryptophan fluorescence assay (section 3.3.2; figures 23-26). The binding isotherms generated from the latter were used to establish specific involvement of the residue in drug binding. Using two different functional assays to identify a mutated residue as a contact residue for a given drug was a key strategy in this project.

Tryptophan fluorescence assays to measure specific binding of the drug examined was also carried out in a P-gp mutant isoform that did not show an altered potency of the drug to stimulate ATP hydrolysis. This was done to establish the specificity of the tryptophan fluorescence assay in identifying contact residues, since theoretically, any P-gp mutant that did not show an altered potency to stimulate ATP hydrolysis, should also not show any alteration in the K_{App} for the drug being assessed. This validated that the change in ATPase activity was a direct result of altered interaction between P-gp and the drug. Any mutation that reduced the potency of any of the four ‘marker’ drugs to stimulate ATP hydrolysis and displayed a shift in the K_{App}, was deemed to

be directly involved in the binding of that drug and was designated as a contact residue. A mutation that reduced the potency of the drug to stimulate ATP hydrolysis but did not show an associated change in the K_{App} was considered important in inter-domain communication but not directly involved in drug binding.

The subsequent sections focus on identifying contact residues at each of the four pharmacologically distinct drug binding sites.

3.4.1 Contact residues involved in the binding of nicardipine

The potency of the P-gp modulator nicardipine to stimulate ATP hydrolysis was measured in all isoforms (table 3, p96). In cys-less P-gp, nicardipine stimulated ATP hydrolysis 2.0 ± 0.3-fold from the basal rate, with a potency of 1.10 ± 0.40 µM. The potency with which nicardipine stimulated ATP hydrolysis in the mutants L65C (3.53 ± 1.17 µM), M197C (2.37 ± 0.89 µM), F336C (1.55 ± 0.37 µM), and V982C (1.57 ± 0.63 µM) was not significantly different to that in cys-less P-gp. Mutations at these residues did not affect the binding of P-gp to nicardipine.

Three mutants did show significantly ($p<0.05$) altered potencies for nicardipine compared to cys-less P-gp. The mutants A311C and T769C showed a reduction in nicardipine potency to stimulate ATP hydrolysis by approximately three-fold at EC_{50} = 3.19 ± 0.98 µM and EC_{50} = 3.46 ± 0.97 µM, respectively. The greatest reduction was observed in the mutant F978C, where the potency for nicardipine to stimulate ATP hydrolysis was reduced to 19.5 ± 6.20 µM. Despite the differences in potencies, none of the seven mutations affected the extent of stimulation from the basal rate (1.7 – 3.5-fold) following addition of nicardipine (table 3, p96).

For the three mutants that showed altered potencies, the tryptophan fluorescence assay was undertaken to determine whether the change in potency for nicardipine to

stimulate ATP hydrolysis in A311C, T769C, and F978C, was a result of impaired binding or defective inter-domain coupling. The apparent binding affinity of nicardipine in cys-less P-gp was established as K_{App} = 43 ± 4 µM at a capacity of B_{max} = 44 ± 4 r.f.u. All three P-gp mutants showed significantly different (*p<0.05*) binding affinities for nicardipine. For mutants A311C (K_{App} = 23 ± 1 µM) and F978C (K_{App} = 24 ± 3 µM), the K_{App} was reduced, which indicated increased apparent affinity for nicardipine binding to the P-gp protein. This may suggest that the residue positions are involved in binding but the mutation to cysteine impacts the affinity alternatively. This surprising finding may have resulted from the mutation affecting conformational changes in the TMDs associated with nicardipine interaction, thus altering the tryptophan fluorescence spectrum.

In contrast, the P-gp mutant T769C had a K_{App} value for nicardipine binding that was beyond the range of concentration used in the tryptophan fluorescence assay. In fact, it was not possible to reach higher concentrations due to solubility issues with nicardipine. Thus, it was not possible to accurately assign the K_{App} and B_{max} values for nicardipine in T769C, and the K_{App} was assigned a value of >100µM. Threonine 769 of P-gp was established as a contact residue for nicardipine since the mutation at this residue significantly impaired the binding of nicardipine with P-gp. T769 likely resides within the nicardipine binding site.

Table 3: Summary of the effects of cysteine mutations on the interaction of P-gp with nicardipine. Dose response relationships of ATP hydrolysis as a function of nicardipine concentration was generated for each of the P-gp mutant isoforms and the cys-less P-gp control protein using a colorimetric assay (refer to methods section). The potency to stimulate ATP hydrolysis (EC_{50}), and the degree of stimulation (fold-stimulation) was determined from non-linear regression of the general dose-response relationship. The tryptophan fluorescence assay was used to measure direct binding of nicardipine to specific P-gp mutants. The change in fluorescence at each concentration

of nicardipine was used to generate a binding isotherm and non-linear regression used to determine the two parameters, K_{App} (apparent binding affinity) and B_{max} (capacity of binding).

A statistically significant difference is indicated by ***** (*p<0.05*); a value of >100μM indicates a binding affinity beyond the range of drug concentrations used, thus making accurate assignment of parameters impossible; 'n.d.' refers to not determined. Data is the mean ± SEM from ≥4 independent purifications with individual values shown in parentheses next to each mutant.

P-gp mutant	**ATP Hydrolysis**		**Tryptophan Fluorescence**	
	Potency (μM)	**Fold Stimulation**	**K_{App} (μM)**	**B_{max} (Δr.f.u.)**
Cys-less (10)	1.10 ± 0.40	2.0 ± 0.3	43 ± 4	44 ± 4
L65C (4)	3.53 ± 1.17	1.7 ± 0.1	n.d.	n.d.
M197C (4)	2.37 ± 0.89	2.3 ± 0.4	n.d.	n.d.
A311C (8)	**3.19 ± 0.98***	2.6 ± 0.3	**23 ± 1***	29 ± 5
F336C (4)	1.55 ± 0.37	2.2± 0.3	n.d.	n.d.
T769C (6)	**3.46 ± 0.97***	3.5 ± 0.4	**n.d.**	n.d.
F978C (7)	**19.5 ± 6.20***	2.3 ± 0.3	**24 ± 3***	26 ± 4
V982C (4)	1.57 ± 0.63	3.4 ± 0.5	n.d.	n.d.

3.4.2 Contact residues involved in the binding of vinblastine

The potency of vinblastine to stimulate ATP hydrolysis in cys-less P-gp was EC_{50} = 1.78 ± 0.22 µM, with a fold-stimulation of 1.59 ± 0.14. All seven mutants displayed similar extents of ATP hydrolysis stimulation by vinblastine, ranging from 1.2 – 3.3-fold increases in the basal activity (table 4, p99).

The potency to stimulate ATP hydrolysis was similar for five of the mutants compared to cys-less P-gp; namely L65C (1.37 ± 0.70 µM), A311C (3.34 ± 1.02 µM), F336C (3.17 ± 0.47 µM), T769C (1.24 ± 0.39 µM), and V982C (2.34 ± 0.91 µM). Therefore, these residues were not considered to be involved in the binding of vinblastine. This was confirmed for L65C, F336C, and V982C, by the tryptophan fluorescence assay. The apparent binding affinities (K_{App}) for L65C, F336C, and V982C, were 6.0 ± 0.5 µM, 11.7 ± 1.3 µM, and 7.2 ± 2.5 µM, respectively, which was not significantly different to that of cys-less P-gp (K_{App} = 6.8 ± 0.8 µM; B_{max} = 32.9 ± 4.2 r.f.u.).

However, two of the mutants, M197C and F978C, did show significantly different (*p<0.05*) potencies for vinblastine to stimulate ATP hydrolysis. Vinblastine potency in the mutant M197C was 6.56 ± 1.67 µM, an approximately four-fold decrease compared to cys-less P-gp. F978C showed a greater reduction in potency with an EC_{50} = 9.16 ± 1.79 µM. Thus, mutations at both these residues did alter the interaction of vinblastine with P-gp, however whether this was a result of defective binding or impaired inter-domain communication was addressed with the tryptophan fluorescence assay.

The apparent binding affinity of vinblastine in the mutant M197C was significantly reduced (*p<0.05*) to a K_{App} of 21.4 ± 5.4 µM with no effect on the binding capacity (B_{max} = 33.4 ± 8.7). Thus, methionine 197 in P-gp is involved in directly binding

vinblastine, and mutating this residue resulted in a significantly reduced potency of vinblastine to stimulate ATP hydrolysis, as well as an associated reduction in the binding affinity for vinblastine.

There was no associated change in the tryptophan fluorescence spectrum of F978C. The binding affinity of vinblastine was not significantly altered (K_{App} = 7.2 ± 2.5 µM) in the mutant F978C. Despite the significantly reduced potency of vinblastine to stimulate ATP hydrolysis in, F978C was not involved in direct binding of vinblastine as the binding affinity was unchanged. F978C instead impaired the communication between the vinblastine binding site in the TMD, and the NBDs, affecting ATP hydrolysis.

Using the two different functional assays allowed for the establishment of M197 as being either in, or proximal to, the vinblastine binding site. F978 however, does not lie within the vinblastine binding site in P-gp.

Table 4: Summary of the effects of cysteine mutations on the interaction of P-gp with vinblastine. Dose response relationships of ATP hydrolysis as a function of vinblastine concentration was generated for each of the P-gp mutant isoforms and the cys-less P-gp control protein using a colorimetric assay (refer to methods section). The potency to stimulate ATP hydrolysis (EC_{50}), and the degree of stimulation (fold-stimulation) was determined from non-linear regression of the general dose-response relationship. The tryptophan fluorescence assay was used to measure direct binding of vinblastine to specific P-gp mutants. The change in fluorescence at each concentration of vinblastine was used to generate a binding isotherm and non-linear regression used to determine the two parameters, K_{App} (apparent binding affinity) and B_{max} (capacity of binding).

A statistically significant difference is indicated by ***** (*p<0.05*); 'n.d.' refers to not determined. Data is the mean ± SEM from ≥4 independent purifications with individual values shown in parentheses next to each mutant.

P-gp mutant	ATP Hydrolysis		Tryptophan Fluorescence	
	Potency (μM)	**Fold Stimulation**	**K_{App} (μM)**	**B_{max} ($\Delta\lambda_{em}$)**
Cys-less (8)	1.78 ± 0.22	1.6 ± 0.1	6.8 ± 0.8	32.9 ± 4.2
L65C (6)	1.37 ± 0.70	1.3 ± 0.1	6.0 ± 0.5	29.3 ± 0.7
M197C (6)	**6.56 ± 1.67***	2.1 ± 0.6	**21.4 ± 5.4***	33.4 ± 8.7
A311C (4)	3.34 ± 1.02	1.7 ± 0.1	n.d.	n.d.
F336C (6)	3.17 ± 0.47	1.7 ± 0.2	11.7 ± 1.3	22.3 ± 0.4
T769C (4)	1.24 ± 0.39	3.3 ± 0.7	n.d.	n.d.
F978C (6)	**9.16 ± 1.79***	2.9 ± 1.5	9.2 ± 1.5	24 ± 1.0
V982C (6)	2.34 ± 0.91	1.2 ± 0.1	7.2 ± 2.5	40 ± 4.8

3.4.3 Contact residues involved in the binding of rhodamine 123

Rhodamine 123 is a fluorescent dye that is known to be transported by P-gp. Of the four compounds tested, rhodamine 123 had the lowest potency to stimulate ATP hydrolysis in cys-less P-gp with an EC_{50} of 255 ± 56 μM and a 1.8 ± 0.2-fold increase in basal activity (table 5, p102).

The P-gp mutants L65C, F336C, and V982C, showed altered potencies for rhodamine 123 to stimulate ATP hydrolysis. Residue L65C displayed a significantly reduced ($p<0.05$) potency of rhodamine 123 to stimulate ATP hydrolysis EC_{50} = 691 ± 132 μM. The apparent binding affinity was also significantly reduced approximately 2-fold to K_{App} = 89 ± 25 μM, compared to cys-less P-gp control (K_{App} = 40 ± 3 μM).

Similarly, mutating residue V982 to a cysteine also resulted in both a significantly reduced potency of rhodamine 123 to stimulate ATP hydrolysis (EC_{50} = 1181 ± 357 µM), as well as a significant reduction in the apparent binding affinity to P-gp (K_{App} = 73 ± 13 µM). Both residues L65C and V982C were therefore identified as contact residues for rhodamine 123 binding.

In contrast, F336C showed a significantly increased (*p<0.05*) potency for rhodamine 123 to stimulate ATP hydrolysis, with an EC_{50} = 68 ± 8 µM compared to cys-less (EC_{50} = 255 ± 56 µM). Despite this apparent improvement in the potency to stimulate ATP hydrolysis, the tryptophan fluorescence assay resulted in an inconclusive binding isotherm, making it impossible to determine an accurate binding affinity or KApp value. Using any higher concentration of rhodamine 123 resulted in the drug precipitating in solution and F336C was assigned a K_{App} value >100µM. Therefore, F336 significantly reduced the affinity of rhodamine 123 to bind to P-gp and was thus assigned as a contact residue. The observed increased potency to stimulate ATP hydrolysis may occur by the residue mutation enhancing the coupling process to the NBDs.

As observed for nicardipine and vinblastine, the mutant F978C showed a significantly altered potency for rhodamine 123 to stimulate ATP hydrolysis. Rhodamine 123 failed to elicit any stimulation of ATP hydrolysis in F978C P-gp (table 5, p102). This may suggest that the mutation in residue F978 prevented the binding of rhodamine 123 to P-gp altogether. However, although the binding was significantly reduced as shown by the tryptophan fluorescence assay (K_{App} is >100µM), it was not abrogated. This would suggest that F978 is not only involved in the binding of rhodamine 123, but also in facilitating communication between the TMDs and the NBDs.

The combination of the two assays allowed successful distinction between the two contact residues that were also important in inter-domain coupling (F336 and F978), and the two that were only important in the binding of rhodamine 123 (L65 and V982).

L65C, F336C, F978C, and V982C, are all defined as contact residues for rhodamine 123 and likely reside within its binding site on P-gp. Mutating any of these residues resulted in reduced potencies to stimulate ATP hydrolysis, or a reduced affinity for rhodamine 123 binding, or both. The tryptophan fluorescence assays were also undertaken on three further mutants; M197C, A311C, and T769C. None of the mutations altered the potencies for rhodamine 123 to stimulate ATP hydrolysis or their binding affinities compared to cys-less P-gp (table 5, p102). Similarly, the extent of the ATPase activity stimulation was not significantly different in any of the seven mutants.

Table 5: Summary of the effects of cysteine mutations on the interaction of P-gp with rhodamine 123. Dose response relationships of ATP hydrolysis as a function of rhodamine 123 concentration was generated for each of the P-gp mutant isoforms and the cys-less P-gp control protein using a colorimetric assay (refer to methods section). The potency to stimulate ATP hydrolysis (EC_{50}), and the degree of stimulation (fold-stimulation) was determined from non-linear regression of the general dose-response relationship. The tryptophan fluorescence assay was used to measure direct binding of rhodamine 123 to specific P-gp mutants. The change in fluorescence at each concentration of rhodamine 123 was used to generate a binding isotherm and non-linear regression used to determine the two parameters, K_{App} (apparent binding affinity) and B_{max} (capacity of binding).

A statistically significant difference is indicated by ***** (*p<0.05*); a value of >100μM indicates a binding affinity beyond the range of drug concentrations used, thus making accurate assignment of parameters impossible; 'n.d.' refers to not determined. Data is the mean ± SEM from ≥4 independent purifications with individual values shown in parentheses next to each mutant.

P-gp mutant	**ATP Hydrolysis**		**Tryptophan Fluorescence**	
	Potency (μM)	**Fold Stimulation**	**K_D (μM)**	**B_{max} (Δr.f.u.)**
Cys-less (13)	255 ± 56	1.8 ± 0.2	40 ± 3	30 ± 7
L65C (8)	**691 ± 132***	1.3 ± 0.04	**89 ± 25***	39 ± 3
M197C (6)	167 ± 9	2.0 ± 0.4	36 ± 5	20 ± 6
A311C (8)	228 ± 82	1.5 ± 0.01	40 ± 3	22 ± 3
F336C (5)	**68 ± 8***	1.7 ± 0.1	**>100**	n.d.
T769C (6)	499 ± 99	2.3 ± 0.6	48 ± 5	17 ± 2
F978C (4)	**No Response**	No Response	**>100**	n.d.
V982C (6)	**1181 ± 357***	1.8 ± 0.2	**73 ± 13***	36 ± 4

3.4.4 Contact residues involved in the binding of paclitaxel

Paclitaxel is an anti-cancer agent widely used in the treatment of breast, lung, and ovarian cancers, among others. It is also a known substrate of P-gp. In cys-less P-gp, paclitaxel stimulated ATP hydrolysis by 2.2 ± 0.3-fold, with the greatest potency of EC_{50} = 0.55 ± 0.09 μM, amongst the four drugs tested. All seven mutants had a

similar degree of stimulation of ATP hydrolysis to cys-less P-gp, ranging from 1.7 – 2.9-fold increase in basal activity. The binding affinity of paclitaxel in cys-less P-gp was K_{App} = 26 ± 6 µM (table 6, p105).

Of the seven mutants, only two, A311C and F987C, resulted in a significant (*p<0.05*) reduction in the potency of paclitaxel to stimulate ATP hydrolysis. In A311C, the potency was reduced over 5-fold to EC_{50} = 2.89 ± 1.40 µM. A311C showed an associated change in the fluorescence emission spectrum, translating to a significantly reduced (*p<0.05*) affinity for binding paclitaxel (K_{App} = 56 ± 10 µM), compared to cys-less P-gp (K_{App} = 26 ± 6 µM). Therefore, mutating alanine 311 to a cysteine directly affected the binding of paclitaxel to P-gp, and it was assigned as a contact residue, residing within or proximal to the paclitaxel binding site.

Mutation of residue F978 to cysteine resulted in an approximately 8-fold decrease in potency of paclitaxel to stimulate ATP hydrolysis with an EC_{50} of 4.34 ± 1.10 µM. Despite the change in potency, F978C did not show a significantly reduced binding affinity for paclitaxel to F987C P-gp (K_{App} = 22 ± 2 µM), compared to cys-less P-gp. Therefore, similar to the observed interaction of vinblastine and nicardipine with F978C P-gp, the mutation in this residue did not alter the binding of paclitaxel to P-gp. The decrease in potency to stimulate ATP hydrolysis further supports the involvement of residue 978 in TM12 of P-gp in the facilitation of inter-domain coupling.

The other mutants, L65C (EC_{50} = 1.16 ± 0.38), M197C (EC_{50} = 0.49 ± 0.17), F336C (EC_{50} = 0.54 ± 0.10), T769C (EC_{50} = 0.56 ± 0.11), and V982C (EC_{50} = 0.71 ± 0.22), did not result in any perturbation in the interaction between P-gp and paclitaxel and showed no significant difference in potency to stimulate hydrolysis compared to cys-

less P-gp (EC_{50} = 0.55 ± 0.09). In addition, the affinity with which mutants L65C and M197C bound paclitaxel was also measured, and the K_{App} values were 21 ± 10 and 15 ± 10 µM, respectively, further supporting no involvement in paclitaxel binding (table 6, p105). Residue A311C was the only contact residue assigned for paclitaxel binding.

3.5 Summary of Results

Table 7 summarises the results of the two assays used to identify the contact residues for each of the four compounds. For nicardipine, T769C was assigned as a contact residue as it resulted in both a decrease in potency to stimulate ATP hydrolysis, and it shifted the K_{App} for binding nicardipine to a lower affinity. Though nicardipine showed a decreased potency to stimulate ATP hydrolysis in both A311C and F978C, neither mutant was associated with a decrease in the binding affinity for nicardipine.

Rhodamine 123 was assigned the greatest number of contact residues including L65C, F336C, F978C, and V982C, as all four showed a decrease in the affinity with which they bound the drug. Altered interaction of P-gp with vinblastine and paclitaxel were associated with mutations M197C and A311C, respectively. In both cases, the potency with which the drug stimulated ATP hydrolysis, and the binding affinity were reduced.

F978C resulted in a decrease in potency for nicardipine, vinblastine, and paclitaxel to stimulate ATP hydrolysis. However, there was no associated decrease in the apparent binding affinities compared to cys-less P-gp, thus it was not assigned as a contact residue for any of these drugs.

Table 6: Summary of the effects of cysteine mutations on the interaction of P-gp with paclitaxel. Dose response relationships of ATP hydrolysis as a function of paclitaxel concentration was generated for each of the P-gp mutant isoforms and the cys-less P-gp control protein using a colorimetric assay (refer to methods section). The potency to stimulate ATP hydrolysis (EC_{50}), and the degree of stimulation (fold-stimulation) was determined from non-linear regression of the general dose-response relationship. The tryptophan fluorescence assay was used to measure direct binding of paclitaxel to specific P-gp mutants. The change in fluorescence at each concentration of paclitaxel was used to generate a binding isotherm and non-linear regression used to determine the two parameters, K_{App} (apparent binding affinity) and B_{max} (capacity of binding).

A statistically significant difference is indicated by ***** (*p<0.05*); 'n.d.' refers to not determined. Data is the mean ± SEM from ≥3 independent purifications with individual values shown in parentheses next to each mutant.

P-gp mutant	**ATP Hydrolysis**		**Tryptophan Fluorescence**	
	Potency (μM)	**Fold Stimulation**	**K_D (μM)**	**B_{max} (Δr.f.u.)**
Cys-less (6)	0.55 ± 0.09	2.2 ± 0.3	26 ± 6	6 ± 2
L65C (7)	1.16 ± 0.38	1.9 ± 0.2	21 ± 10	4 ± 1
M197C (10)	0.49 ± 0.17	1.7 ± 0.1	15 ± 10	5 ± 1
A311C (7)	**2.89 ± 1.40***	1.8 ± 0.2	**56 ± 10***	9 ± 2
F336C (3)	0.54 ± 0.10	1.9 ± 0.1	n.d.	n.d.
T769C (3)	0.56 ± 0.11	2.6 ± 0.1	n.d.	n.d.
F978C (7)	**4.34 ± 1.10***	2.9 ± 0.9	22 ± 2	5 ± 0.2
V982C (3)	0.71 ± 0.22	2.5 ± 0.1	n.d.	n.d.

Table 7: Summary of the effects of TMD mutations on the interaction of P-gp with the four compounds. The effects of each mutation on the EC_{50} (potency) and K_{App} (binding affinity) of nicardipine, vinblastine, rhodamine 123, and paclitaxel, are shown as either no change (↔), a decrease (↓), or an increase (↑). Values not determined are left blank and identified contact residues are shown as a **green tick** (√).

P-gp mutant	NICARDIPINE			VINBLASTINE			RHODAMINE 123			PACLITAXEL		
	EC_{50}	K_{App}	Contact residue	EC_{50}	K_{App}	Contact residue	EC_{50}	K_{App}	Contact residue	EC_{50}	K_{App}	Contact residue
L65C	↔		✗	↔	↔	✗	↓	↓	√	↔	↔	✗
M197C	↔		✗	↓	↓	√	↔	↔	✗	↔	↔	✗
A311C	↓	↑	✗	↔		✗	↔	↔	✗	↓	↓	√
F336C	↔		✗	↔	↔	✗	↑	↓	√	↔		✗
T769C	↓	↓	√	↔		✗	↔	↔	✗	↔		✗
F978C	↓	↑	✗	↓	↔	✗	↓	↓	√	↓	↔	✗
V982C	↔		✗	↔	↔	✗	↓	↓	√	↔		✗

Chapter 4:
DISCUSSION

4.1 Findings of current investigation

P-glycoprotein (P-gp) is the most characterised MDR transporter and recognises more than 300 structurally and chemically distinct compounds [62]. Amongst these compounds are hundreds of conventional cytotoxic drugs which cause cell death by interfering with the integrity of DNA replication in rapidly dividing cancer cells. Many tumour types overexpress P-gp [18, 24, 192], which extrudes these chemotherapeutic agents and prevents them from reaching their cellular targets. Many of the newer therapies, including those that specifically target key molecular pathways in cancer cells, are also substrates of P-gp [193]. Therefore, P-gp has remained a viable target for the treatment of cancer since the discovery of its role in MDR five decades ago.

Studies have identified several contact residues in P-gp implicated in drug binding and supported the existence of at least four pharmacologically distinct drug binding sites (DBSs) [50, 131, 194-196]. However, until now, their spatial separation remained unclear. The present investigation employed cysteine mutagenesis to identify several contact residues implicated in the binding of drugs at each of these four pharmacologically distinct binding sites. For the first time, the present investigation was able to show that the binding sites were also spatially distinct and are connected through a single translocation pathway in the central cavity. Several mutagenesis and structural studies have identified that various drugs bind within the large (~6000Å) central cavity of the TMD [50, 131, 194], and that it is accessible to the aqueous environment [197].

However, the present investigation provides evidence that three of the four identified DBSs lie outside the central cavity. Biochemical assays identified contact residues for rhodamine 123 (L65, F336, F978, and V982), nicardipine (T769), paclitaxel (A311), and vinblastine (M197), as spatially distinct to one another. Only one of the three drugs, rhodamine 123, bound within the central cavity close to the apex. The other three drugs, vinblastine, paclitaxel and nicardipine, had contact residues located in the outside of the central cavity. The binding sites for nicardipine and vinblastine were located at the protein-lipid interface. The binding site for paclitaxel was located close to the central cavity but embedded within the TMD. These contact residues and their locations are identified in figure 28, a homology model of P-gp (PDB: 4M1M) based on the crystal structure of mouse P-gp in a nucleotide free stage [50]. Additionally, we hypothesise that as the catalytic cycle progresses, P-gp undergoes conformational changes that allows drugs to be ‘relocated’ from the lipid-protein interface to the central cavity, allowing it to transition into the translocation pore.

4.2 Experimental approach of current investigation

A cysteine-scanning mutagenesis approach was used in identifying potential contact residues based on existing pharmacological and structural data obtained from the 3.8Å crystal structure of murine P-gp in a nucleotide free state [50, 157]. Though there exist many three-dimensional structures of P-gp in different conformations across different organisms [52, 58, 198-200], murine P-gp is considered ideal for homology modelling due to its 87% sequence identity with human P-gp, and 100% sequence identify of the residues lining the drug binding cavity with human P-gp [201].

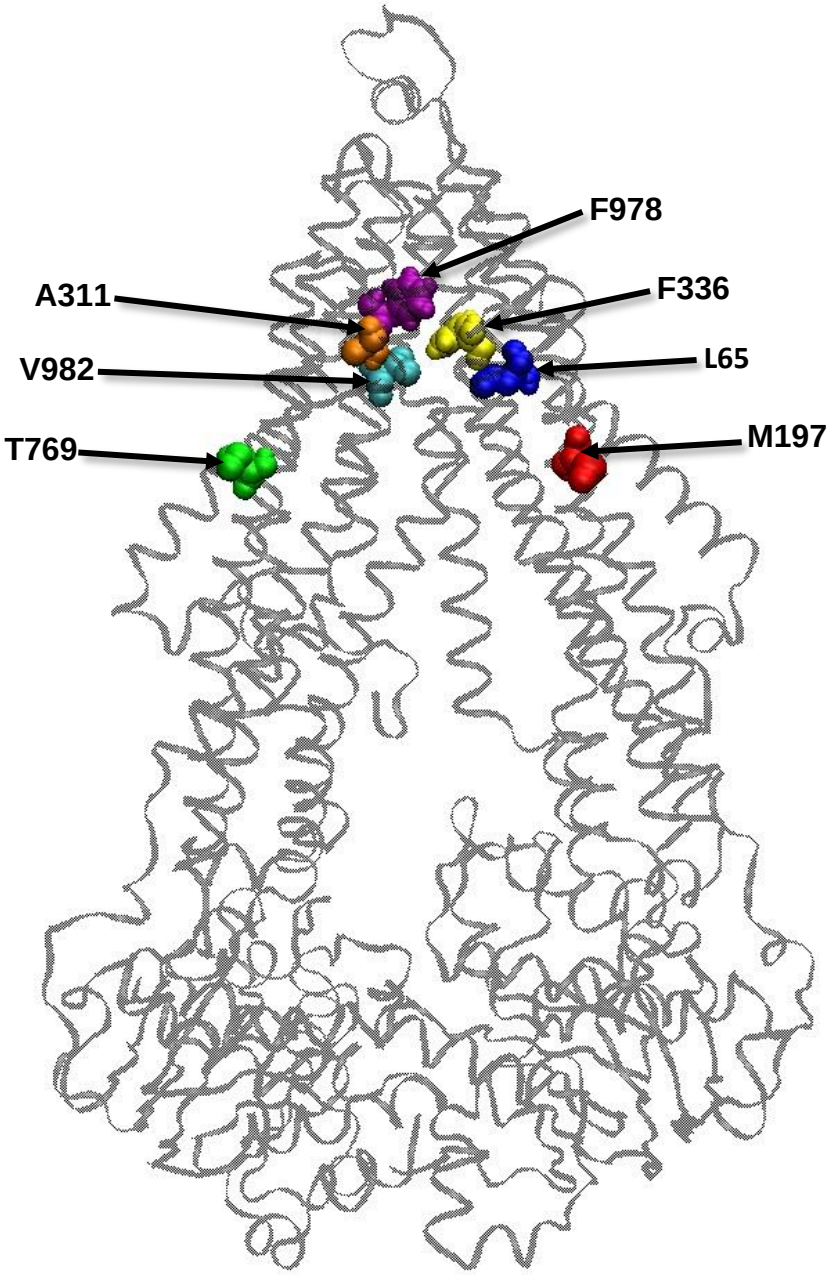

Figure 28: P-gp homology model showing contact residues. A homology model of human P-gp made using the mouse P-gp structure (PDB: 4M1M), showing the distribution of residues that were mutated to cysteines in the current investigation.

Seven residues were mutated to cysteines in cysteine-less P-gp, and biochemical assays were used to identify the contact residue for each of the four compounds evaluated. Previous detailed characterization of cys-less P-gp [184] revealed that substitution of cysteines to serines does not alter the overall function compared to Wild-type (wt) P-gp. Though there were subtle difference in the ATPase activity of

cys-less P-gp compared to wt P-gp in the presence of nicardipine, these differences were not due to altered binding, but rather due to different routes of communication to the NBDs. The cysteine mutations in P-gp did not significantly affect the Michaelis-Menten parameters of ATP hydrolysis. The study also showed that drug interactions with the TMDs of P-gp, as well as allosteric coupling, was unaffected by cysteine substitutions. It has also been shown that cys-less P-gp and wt P-gp have similar transport competencies [202]. The present investigation therefore used a cys-less P-gp construct to introduce cysteine mutations and report on drug binding based on evidence that endogenous cysteines are not critical in drug binding, ATP hydrolysis, or in the initiation of ATP hydrolysis following binding of drug. Additionally, modifications can be done under physiological conditions [135, 184]. Therefore, introduction of cysteine residues in cys-less P-gp allowed elucidation of specific drug-protein interactions in the current investigation.

The translocation of drugs by P-gp is coupled to ATP hydrolysis at the NBDs [203]. In the presence of a substrate or modulator, the NBDs form a ‘sandwich’ dimer [204, 205]. This allows binding and hydrolysis of ATP, switching the P-gp conformation from high- to low-affinity and subsequent extrusion of the substrate to the extracellular membrane. Binding of drug at the TMDs promotes coupling of the TMDs and the NBDs during this catalytic cycle [120]. Thus, alteration in the ATP hydrolysis rate of a mutant P-gp can report on the importance of the residue in drug binding [121, 122]. None of the seven cysteine insertions in the present investigation caused a gross perturbation of P-gp ATPase activity (results section, table 2). This agrees with previous work which showed these mutant isoforms as functional [131, 148, 153, 206]. Contact residues were assigned for a drug if a given mutation resulted in reduced potency of the drug to stimulate ATPase activity (EC_{50}) in P-gp, and if there

was a subsequent shift to a lower affinity (K_{App}) interaction between the drug and P-gp (results section: tables 3-6).

4.3 Scope of current investigation

To date, many experimental efforts including mutagenesis and pharmacological studies have been used to explore the molecular details of drug binding to P-gp. Computational studies too have been used to reveal the molecular details on an atomic level. Docking studies are entirely reliant on the existence of a high-resolution P-gp crystal structure where the secondary structural motifs and sidechains are resolved. To date there exist several P-gp structures that provide us with vital information regarding drug binding and transport. However, the key requirement for crystallisation is to immobilise the protein which can preclude the conformational flexibility of P-gp during drug binding and translocation [207, 208]; an issue that molecular dynamic (MD) simulation aims to overcome. However, MD simulations used to be limited by the capacity of the timescale previously employed, which ranged from 100-200ns due to the requirement of a large computational system size. Since then, technological advances enable much longer simulations (500ns to the range of microseconds are now feasible), but they are still restricted in their ability to capture the large conformational changes induced following drug binding to P-gp.

Docking and MD simulations of P-gp drug binding can measure the energetics of binding, resulting in the assignment of residue 'hotspots', which are interactions between the substrate and P-gp [209]. For example, Ferreira et al., described three putative drug binding sites by performing a docking study of the murine crystallographic P-gp structure using a database of 68 molecules [201]. Using umbrella sampling techniques measuring PMF (potential of mean force), Subramanian et al. identified transport-competent minimum free energy binding

locations of several compounds in murine P-gp [194, 210]. During a 100 ns MD simulation, Zhang et al. studied the substrate promiscuity of P-gp by identifying the spontaneous interactions of doxorubicin and paclitaxel with human P-gp [211]. However, MD simulations can be limited in its ability to characterise the vast number of conformational changes that P-gp undergoes upon drug binding; something targeted MD simulations try to overcome. Umbrella sampling techniques to obtain PMFs [212], and targeted MD simulations [213, 214], have been useful in investigating the conformational changes (inward- to outward-facing) of human P-gp both in the absence or presence of substrates, as well as in presenting the transport pathway and key residues for some substrates [215, 216].

Similarly, large scale mutagenesis studies have identified the relative contributions of various contact residues on the binding and transportation of substrates, and pharmacological studies have identified multiple substrate binding sites. As discussed in the introduction, cysteine, alanine, and arginine mutagenesis approaches have identified clusters of residues throughout the TMDs, NBDs, and intracellular loops in drug binding and transport, but without any indication of the spatial proximity of any distinct binding sites. The predictive information provided by docking studies and MD simulations can be corroborated with molecular studies such as mutagenesis experiments, and together provide strong experimental evidence in identifying contact residues and drug binding sites. This information has provided the foundation of the choices of residues mutated to cysteines in the current investigation.

The strength of our current investigation in identifying the drug binding sites of four pharmacologically distinct compounds, lies in combining cysteine mutagenesis and using biochemical assays to measure the effect on ATPase hydrolysis, with direct

measurement of drug binding affinity using the tryptophan fluorescence assay. Conformational changes following drug binding to P-gp result in a shift in the tryptophan fluorescence emission spectrum in a dose-dependent manner, thus establishing residues of interest as specifically being involved in drug binding.

The subsequent sections will discuss in detail the findings of this study, how it corroborates with existing knowledge of the nature and location of the drug binding sites, and what it contributes towards characterising the drug binding sites in P-gp.

4.4 Evidence of drug binding site within the central cavity

Of the four evaluated compounds, rhodamine 123 was the only one with more than one distinct contact residue identified. Rhodamine 123 belongs to a class of rhodamine dyes known to be transported by P-gp [217]. The four contact residues identified for rhodamine 123 include L65, F336, F978, and V982. All four residues are located within the central cavity of P-gp towards the apical end of the protein and near the central plane of the TMD (figure 28). Many studies support a central location within the internal cavity as a key area for P-gp modulation [113, 137, 148, 218, 219].

Two key mutagenesis studies investigating the binding site of rhodamine 123, or the R-site, localised residues within the lining of the central cavity, particularly those located on TM6 and TM12. Loo et al. identified key residues involved in rhodamine binding by monitoring the change in ATPase activity [131]. Following insertion of cysteines at 252 residues, a thiol-reactive analog of rhodamine (MTS-rhodamine) was used to identify several contact residues across numerous TM segments. Residues were identified based on MTS-rhodamine inhibition of the activity of single cysteine mutants. However, due to the highly reactive nature of the MTS group, to further refine the key residues involved in rhodamine binding, a protection from

inhibition assay was done, where the rationale involved was that rhodamine B when added first would occupy the drug binding site and therefore prevent the MTS-rhodamine from binding to these specific cysteine residues. This protected the mutant from inactivation if it was close to or within the rhodamine binding site. Pre-incubation with rhodamine B prior to addition of MTS-rhodamine resulted in the protection of five mutants, I340C (TM6), A841C (TM9), L975C (TM12), V981C (TM12), and of interest, residue V982C (TM12), implicating them in the binding of rhodamine B.

Through our current investigation, V982C was identified as a contact residue for rhodamine 123 because it significantly decreased the potency of rhodamine 123 to stimulate the ATPase activity of P-gp and resulted in a significant decrease in the binding affinity of rhodamine 123 to P-gp as measured by the tryptophan fluorescence assay (table 6, p105). This residue has also been implicated in substrate transport of colchicine and vinblastine in earlier studies [133].

L65 located in TM1 has also been identified as a key residue in binding of verapamil through a cysteine-scanning mutagenesis study [132] and reaction with MTS-verapamil (protection of inhibition assay). The study also tested whether rhodamine B affected the labelling of L65 by MTS-verapamil, but did not find any effect, indicating that verapamil and rhodamine B interacted with P-gp at separate sites in the drug binding pocket. Using a different approach which involved insertion of arginine residues at sites on TM1 and TM3, TM segments predicted to line the drug-binding pocket, Loo and Clarke [220] further implicated the importance of L65 in drug binding. L65R mutation resulted in a significant reduction in the apparent affinity of vinblastine, but not of rhodamine B. This is contrary to the findings of the present investigation which identifies L65 as a key residue in rhodamine 123 binding. In the

present investigation, the residue was mutated to a cysteine, which is a lot more conservative. However, in the above-mentioned study L65 was mutated to an arginine, which is negatively charged and could result in different drug-P-gp interactions compared with those in the presence of a lysine or cysteine at residue 65. This could explain the observed differences in implicating L65C as a contact residue for rhodamine 123 in the present investigation, but not L65R in previous investigations.

Further to this, arginine-enhancer mutation and arginine-scanning mutagenesis studies done by Loo and Clarke [221] on all TM segments of a P-gp mutant (G251V) with defective folding, identified F336 as a key residue in drug binding. Insertion of arginine at 237 residues resulted in significant alterations in P-gp-drug interactions for some mutants, leading to the identification of key residues involved in drug binding. F336R (TM6) mutant resulted in a significant decrease in the apparent affinity of rhodamine B to interact with P-gp. The current investigation identified F336 as another contact residue for rhodamine 123 binding to P-gp (results section, table 5).

Both cysteine and arginine mutagenesis studies [137, 219] identified residues localised in the transmembrane helices lining the central cavity comprising the translocation pathway. Majority of the residues were located on TM6 (L339, I340, A342, F343), and TM12 (L975, V981, G984, A985), suggesting that TM helices 2, 3, 5, 7-11 are organised to form a funnel shaped DBP (drug binding pocket). Many of the pool of identified residues were located at the TMD interface facing the hypothetical central DBP.

The vast number of candidate residues identified by mutagenesis studies were also in broad agreement with those identified using Molecular Dynamic (MD) simulations and docking approaches, as well as by Aller et al, which included residues V982 and F978 [166, 194]. The publication of the murine crystallographic structure (PDB; 3G5U) provided structural insights that defined the DBP as a large internal chamber of ~6000Å, opening to the intracellular compartment and the lipid interface through two designated gates (one formed by TM4/6 and the other by TM10/12) [201] and capable of simultaneous binding of more than one substrate [108, 136, 137, 148, 154].

The murine crystallographic structure (87% sequence similarity to human P-gp) was resolved with two SSS and one RRR enantiomers of QZ59, a selenohexapeptide inhibitor within the putative drug-binding pocket [50]. The co-crystallisation with QZ59 allowed localisation and characterisation of the H- and R-sites by studying their inhibition mechanisms. This study showed that the H-site broadly overlapped the binding groove of QZ59, but that the R-site only partially shared it. Docking with the thiol-reactive analog of rhodamine (MTS-rhodamine) showed that the R-site overlapped the most embedded binding location of the SSS enantiomer, but not the RRR enantiomer [166]. A more recent human-mouse chimeric structure of P-gp revealed that two molecules of zosuquidar (a third generation P-gp inhibitor) could also bind in the central cavity at the same time [55], providing further evidence of a large central binding pocket capable of binding more than one drug at a time. The location of the residues identified by both Aller et al. [50] and Alam et al. [55] were in close agreement with those identified through mutagenesis studies undertaken by Loo and Clarke as described, and with those identified in the present investigation.

Additionally, a recent study combining docking and MD simulations identified contact residues for the transport of verapamil and doxorubicin [209]. Doxorubicin is a known P-gp substrate that binds to the R-site (rhodamine 123 binding site). The study identified residues in TM1 (including L65), TM6 (including F336), and TM12 (including V982) as important contact residues and were all located in the DBP of the TMDs of P-gp. These findings are also partially consistent with a previous study [216] which identified TM6 and TM12 as the common TM helices important in transporting daunorubicin, also known to bind at the R-site. Ferriera et al., also located L336 in the designated R-site [201]. The location of these residues is proposed to be in the TMD interface facing the central DBP. These findings were consistent with those of the current investigation which identified all three residues (L65, F336, and V982) as contact residues for rhodamine 123 which binds at the R-site like doxorubicin and daunorubicin.

Modelling studies calculate the R-site pocket volume to be 1900 ± 300 $Å^3$ [201]. Literature defines the location of the R-site as being in the cytoplasmic inner leaflet C-terminal position, thus accessible from the inner bilayer leaflet, as well as the cytoplasm. The current investigation designates the R-site near the apex of P-gp within the large central cavity. It is predominantly non-polar, containing aromatic amino acids [222]. This fits in with previous studies supporting that most of the drug binding to P-gp occurred in the cytoplasmic, aqueous environment and binding was driven by hydrophobic interactions between substrates and P-gp [223].

In summary, the current investigation identified four hydrophobic contact residues that mediate interactions of rhodamine 123 with P-gp (L65, F336, F978, and V982). These residues do share some overlap with those identified in the above-mentioned

studies but are strengthened using direct measurement of drug binding, thus localising the drug binding site of rhodamine 123 within the central cavity.

4.5 Evidence of drug binding sites outside the central cavity

The publication of the 2009 murine P-gp crystallographic structure [50] proved to be a major turning point in MDR research, establishing the size and aqueous nature of the large internal drug-binding pocket [224]. Interestingly, it also provided evidence that the central cavity could be accessed from both the cytoplasm and lipid bilayer through two ‘entrance gates’. These gates are located between TM helices 4/6 and 10/12 [50] and movement of drugs through them would hence require points of interactions in the lipid-protein interface. Thus, it is possible for drugs to have contact residues that lie outside the central cavity of P-gp. The present investigation identified the binding sites of the three other compounds, nicardipine, paclitaxel, and vinblastine to lie outside the central cavity, in contrast to the location of rhodamine 123 (figure 32).

For nicardipine, the identified contact residue T769C was located at the protein-lipid interface of P-gp. Mutation of residue T769 to a cysteine resulted in significantly decreased potency of the compound to stimulate ATP hydrolysis, as well a significantly reduced apparent binding affinity to P-gp. Interestingly, mutation of another residue, A311C, also resulted in a significantly reduced ATPase hydrolysis activity of nicardipine, but this did not translate to a reduced overall apparent binding affinity (K_{App}) (refer to results section). A311C was identified as a contact residue for paclitaxel instead, as it resulted in both an altered potency to stimulate ATP hydrolysis in P-gp, as well as a significantly reduced binding affinity. The current investigation localised the contact residue for paclitaxel outside the central cavity, closer to the extracellular region of the transmembrane domain compared to

rhodamine 123. Similarly to nicardipine, the single identified contact residue for vinblastine (M197) was also located outside the central cavity and at a more cytoplasmic location near the protein-lipid interface, compared to rhodamine 123 (figure 32).

The below sections discuss how these findings fit into existing hypotheses, and mechanistic studies that support the binding of drugs outside of the central cavity.

4.5.1 Drugs can access P-gp through ‘gates’

As mentioned above, the existence of ‘entrance gates’ through the lipid bilayer, could explain binding of drugs outside the central cavity. This is supported by a photoaffinity labelling study by Pleban et al. [113] that suggested TM helices formed the ‘gates’ (TM3/11 and TM5/8) at the protein-lipid interface, where substrates first interact with P-gp before entering the central binding site (refer to Introduction section) (figure 29). Of particular interest was that M197 (TM3), A311 (TM5), T769 (TM8), and F951 (TM11) were the most frequently identified residues in the study, and molecular modelling predicted that M197/F951 and A311/T769 form the two protein binding sites in P-gp. Previous cross-linking studies [130, 219, 225] have also provided support for the P-gp protein homology model generated in the above study, identifying the spatial proximity of TM helices 2/11 and 5/8.

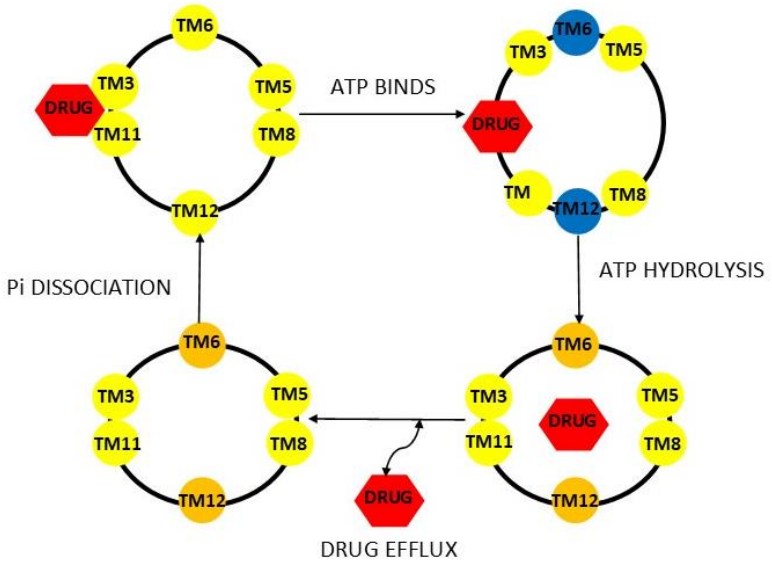

Figure 29: The two-step model of drug translocation by P-gp. Schematic representation of some of the key helices involved in drug translocation, including TM3/11 and TM5/8 forming the two entrance gates. Upon drug interaction and ATP binding, the TM helices undergo conformational changes (shown by a change in colour), switching from high to low affinity binding sites following ATP hydrolysis and resetting of the conformation. *Figure adapted from Crowley et al., 2010 [114].*

The current investigation identified three of the above four listed residues - M197 (TM3), A311 (TM5), and T769 (TM8) – as contact residues implicated in drug binding in P-gp. Despite efforts to generate and express the mutant isoform F951C, we failed to produce enough recombinant baculovirus to express the mutant P-gp in insect cells. Although we used different drugs to study the interactions of residues with substrates, both investigations were in broad agreement with respect to the identification of contact residues that contributed to the binding sites in P-gp. Propafenone analogues chosen in the study conducted by Pleban et al., suggested that TM helices 3/11 and 5/8 contributed to two separate individual binding sites for propafenone since the distance between the two TMD/TMD interfaces were too large to contribute towards a single binding site. This is similar to that seen for daunorubicin, known to bind at more than one site with different affinities [164].

4.5.2 Is P-gp a hydrophobic ‘vacuum cleaner’ or a drug ‘flippase’?

The location of the above residues external to the central cavity can also be explained by the existing hydrophobic ‘vacuum cleaner’ hypothesis of P-gp substrate transport mechanism. As described previously, P-gp is believed to operate in an alternating access model whereby the inward-facing conformation allows for binding of the drugs in the cytosolic side, and following ATP hydrolysis, this switches to the outward-facing extracellular conformation and release of drug.

Also of interest is the environment in which P-gp captures its substrates, as it provides key information on P-gp-drug interactions since the forces driving drug binding would differ significantly depending on whether the interaction takes place in the aqueous phase or the lipid phase. Substrates of P-gp are typically hydrophobic and amphipathic, and often, but not always, contain a positively charged N atom and aromatic rings [22, 69]. It has been observed that binding to the protein is a two-step process involving first partitioning of the substrate into the lipid bilayer, followed by its interaction with the binding pocket located within the TMDs. Early work supported the efflux of drugs by P-gp directly from within the membrane rather than the aqueous phase [226], and a key primary determinant of the recognition of a drug for transport by P-gp is thus its presence within the membrane inner leaflet. There is therefore a clear opportunity for the drugs to bind at the lipid-protein interface of these TMDs as demonstrated by the identified contact residues of nicardipine and vinblastine in the present study.

In an early study [227], a photolabile lipophilic membrane probe, [^{125}I]INA, was used to label an intact functional P-gp in living tumour cells to study the mechanism of interaction and transit of drugs through the transporter. Following photoactivation by UV light, this probe generates reactive by-products that bind to membrane proteins,

selectively those which have domains embedded in the lipid phase of the membrane, such as P-gp. This method allowed for a possible approach to trace the pathway of drugs through the hydrophobic domains of the multidrug transporter and suggested that P-gp may be interacting with its substrates within the membrane. Along with other similar observations, this led to the proposal that P-gp acts as a hydrophobic 'vacuum cleaner' (figure 30) by Higgins and Gottesman [228]. According to this model, P-gp 'scoops up' lipophilic molecules from the lipid milieu and expels them from the membrane into the extracellular environment using a pumping action. This results in a concentration gradient across the plasma membrane with a higher substrate concentration in the external aqueous phase [50, 229]. P-gp is thus able to intercept substrates before they enter the cytosol, protecting the cell from exposure to potentially toxic molecules [22].

The 'flippase' model (figure 30) also sees substrates interacting with P-gp at the lipid annulus, but unlike in the hydrophobic 'vacuum cleaner' model, drugs are transported from one leaflet to the other whilst still in the annulus [22, 229]. P-gp translocates hydrophobic drugs across the membrane in an ATP-dependent fashion, moving them from the cytoplasmic to the extracellular membrane leaflet. The drugs partition into the lipid membrane and spontaneously translocate to the cytoplasmic leaflet where it can gain access to the substrate-binding pocket of P-gp located within the bilayer exterior. The drugs are then subsequently effluxed into the extracellular environment [228]. As mentioned earlier, substrates of P-gp tend to be amphiphilic, either electrically neutral, or cationic. They tend to orient their hydrophobic part towards the hydrophobic fatty acyl chain region of lipids, and their polar part towards the polar head group region of lipids [223]. This results in a 'flipping' movement of an amphiphilic molecule from one leaflet to the other. The rate of spontaneous

movement across the lipid bilayer is low for many P-gp substates, thus the concentration of drugs in the lipid phase are significantly higher than in the aqueous phase since amphiphilic drugs can partition easily into lipid membranes. The 'flippase' activity therefore gives rise to a substrate concentration gradient across the membrane, resulting in rapid equilibration of the drug in the outer leaflet with the external medium [22]. More recently, this model is being addressed as the "floppase" model as the movement from the inner to the outer leaflet was defined as 'flopping', whereas the inverse was 'flipping'. When drugs are transported to the extracellular environment, it is a result of P-gp 'flopping' [223]. Omote and Al-Shawi provided evidence [230] of this "floppase" activity by investigating the transport of permanently charged spin-labelled verapamil which cannot passively diffuse across the membrane.

Sharom et al. [174] mapped the location of the H-site to the cytoplasmic membrane leaflet of P-gp, consistent with the idea of P-gp working as a drug "flippase". Additionally, using the fluorescence characteristics of certain P-gp substrates, Lugo and Sharom [176] were able to characterise both H- and R-sites as being very hydrophobic, therefore unlikely to be located close to an opening onto an aqueous chamber as described earlier [150]. However, though Sharom et al. [176, 177] mapped the potential location of the H- and R-sites within the cytoplasmic leaflet of the lipid bilayer, it did not exclude the existence of a common central drug binding site. A later study by Shapiro et al. [165] using the fluorescent dye Hoechst 33342 provided direct evidence of drug transport from within the membrane. They showed that the specific rate of transport was directly proportional to the amount of the dye in the lipid phase, supporting that P-gp removes Hoechst 33342 from the lipid membrane.

Thus, binding of P-gp substrates within the lipid bilayer may help explain the broad substrate specificity of P-gp since the volume of the lipid bilayer compared to the aqueous phase is relatively small and a lipophilic substance can reach high concentrations within the lipid phase much quicker and thus does not need to be recognised with high affinity by P-gp [223]. According to this observation, it can be said that P-gp transports substrates down a concentration gradient from the lipid phase to the aqueous environment. The energy generated by ATP hydrolysis in this case, instead of being used to transport a substrate against a concentration gradient, would be to overcome the lipid membrane-aqueous partition coefficient since the lipophilic substrate in question would prefer the lipid membrane environment over the aqueous cavity of P-gp [160]. Other transport studies [161, 170, 231] using plasma membrane vesicles, reconstituted P-gp, and intact MDR cells, also demonstrated that several other fluorescent substrates in addition to Hoechst 33342, including LDS-751 and a rhodamine derivative, were all extracted from the cytoplasmic membrane leaflet.

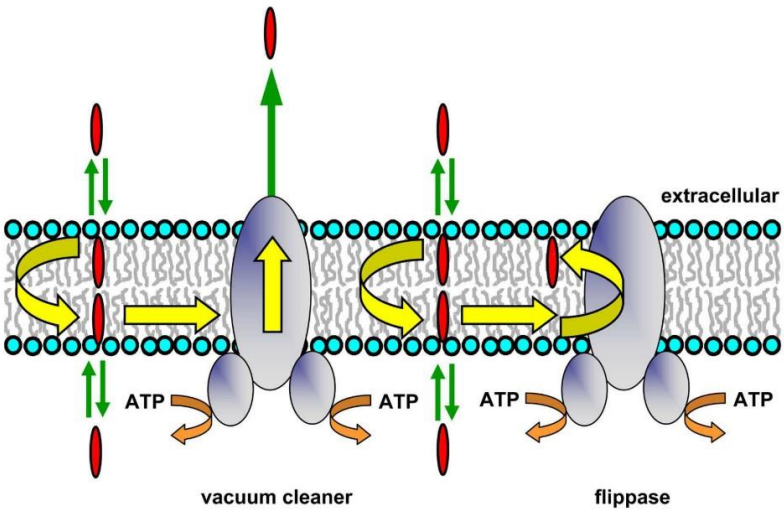

Figure 30: The hydrophobic vacuum cleaner and drug flippase models of P-gp function. Schematic representation of the two models discussed. Drug is shown in red, with the green arrows showing the direction of movement and the yellow arrows representing the concentration gradients within the lipid bilayer and translocation pore. *Figure abstracted from Sharom, 2014 [229].*

The hydrophobic ‘vacuum cleaner’ model supports the observation in the current investigation that the identified locations of the contact residues of nicardipine, vinblastine, and paclitaxel lie outside the central cavity. The data from MD simulations, biochemical assays, and drug permeation profiles [41, 50, 155, 201, 204, 226, 232], suggest that P-gp acts according to the hydrophobic ‘vacuum cleaner’ model and that all but one stage of drug efflux (drug permeation, entry into the DBP, and ATP hydrolysis resulting in drug release) are energetically favourable. P-gp therefore seems to act as a ‘facilitator’, allowing drugs to pass directly from the cytoplasmic leaflet into the extracellular environment, bypassing the drug ‘flip-flop’ mechanism between membrane leaflets. This results in a lower intracellular concentration. However, for drug release to occur, the binding affinities at the DBSs must shift from high to low. These conformational changes are intimately linked to ATP binding and hydrolysis at the NBDs [224].

4.5.3 The four pharmacologically distinct drug binding sites are also spatially distinct

The current investigation not only supported the existence of four pharmacologically distinct drug binding sites [157], but also for the first time provided evidence of their distinct spatial relationship (figure 32). The location of these residues allowed us to support the existence of DBSs within the central cavity and propose the existence of transport-competent alternate drug binding sites at the lipid-protein interface, allowing extraction of the drugs from the bilayer.

The existence of pharmacologically distinct drug binding sites at spatially distinct locations inside and outside the central cavity are in contrast with the findings of Chufan et al. [158] who proposed that P-gp has multiple binding sites for the same substrate. According to this model, mutating a residue that forms a part of the drug-

binding site would affect the biochemical properties of P-gp in such a way that it would alter the drug interaction with the mutant protein, rather than prevent its binding altogether. The study suggested that a substrate has more than one transport-capable binding site (secondary sites) to which it can bind upon mutations within the primary binding site. The existence of several similar binding sites (secondary sites) for any one substrate within the central cavity would thus enable efficient binding and transport of the substrate despite a mutation at its primary binding site [233].

The present investigation provides evidence for a multisite model of drug binding in P-gp where distinct binding sites exist for a class of substrate/modulator. This is supported by numerous studies as discussed in detail in the introduction. Briefly, Shapiro and colleagues established the existence of at least two distinct, but positively co-operative sites [155]. The R-site and the H-site also shared overlapping specificities. Martin and Callaghan et al. [178] used an equilibrium drug binding assay to directly and quantitatively measure the affinity of drug interactions with P-gp of the anthranilic acid derivative, XR9576, and a variety of P-gp substrates including vinblastine and paclitaxel, further supporting a multisite drug binding model for P-gp. The data suggested that XR9576 interacted non-competitively with vinblastine and paclitaxel at a site distinct to their binding sites but could effectively block transport of both cytotoxic agents.

The use of P-gp inhibitors has also supported binding at multiple drug binding sites. Studies have shown that in cells overexpressing P-gp, two inhibitors - elacridar and tariquidar, could both be transported as substrates at low concentrations [234]. This observation was explained in a recent study by Nosol and Locher et al. [200] using cryo-EM structures of nanodisc-reconstituted P-gp in complex with the Fab fragment

of MRK16. MRK16 is an inhibitory monoclonal antibody that prevents substrate release at the external membrane, without interfering with drug binding or ATPase activity. This complex was either bound to a substrate (vincristine) or a potent inhibitor (zosuquidar, elacridar, or tariquidar) of P-gp. Small-molecule inhibitors are expected to bind to the TMDs and compete with P-gp substrates for binding within the central DBP. However, the five resolved cryo-EM structures in the study captured an occluded conformation of P-gp with TM4 and TM10 kinked towards the pseudosymmetric axis of the protein, forming a cytoplasmic gate at the entrance of the DBP. At low (nanomolar) concentrations of the inhibitors, transport was possible only if a single molecule bound the central binding cavity. However, at higher (micromolar) concentrations, two molecules bound. One of these molecules adopted a globular, U-shaped conformation, fully inside the central binding pocket, and acted as a substrate. The second molecule adopted an L-shaped conformation and extended beyond the central DBP to the cytoplasmic gate and acted as a non-competitive inhibitor. This cavity or “access tunnel”, connected to the central cavity by a vestibule, provided access to small solutes from the cytoplasm to the central DBP (figure 31).

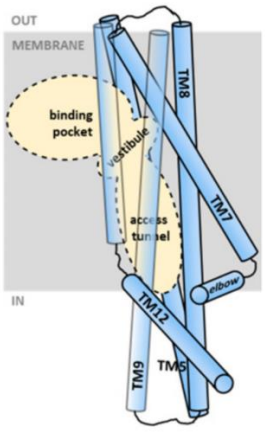

Figure 31: Schematic representation of the access tunnel and vestibule in the occluded conformation of P-gp. Figure shows the drug-binding pocket, vestibule, and access tunnel within P-gp. Key TM helices are shown as cylinders, surrounding the access tunnel, as explained in detail in the text above. *Figure abstracted from Nosol et al., 2020 [200].*

This supports binding of drugs outside the central cavity, as observed in the current investigation. Additionally, the access tunnel was reported to be closer to the C-terminal half of P-gp and surrounded by TM helices 5, 7, 8, 9, and 12. TM12 played a key role in the plasticity of the drug binding pocket. TM9 was important in distinguishing substrates from inhibitors by moving into the space provided by the access tunnel when a substrate was bound, thus initiating the peristaltic extrusion mechanism. Inhibitors, unlike substrates, could bind in pairs and binding at the access tunnel prevented movement of TM9. Some of the conserved residues in the access tunnel agreed with previous mutagenesis studies and the present investigation [235, 236]. However, in contrast to the present investigation which found V982 as a contact residue for rhodamine 123, Nosol et al. reported that mutagenesis of V982 did not significantly alter substrate transport but did interfere with inhibition by tariquidar [158].

Additionally, as discussed above, several of the contact residues identified by Pleban et al. [113] and Loo and Clark [132, 148, 206, 220, 221, 237] also agreed with the current investigation (refer to section 4.4 and 4.5.1). However, in our study, we used P-gp substrates that are pharmacologically distinct and known to bind at a single class of site previously identified in P-gp [157]. We thus propose that the R-site (and the overlapping H-site) is in the central cavity of P-gp, proximal to the ‘apex’ or closure point of the cavity. The contact residues identified for vinblastine and nicardipine, M197 and T769, respectively, are spatially separated by approximately 33Å (predicted by the PDB 4M1M molecular model of P-gp) and located towards the cytoplasmic face of P-gp, within the inner hemi-leaflet of the membrane. These findings are supported by that of a previous study [238] which, characterised the interactions of vinblastine to P-gp during the different stages of the catalytic cycle

using a series of radioligand binding experiments, and identified a single class of high affinity binding site. Nicardipine and vinblastine have been shown to exhibit complex allosteric interactions with P-gp, whereby binding of one effect the dissociation of the other, but binding occurs at distinct pharmacologically classed binding sites [157, 179]. Contrary to the location of the contact residues for vinblastine and nicardipine, the current investigation identified the contact residue of paclitaxel (A311) to be located within the plane of the outer leaflet of the bilayer.

Taken together the findings of the present investigation add experimental support to the evidence of multiple drug binding sites, that are distinct in their transport or modulatory function. More notably, we provide new information that these distinct drug binding sites are also spatially separate, existing not just in the central cavity but also outside at the lipid-protein interface.

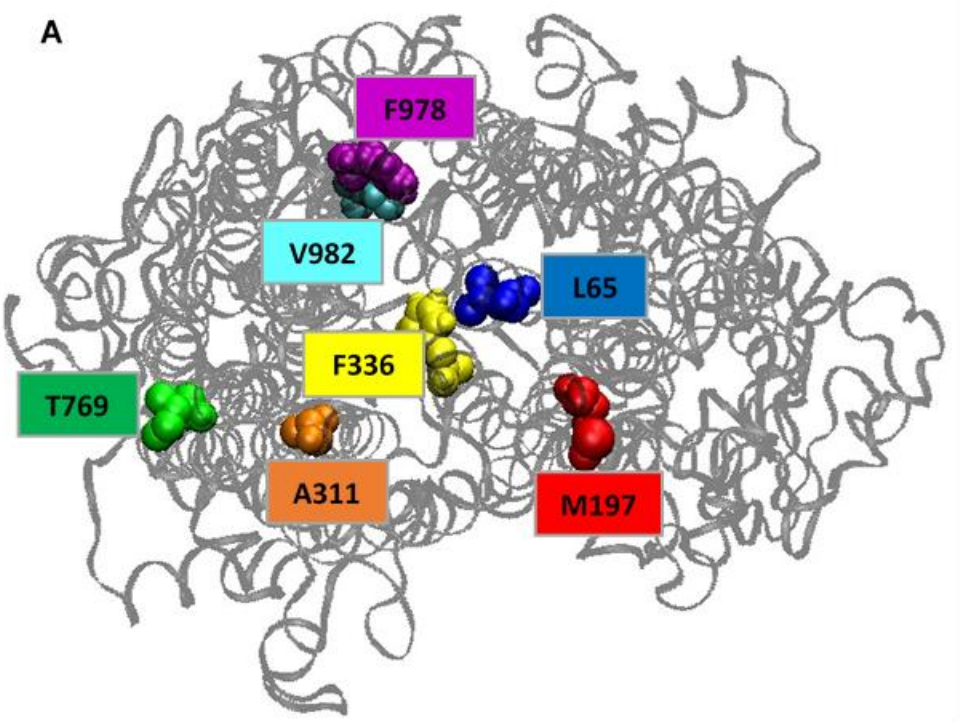

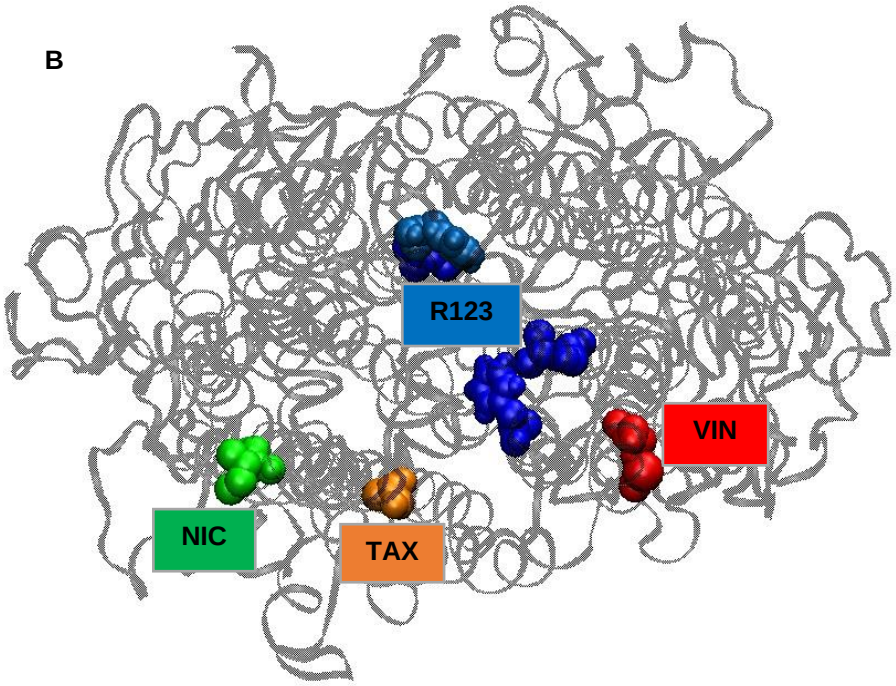

Figure 32: Top view of a P-gp homology model (PDB: 4M1M) showing contact residues. (A) shows the distribution of residues that were mutated to cysteines in the current investigation. **(B)** shows the four pharmacologically distinct drugs (NIC = nicardipine, TAX = paclitaxel, VIN = vinblastine, and R123 = rhodamine 123), that were used in the current investigation. The labels placed proximal to their identified contact residues, indicating four spatially distinct drug binding sites.

4.6 The importance of residue F978 in P-gp drug translocation

Finally, we also addressed the question: do the multiple binding sites operate through a single translocation pathway? Results with one mutation certainly support this. Specifically, the F978C mutation affected the binding of rhodamine 123 to P-gp but also altered the interactions of all four drugs with P-gp. There was a significant reduction in the ability of all four drugs to stimulate ATPase activity in P-gp (tables 3-6 in Results section 3.4). Given the spatial separation of the drug binding sites, this commonality can best be explained by the presence of a common translocation route. F978 is located close to the central cavity, lining the proposed R-site. This finding is consistent with previous data from studies [142, 220, 221, 239] showing

that residues in the vicinity of F978 are implicated to reside within the translocation pore of P-gp both through MD simulation studies and mutagenesis studies.

As mentioned earlier, P-gp is comprised of two homologous halves, each comprising six transmembrane (TM) helices and one cytoplasmic NBD. Intracellular loops between TM6 and NBD1 and TM12 and NBD2 link the TMD and NBD in each half. Additional short intracellular coupling helices form non-covalent bonds between TMD-NBD [50, 240, 241]. Therefore, TM6 and TM12 are key in facilitating the communication between ATP hydrolysis at the NBD and drug binding and translocation in the TMD [142-145, 242]. Mutations in key residues along these helices can therefore perturb the interdomain communication between TMDs and NBDs and alter the translocation process.

Residue F978 is located on TM helix 12, in a densely packed region of P-gp, on a helix-helix interface, and contributes to helix-helix TM12-TM1 stabilisation by hydrophobically interacting with F72 [142]. The mutation F978C is located on the membrane-embedded region of TM12 near the extracellular protein-lipid interface. It is part of a conserved sequence motif present in TM12 and TM6. Mutation prevents hydrophobic interactions between TM12-TM1, resulting in a reduction in P-gp activity. Residue F978 has also been previously implicated in drug binding [142, 143, 237, 240]. Mutation has shown significantly reduced ATPase activity, nucleotide binding, and drug-protein interactions, supported by the current investigation. Interestingly, mutations in TM6 did not show a similar reduction in ATPase activity in the presence of all drugs, in agreement with previous studies. It is likely that TM6 and TM12 communicate with NBD1 and NBD2, respectively, in an asymmetrical manner, possibly due to differences in interdomain interactions [142].

van Wonderen et al. [243] utilising an EPR spectroscopic technique, analysed the residue microenvironment in significantly more detail to understand the dynamic changes that selected residues underwent during the transport process. Four residues including two that are proximal to residue F978 (A980 in TM12 and F343 in TM6) were mutated and an MTSL paramagnetic probe attached. The resultant EPR spectra supported an 'alternating access' [45, 58, 61, 243] model whereby the helices lining the cavity undergo significant conformational changes during the ATP hydrolytic transport process, allowing for greater aqueous accessibility of the central cavity to the extracellular region. Therefore, a mutation at any of these residues could interfere with the necessary conformational changes required for drug translocation.

Another recent study [240] developed a human P-gp homology model based on the murine P-gp crystallographic structure in the inward-facing *apo* state (PDB: 4Q9H), and refined it using MD simulations to then analyse the effects of four mutations, including F978A, on drug specificity and efflux. The results of this study proposed that a mutation at F978 induced repacking of TM helices, affecting the portals of drug entry into the central cavity or the DBP by changing the crossing helices TM4/5 and TM10/11 that are important in NBD dimerisation. This repacking changed the volume, shape and polarity of the drug binding sites lining the central cavity, affecting binding at the H- and R-sites. Specific mutations at these sites resulted in significant changes to substrate binding sites (SBSs) [201, 240]. This suggests a communication pathway between the residue location and the SBSs through the functional TM6 and TM12 [156, 157, 162].

The findings of the current investigation also corroborated findings from another study [244] that emphasised the importance of F978 in facilitating the alternating access mechanism of drug transport in P-gp, where substrate translocation is

powered by ATP hydrolysis. Using molecular modelling, biochemical and transport assays, the study identified how the two phenylalanine residues, F978 and F728, interacted with two tyrosine residue Y953 and Y310, respectively, in an edge-to-face conformation and resulted in reorientation of the tyrosine residues in such a way that they were able to form hydrogen bond contacts with potent inhibitors of P-gp. The two structural motifs (F978-Y953 and F728-Y310) were therefore essential for drug-mediated inhibition of ATP hydrolysis by P-gp. The structural information suggested that this interaction locked the TM helices in a conformation before the outward opening of the TMDs. It inhibited the opening of the apex to create access from the extracellular environment, as well as closing the cytosolic entrance.

Taken together, the significantly reduced ATPase activity observed with F978C appears to be a result of reduced nucleotide binding. Considering the residue is located at the extracellular end of the helix and a considerable distance from the site of ATP binding and hydrolysis in the NBDs, it adds further support to the findings of previous studies [150, 238, 245-249] which have highlighted the cooperativity between these two domains, and the importance of coupling in initiating drug translocation. The current investigation therefore adds evidence supporting the key role of TM12 in coordinating the necessary conformational changes in the TMDs following ATP hydrolysis in the NBDs. F978 is an importance residue, forming a part of the common drug translocation route and its mutation resulted in significantly reduced ATPase activity of P-gp in the presence of all four drugs investigated.

4.7 Scientific impact of the current investigation

Modulating the efflux of chemotherapeutic drugs by P-gp has been a long-investigated strategy in overcoming MDR in cancer cells. Due to the complexity of the efflux mechanism and the limited understanding of the molecular basis of

polyspecificity, inhibitors of P-gp have achieved only moderate clinical success. However, since its discovery over 40 years ago, long strides have been made in understanding this enigmatic transporter. We currently have several structures/homologues of P-gp, which when combined with advanced MD simulations and biochemical assays, have provided us with key information towards understanding the efflux mechanism of P-gp by confirming the entrance gate [224], establishing the behaviour of ATP binding and hydrolysis [232, 239], defining the translocation pathway [215, 216], characterising the drug binding sites [201], and investigating the influence of the environment on substrate recognition [222, 250, 251].

The present investigation provided key information in further characterising the drug binding sites by identifying the contact residues of four pharmacologically distinct compounds, rhodamine 123, vinblastine, nicardipine, and paclitaxel. Though previous studies have established that each of these compounds bound at pharmacologically distinct drug binding sites in P-gp, the spatial distribution of these binding sites was unknown. We identified the location of the four pharmacologically distinct sites to be spatially distinct, with one site located within the central cavity, and the other three outside the central cavity at the lipid-protein interface (in the lipid milieu). The presence of binding sites in the annular region is also supported by a recent study by Nosol and Locher et al. [200]. This information along with the evidence for F978 being a key residue in TM12, provides vital insight into the physical mechanism of coupling drug-binding events and the ATP hydrolysis cycle, as well as support for the alternating access mechanism of drug translocation through a common pore. We thus propose that as P-gp responds to stimuli from the NBDs, it undergoes conformational changes that allow the drugs to be actively relocated to the central

cavity of P-gp (after initial binding). As the drugs transition into the translocation pore, the cavity then reorients to open to the extracellular environment, shutting the cytosolic end.

The findings of the current investigation can be coupled with higher resolution structural data and further mutagenesis to refine the location of the distinct drug binding sites in P-gp. This will help describe the molecular interactions between drugs and the peptide chains, shedding light on the pharmacophoric elements for interaction with P-gp and the basis of the polyspecificity displayed by P-gp. Thus, spatial identification of the four pharmacologically distinct binding sites in the current investigation will improve our understanding of the environment of the binding sites and better characterise substrates of P-gp. This will direct rational chemical design of more potent inhibitors or compounds that are not substrates of P-gp.

Currently, interest in P-gp as a pharmacological target in cancer therapy has petered due to limited success in inhibiting it over the past few decades. However, renewed interest can be engendered through elucidation of the drug-binding site structure, and the pharmacophore of drug substrates. The fundamental scientific work presented in this current investigation adds to this much needed research. Thus, the ability to pharmacologically modulate expression and function of P-gp through fundamental research will provide the language for translation, vital in changing perspectives of P-gp as a viable target in overcoming MDR.

REFERENCES

1. Carlsen, S.A., J.E. Till, and V. Ling, *Modulation of membrane drug permeability in Chinese hamster ovary cells.* Biochim Biophys Acta, 1976. **455**(3): p. 900-12.
2. Juliano, R.L. and V. Ling, *A surface glycoprotein modulating drug permeability in Chinese hamster ovary cell mutants.* Biochim Biophys Acta, 1976. **455**(1): p. 152-62.
3. Juranka, P.F., R.L. Zastawny, and V. Ling, *P-glycoprotein: multidrug-resistance and a superfamily of membrane-associated transport proteins.* FASEB J, 1989. **3**(14): p. 2583-92.
4. Mansoori, B., et al., *The Different Mechanisms of Cancer Drug Resistance: A Brief Review.* Adv Pharm Bull, 2017. **7**(3): p. 339-348.
5. Housman, G., et al., *Drug resistance in cancer: an overview.* Cancers (Basel), 2014. **6**(3): p. 1769-92.
6. Michael, M. and M.M. Doherty, *Tumoral drug metabolism: overview and its implications for cancer therapy.* J Clin Oncol, 2005. **23**(1): p. 205-29.
7. Rodriguez-Antona, C. and M. Ingelman-Sundberg, *Cytochrome P450 pharmacogenetics and cancer.* Oncogene, 2006. **25**(11): p. 1679-91.
8. Townsend, D.M. and K.D. Tew, *The role of glutathione-S-transferase in anti-cancer drug resistance.* Oncogene, 2003. **22**(47): p. 7369-75.
9. Rivlin, N., et al., *Mutations in the p53 Tumor Suppressor Gene: Important Milestones at the Various Steps of Tumorigenesis.* Genes Cancer, 2011. **2**(4): p. 466-74.
10. Soengas, M.S., et al., *Apaf-1 and caspase-9 in p53-dependent apoptosis and tumor inhibition.* Science, 1999. **284**(5411): p. 156-9.
11. Holohan, C., et al., *Cancer drug resistance: an evolving paradigm.* Nat Rev Cancer, 2013. **13**(10): p. 714-26.
12. Slamon, D.J., et al., *Studies of the HER-2/neu proto-oncogene in human breast and ovarian cancer.* Science, 1989. **244**(4905): p. 707-12.
13. Dieras, V., et al., *[Trastuzumab (Herceptin) and breast cancer: mechanisms of resistance].* Bull Cancer, 2007. **94**(3): p. 259-66.
14. Bonanno, L., A. Favaretto, and R. Rosell, *Platinum drugs and DNA repair mechanisms in lung cancer.* Anticancer Res, 2014. **34**(1): p. 493-501.
15. Selvakumaran, M., et al., *Enhanced cisplatin cytotoxicity by disturbing the nucleotide excision repair pathway in ovarian cancer cell lines.* Cancer Res, 2003. **63**(6): p. 1311-6.
16. Gottesman, M.M., T. Fojo, and S.E. Bates, *Multidrug resistance in cancer: role of ATP-dependent transporters.* Nat Rev Cancer, 2002. **2**(1): p. 48-58.
17. Modok, S., H.R. Mellor, and R. Callaghan, *Modulation of multidrug resistance efflux pump activity to overcome chemoresistance in cancer.* Curr Opin Pharmacol, 2006. **6**(4): p. 350-4.
18. Gottesman, M.M., I. Pastan, and S.V. Ambudkar, *P-glycoprotein and multidrug resistance.* Curr Opin Genet Dev, 1996. **6**(5): p. 610-7.
19. Wang, Z., et al., *P-glycoprotein substrate models using support vector machines based on a comprehensive data set.* J Chem Inf Model, 2011. **51**(6): p. 1447-56.
20. Callaghan, R., F. Luk, and M. Bebawy, *Inhibition of the multidrug resistance P-glycoprotein: time for a change of strategy?* Drug Metab Dispos, 2014. **42**(4): p. 623-31.

21. Gottesman, M.M. and V. Ling, *The molecular basis of multidrug resistance in cancer: the early years of P-glycoprotein research.* FEBS Lett, 2006. **580**(4): p. 998-1009.
22. Sharom, F.J., *The P-glycoprotein multidrug transporter.* Essays Biochem, 2011. **50**(1): p. 161-78.
23. Sharom, F.J., *Shedding light on drug transport: structure and function of the P-glycoprotein multidrug transporter (ABCB1).* Biochem Cell Biol, 2006. **84**(6): p. 979-92.
24. Ambudkar, S.V., et al., *Biochemical, cellular, and pharmacological aspects of the multidrug transporter.* Annu Rev Pharmacol Toxicol, 1999. **39**: p. 361-98.
25. Smit, J.W., et al., *Absence or pharmacological blocking of placental P-glycoprotein profoundly increases fetal drug exposure.* J Clin Invest, 1999. **104**(10): p. 1441-7.
26. Thiebaut, F., et al., *Immunohistochemical localization in normal tissues of different epitopes in the multidrug transport protein P170: evidence for localization in brain capillaries and crossreactivity of one antibody with a muscle protein.* J Histochem Cytochem, 1989. **37**(2): p. 159-64.
27. Jonker, J.W., et al., *Role of blood-brain barrier P-glycoprotein in limiting brain accumulation and sedative side-effects of asimadoline, a peripherally acting analgaesic drug.* Br J Pharmacol, 1999. **127**(1): p. 43-50.
28. Bodo, A., et al., *The role of multidrug transporters in drug availability, metabolism and toxicity.* Toxicol Lett, 2003. **140-141**: p. 133-43.
29. Schinkel, A.H., *P-Glycoprotein, a gatekeeper in the blood-brain barrier.* Adv Drug Deliv Rev, 1999. **36**(2-3): p. 179-194.
30. Hollenstein, K., R.J. Dawson, and K.P. Locher, *Structure and mechanism of ABC transporter proteins.* Curr Opin Struct Biol, 2007. **17**(4): p. 412-8.
31. Linton, K.J., *Structure and function of ABC transporters.* Physiology (Bethesda), 2007. **22**: p. 122-30.
32. Martinez-Mir, A., et al., *Retinitis pigmentosa caused by a homozygous mutation in the Stargardt disease gene ABCR.* Nat Genet, 1998. **18**(1): p. 11-2.
33. Jacquemin, E. and M. Hadchouel, *Genetic basis of progressive familial intrahepatic cholestasis.* J Hepatol, 1999. **31**(2): p. 377-81.
34. Higgins, C.F. and K.J. Linton, *Structural biology. The xyz of ABC transporters.* Science, 2001. **293**(5536): p. 1782-4.
35. Jones, P.M., M.L. O'Mara, and A.M. George, *ABC transporters: a riddle wrapped in a mystery inside an enigma.* Trends Biochem Sci, 2009. **34**(10): p. 520-31.
36. Zolnerciks, J.K., et al., *Structure of ABC transporters.* Essays Biochem, 2011. **50**(1): p. 43-61.
37. Linton, K.J. and C.F. Higgins, *Structure and function of ABC transporters: the ATP switch provides flexible control.* Pflugers Arch, 2007. **453**(5): p. 555-67.
38. Kerr, I.D., *Structure and association of ATP-binding cassette transporter nucleotide-binding domains.* Biochim Biophys Acta, 2002. **1561**(1): p. 47-64.
39. Ambudkar, S.V., et al., *The A-loop, a novel conserved aromatic acid subdomain upstream of the Walker A motif in ABC transporters, is critical for ATP binding.* FEBS Lett, 2006. **580**(4): p. 1049-55.
40. Zolnerciks, J.K., et al., *The Q loops of the human multidrug resistance transporter ABCB1 are necessary to couple drug binding to the ATP catalytic cycle.* FASEB J, 2014. **28**(10): p. 4335-46.

41. Ambudkar, S.V., I.W. Kim, and Z.E. Sauna, *The power of the pump: mechanisms of action of P-glycoprotein (ABCB1).* Eur J Pharm Sci, 2006. **27**(5): p. 392-400.
42. Senior, A.E. and S. Bhagat, *P-glycoprotein shows strong catalytic cooperativity between the two nucleotide sites.* Biochemistry, 1998. **37**(3): p. 831-6.
43. Dawson, R.J. and K.P. Locher, *Structure of a bacterial multidrug ABC transporter.* Nature, 2006. **443**(7108): p. 180-5.
44. Locher, K.P., A.T. Lee, and D.C. Rees, *The E. coli BtuCD structure: a framework for ABC transporter architecture and mechanism.* Science, 2002. **296**(5570): p. 1091-8.
45. Pinkett, H.W., et al., *An inward-facing conformation of a putative metal-chelate-type ABC transporter.* Science, 2007. **315**(5810): p. 373-7.
46. Zhou, S.F., *Structure, function and regulation of P-glycoprotein and its clinical relevance in drug disposition.* Xenobiotica, 2008. **38**(7-8): p. 802-32.
47. Gottesman, M.M., S.V. Ambudkar, and D. Xia, *Structure of a multidrug transporter.* Nat Biotechnol, 2009. **27**(6): p. 546-7.
48. Rosenberg, M.F., et al., *Structure of the multidrug resistance P-glycoprotein to 2.5 nm resolution determined by electron microscopy and image analysis.* J Biol Chem, 1997. **272**(16): p. 10685-94.
49. Rosenberg, M.F., et al., *Three-dimensional structures of the mammalian multidrug resistance P-glycoprotein demonstrate major conformational changes in the transmembrane domains upon nucleotide binding.* J Biol Chem, 2003. **278**(10): p. 8294-9.
50. Aller, S.G., et al., *Structure of P-glycoprotein reveals a molecular basis for poly-specific drug binding.* Science, 2009. **323**(5922): p. 1718-22.
51. Ward, A.B., et al., *Structures of P-glycoprotein reveal its conformational flexibility and an epitope on the nucleotide-binding domain.* Proc Natl Acad Sci U S A, 2013. **110**(33): p. 13386-91.
52. Li, J., K.F. Jaimes, and S.G. Aller, *Refined structures of mouse P-glycoprotein.* Protein Sci, 2014. **23**(1): p. 34-46.
53. Esser, L., et al., *Structures of the Multidrug Transporter P-glycoprotein Reveal Asymmetric ATP Binding and the Mechanism of Polyspecificity.* J Biol Chem, 2017. **292**(2): p. 446-461.
54. Higgins, C.F., et al., *Structure of the multidrug resistance P-glycoprotein.* Semin Cancer Biol, 1997. **8**(3): p. 135-42.
55. Alam, A., et al., *Structure of a zosuquidar and UIC2-bound human-mouse chimeric ABCB1.* Proc Natl Acad Sci U S A, 2018. **115**(9): p. E1973-E1982.
56. Dawson, R.J., K. Hollenstein, and K.P. Locher, *Uptake or extrusion: crystal structures of full ABC transporters suggest a common mechanism.* Mol Microbiol, 2007. **65**(2): p. 250-7.
57. Higgins, C.F. and K.J. Linton, *The ATP switch model for ABC transporters.* Nat Struct Mol Biol, 2004. **11**(10): p. 918-26.
58. Jin, M.S., et al., *Crystal structure of the multidrug transporter P-glycoprotein from Caenorhabditis elegans.* Nature, 2012. **490**(7421): p. 566-9.
59. Kodan, A., et al., *Structural basis for gating mechanisms of a eukaryotic P-glycoprotein homolog.* Proc Natl Acad Sci U S A, 2014. **111**(11): p. 4049-54.
60. Carey Hulyer, A.R., et al., *Cross-linking, DEER-spectroscopy and molecular dynamics confirm the inward facing state of P-glycoprotein in a lipid membrane.* J Struct Biol, 2020. **211**(1): p. 107513.

61. Pan, L. and S.G. Aller, *Equilibrated atomic models of outward-facing P-glycoprotein and effect of ATP binding on structural dynamics.* Sci Rep, 2015. **5**: p. 7880.
62. Kim, Y. and J. Chen, *Molecular structure of human P-glycoprotein in the ATP-bound, outward-facing conformation.* Science, 2018. **359**(6378): p. 915-919.
63. Callaghan, R., R.C. Ford, and I.D. Kerr, *The translocation mechanism of P-glycoprotein.* FEBS Lett, 2006. **580**(4): p. 1056-63.
64. Senior, A.E., M.K. al-Shawi, and I.L. Urbatsch, *The catalytic cycle of P-glycoprotein.* FEBS Lett, 1995. **377**(3): p. 285-9.
65. Urbatsch, I.L., et al., *Both P-glycoprotein nucleotide-binding sites are catalytically active.* J Biol Chem, 1995. **270**(45): p. 26956-61.
66. Sauna, Z.E. and S.V. Ambudkar, *Characterization of the catalytic cycle of ATP hydrolysis by human P-glycoprotein. The two ATP hydrolysis events in a single catalytic cycle are kinetically similar but affect different functional outcomes.* J Biol Chem, 2001. **276**(15): p. 11653-61.
67. Sauna, Z.E. and S.V. Ambudkar, *Evidence for a requirement for ATP hydrolysis at two distinct steps during a single turnover of the catalytic cycle of human P-glycoprotein.* Proc Natl Acad Sci U S A, 2000. **97**(6): p. 2515-20.
68. Gottesman, M.M. and I. Pastan, *Biochemistry of multidrug resistance mediated by the multidrug transporter.* Annu Rev Biochem, 1993. **62**: p. 385-427.
69. Seelig, A., *A general pattern for substrate recognition by P-glycoprotein.* Eur J Biochem, 1998. **251**(1-2): p. 252-61.
70. Pallis, M. and N. Russell, *Strategies for overcoming p-glycoprotein-mediated drug resistance in acute myeloblastic leukaemia.* Leukemia, 2004. **18**(12): p. 1927-30.
71. van der Holt, B., et al., *The value of the MDR1 reversal agent PSC-833 in addition to daunorubicin and cytarabine in the treatment of elderly patients with previously untreated acute myeloid leukemia (AML), in relation to MDR1 status at diagnosis.* Blood, 2005. **106**(8): p. 2646-54.
72. van den Heuvel-Eibrink, M.M., P. Sonneveld, and R. Pieters, *The prognostic significance of membrane transport-associated multidrug resistance (MDR) proteins in leukemia.* Int J Clin Pharmacol Ther, 2000. **38**(3): p. 94-110.
73. Jekerle, V., et al., *99mTc-Sestamibi, a sensitive probe for in vivo imaging of P-glycoprotein inhibition by modulators and mdr1 antisense oligodeoxynucleotides.* Mol Imaging Biol, 2006. **8**(6): p. 333-9.
74. Pusztai, L., et al., *Phase II study of tariquidar, a selective P-glycoprotein inhibitor, in patients with chemotherapy-resistant, advanced breast carcinoma.* Cancer, 2005. **104**(4): p. 682-91.
75. Walker, J., C. Martin, and R. Callaghan, *Inhibition of P-glycoprotein function by XR9576 in a solid tumour model can restore anticancer drug efficacy.* Eur J Cancer, 2004. **40**(4): p. 594-605.
76. Tsuruo, T., et al., *Overcoming of vincristine resistance in P388 leukemia in vivo and in vitro through enhanced cytotoxicity of vincristine and vinblastine by verapamil.* Cancer Res, 1981. **41**(5): p. 1967-72.
77. Tsuruo, T., et al., *Enhancement of vincristine- and adriamycin-induced cytotoxicity by verapamil in P388 leukemia and its sublines resistant to vincristine and adriamycin.* Biochem Pharmacol, 1982. **31**(19): p. 3138-40.
78. Benson, A.B., 3rd, et al., *Phase I study of vinblastine and verapamil given by concurrent iv infusion.* Cancer Treat Rep, 1985. **69**(7-8): p. 795-9.

79. Tsuruo, T., et al., *Effects of quinidine and related compounds on cytotoxicity and cellular accumulation of vincristine and adriamycin in drug-resistant tumor cells.* Cancer Res, 1984. **44**(10): p. 4303-7.
80. Ramu, A., D. Glaubiger, and Z. Fuks, *Reversal of acquired resistance to doxorubicin in P388 murine leukemia cells by tamoxifen and other triparanol analogues.* Cancer Res, 1984. **44**(10): p. 4392-5.
81. Bartlett, N.L., et al., *Phase I trial of doxorubicin with cyclosporine as a modulator of multidrug resistance.* J Clin Oncol, 1994. **12**(4): p. 835-42.
82. Berman, E., et al., *Phase I trial of high-dose tamoxifen as a modulator of drug resistance in combination with daunorubicin in patients with relapsed or refractory acute leukemia.* Leukemia, 1995. **9**(10): p. 1631-7.
83. Yu, D.K., *The contribution of P-glycoprotein to pharmacokinetic drug-drug interactions.* J Clin Pharmacol, 1999. **39**(12): p. 1203-11.
84. Fox, E. and S.E. Bates, *Tariquidar (XR9576): a P-glycoprotein drug efflux pump inhibitor.* Expert Rev Anticancer Ther, 2007. **7**(4): p. 447-59.
85. Gruber, A., et al., *A phase I/II study of the MDR modulator Valspodar (PSC 833) combined with daunorubicin and cytarabine in patients with relapsed and primary refractory acute myeloid leukemia.* Leuk Res, 2003. **27**(4): p. 323-8.
86. Crowley, E., C.A. McDevitt, and R. Callaghan, *Generating inhibitors of P-glycoprotein: where to, now?* Methods Mol Biol, 2010. **596**: p. 405-32.
87. Kamath, A.V., et al., *P-glycoprotein plays a role in the oral absorption of BMS-387032, a potent cyclin-dependent kinase 2 inhibitor, in rats.* Cancer Chemother Pharmacol, 2005. **55**(2): p. 110-6.
88. Kitazaki, T., et al., *Gefitinib, an EGFR tyrosine kinase inhibitor, directly inhibits the function of P-glycoprotein in multidrug resistant cancer cells.* Lung Cancer, 2005. **49**(3): p. 337-43.
89. Smith, E. and I. Collins, *Photoaffinity labeling in target- and binding-site identification.* Future Med Chem, 2015. **7**(2): p. 159-83.
90. Singh, A., E.R. Thornton, and F.H. Westheimer, *The photolysis of diazoacetylchymotrypsin.* J Biol Chem, 1962. **237**: p. 3006-8.
91. Dorman, G. and G.D. Prestwich, *Benzophenone photophores in biochemistry.* Biochemistry, 1994. **33**(19): p. 5661-73.
92. Dorman, G. and G.D. Prestwich, *Using photolabile ligands in drug discovery and development.* Trends Biotechnol, 2000. **18**(2): p. 64-77.
93. Weber, P.J. and A.G. Beck-Sickinger, *Comparison of the photochemical behavior of four different photoactivatable probes.* J Pept Res, 1997. **49**(5): p. 375-83.
94. Robinette, D., et al., *Photoaffinity labeling combined with mass spectrometric approaches as a tool for structural proteomics.* Expert Rev Proteomics, 2006. **3**(4): p. 399-408.
95. Safa, A.R., *Identification and characterization of the binding sites of P-glycoprotein for multidrug resistance-related drugs and modulators.* Curr Med Chem Anticancer Agents, 2004. **4**(1): p. 1-17.
96. Shi, H., et al., *Cell-based proteome profiling of potential dasatinib targets by use of affinity-based probes.* J Am Chem Soc, 2012. **134**(6): p. 3001-14.
97. Safa, A.R., *Photoaffinity labels for characterizing drug interaction sites of P-glycoprotein.* Methods Enzymol, 1998. **292**: p. 289-307.
98. Safa, A.R., *Photoaffinity labeling of P-glycoprotein in multidrug-resistant cells.* Cancer Invest, 1993. **11**(1): p. 46-56.

99. Safa, A.R., N.D. Mehta, and M. Agresti, *Photoaffinity labeling of P-glycoprotein in multidrug resistant cells with photoactive analogs of colchicine.* Biochem Biophys Res Commun, 1989. **162**(3): p. 1402-8.
100. Safa, A.R., *Photoaffinity analogs for multidrug resistance-related transporters and their use in identifying chemosensitizers.* Drug Resist Updat, 1999. **2**(6): p. 371-381.
101. Wu, Q., et al., *Identification of the domains of photoincorporation of the 3'- and 7-benzophenone analogues of taxol in the carboxyl-terminal half of murine mdr1b P-glycoprotein.* Biochemistry, 1998. **37**(32): p. 11272-9.
102. Nare, B., R.K. Prichard, and E. Georges, *Characterization of rhodamine 123 binding to P-glycoprotein in human multidrug-resistant cells.* Mol Pharmacol, 1994. **45**(6): p. 1145-52.
103. Callaghan, R., *Providing a molecular mechanism for P-glycoprotein; why would I bother?* Biochem Soc Trans, 2015. **43**(5): p. 995-1002.
104. Tamai, I. and A.R. Safa, *Competitive interaction of cyclosporins with the Vinca alkaloid-binding site of P-glycoprotein in multidrug-resistant cells.* J Biol Chem, 1990. **265**(27): p. 16509-13.
105. Tamai, I. and A.R. Safa, *Azidopine noncompetitively interacts with vinblastine and cyclosporin A binding to P-glycoprotein in multidrug resistant cells.* J Biol Chem, 1991. **266**(25): p. 16796-800.
106. Greenberger, L.M., *Major photoaffinity drug labeling sites for iodoaryl azidoprazosin in P-glycoprotein are within, or immediately C-terminal to, transmembrane domains 6 and 12.* J Biol Chem, 1993. **268**(15): p. 11417-25.
107. Greenberger, L.M., et al., *Domain mapping of the photoaffinity drug-binding sites in P-glycoprotein encoded by mouse mdr1b.* J Biol Chem, 1991. **266**(31): p. 20744-51.
108. Dey, S., et al., *Evidence for two nonidentical drug-interaction sites in the human P-glycoprotein.* Proc Natl Acad Sci U S A, 1997. **94**(20): p. 10594-9.
109. Chiba, P., et al., *Synthesis, pharmacologic activity, and structure-activity relationships of a series of propafenone-related modulators of multidrug resistance.* J Med Chem, 1995. **38**(14): p. 2789-93.
110. Peer, M., et al., *Photoaffinity labeling of P-glycoprotein.* Mini Rev Med Chem, 2005. **5**(2): p. 165-72.
111. Ecker, G.F., et al., *Identification of ligand-binding regions of P-glycoprotein by activated-pharmacophore photoaffinity labeling and matrix-assisted laser desorption/ionization-time-of-flight mass spectrometry.* Mol Pharmacol, 2002. **61**(3): p. 637-48.
112. Ecker, G.F., et al., *A three-dimensional model for the substrate binding domain of the multidrug ATP binding cassette transporter LmrA.* Mol Pharmacol, 2004. **66**(5): p. 1169-79.
113. Pleban, K., et al., *P-glycoprotein substrate binding domains are located at the transmembrane domain/transmembrane domain interfaces: a combined photoaffinity labeling-protein homology modeling approach.* Mol Pharmacol, 2005. **67**(2): p. 365-74.
114. Crowley, E. and R. Callaghan, *Multidrug efflux pumps: drug binding--gates or cavity?* FEBS J, 2010. **277**(3): p. 530-9.
115. O'Mara, M.L. and D.P. Tieleman, *P-glycoprotein models of the apo and ATP-bound states based on homology with Sav1866 and MalK.* FEBS Lett, 2007. **581**(22): p. 4217-22.

116. Vandevuer, S., et al., *Predicting the three-dimensional structure of human P-glycoprotein in absence of ATP by computational techniques embodying crosslinking data: insight into the mechanism of ligand migration and binding sites.* Proteins, 2006. **63**(3): p. 466-78.
117. Chen, C.J., et al., *Internal duplication and homology with bacterial transport proteins in the mdr1 (P-glycoprotein) gene from multidrug-resistant human cells.* Cell, 1986. **47**(3): p. 381-9.
118. Loo, T.W. and D.M. Clarke, *Membrane topology of a cysteine-less mutant of human P-glycoprotein.* J Biol Chem, 1995. **270**(2): p. 843-8.
119. Senior, A.E. and D.C. Gadsby, *ATP hydrolysis cycles and mechanism in P-glycoprotein and CFTR.* Semin Cancer Biol, 1997. **8**(3): p. 143-50.
120. Loo, T.W., M.C. Bartlett, and D.M. Clarke, *Drug binding in human P-glycoprotein causes conformational changes in both nucleotide-binding domains.* J Biol Chem, 2003. **278**(3): p. 1575-8.
121. Sarkadi, B., et al., *Expression of the human multidrug resistance cDNA in insect cells generates a high activity drug-stimulated membrane ATPase.* J Biol Chem, 1992. **267**(7): p. 4854-8.
122. Ambudkar, S.V., et al., *Partial purification and reconstitution of the human multidrug-resistance pump: characterization of the drug-stimulatable ATP hydrolysis.* Proc Natl Acad Sci U S A, 1992. **89**(18): p. 8472-6.
123. Doige, C.A., X. Yu, and F.J. Sharom, *ATPase activity of partially purified P-glycoprotein from multidrug-resistant Chinese hamster ovary cells.* Biochim Biophys Acta, 1992. **1109**(2): p. 149-60.
124. Sauna, Z.E., K. Nandigama, and S.V. Ambudkar, *Exploiting reaction intermediates of the ATPase reaction to elucidate the mechanism of transport by P-glycoprotein (ABCB1).* J Biol Chem, 2006. **281**(36): p. 26501-11.
125. Sauna, Z.E., et al., *Catalytic cycle of ATP hydrolysis by P-glycoprotein: evidence for formation of the E.S reaction intermediate with ATP-gamma-S, a nonhydrolyzable analogue of ATP.* Biochemistry, 2007. **46**(48): p. 13787-99.
126. Loo, T.W. and D.M. Clarke, *Inhibition of oxidative cross-linking between engineered cysteine residues at positions 332 in predicted transmembrane segments (TM) 6 and 975 in predicted TM12 of human P-glycoprotein by drug substrates.* J Biol Chem, 1996. **271**(44): p. 27482-7.
127. Loo, T.W. and D.M. Clarke, *The packing of the transmembrane segments of human multidrug resistance P-glycoprotein is revealed by disulfide cross-linking analysis.* J Biol Chem, 2000. **275**(8): p. 5253-6.
128. Loo, T.W. and D.M. Clarke, *Drug-stimulated ATPase activity of human P-glycoprotein requires movement between transmembrane segments 6 and 12.* J Biol Chem, 1997. **272**(34): p. 20986-9.
129. Loo, T.W., M.C. Bartlett, and D.M. Clarke, *Disulfide cross-linking analysis shows that transmembrane segments 5 and 8 of human P-glycoprotein are close together on the cytoplasmic side of the membrane.* J Biol Chem, 2004. **279**(9): p. 7692-7.
130. Stenham, D.R., et al., *An atomic detail model for the human ATP binding cassette transporter P-glycoprotein derived from disulfide cross-linking and homology modeling.* FASEB J, 2003. **17**(15): p. 2287-9.
131. Loo, T.W. and D.M. Clarke, *Location of the rhodamine-binding site in the human multidrug resistance P-glycoprotein.* J Biol Chem, 2002. **277**(46): p. 44332-8.

132. Loo, T.W., M.C. Bartlett, and D.M. Clarke, *Transmembrane segment 1 of human P-glycoprotein contributes to the drug-binding pocket.* Biochem J, 2006. **396**(3): p. 537-45.
133. Loo, T.W. and D.M. Clarke, *Identification of residues in the drug-binding site of human P-glycoprotein using a thiol-reactive substrate.* J Biol Chem, 1997. **272**(51): p. 31945-8.
134. Loo, T.W. and D.M. Clarke, *Identification of residues in the drug-binding domain of human P-glycoprotein. Analysis of transmembrane segment 11 by cysteine-scanning mutagenesis and inhibition by dibromobimane.* J Biol Chem, 1999. **274**(50): p. 35388-92.
135. Loo, T.W. and D.M. Clarke, *Identification of residues within the drug-binding domain of the human multidrug resistance P-glycoprotein by cysteine-scanning mutagenesis and reaction with dibromobimane.* J Biol Chem, 2000. **275**(50): p. 39272-8.
136. Loo, T.W. and D.M. Clarke, *Defining the drug-binding site in the human multidrug resistance P-glycoprotein using a methanethiosulfonate analog of verapamil, MTS-verapamil.* J Biol Chem, 2001. **276**(18): p. 14972-9.
137. Loo, T.W. and D.M. Clarke, *Determining the dimensions of the drug-binding domain of human P-glycoprotein using thiol cross-linking compounds as molecular rulers.* J Biol Chem, 2001. **276**(40): p. 36877-80.
138. Devine, S.E., V. Ling, and P.W. Melera, *Amino acid substitutions in the sixth transmembrane domain of P-glycoprotein alter multidrug resistance.* Proc Natl Acad Sci U S A, 1992. **89**(10): p. 4564-8.
139. Loo, T.W. and D.M. Clarke, *Functional consequences of phenylalanine mutations in the predicted transmembrane domain of P-glycoprotein.* J Biol Chem, 1993. **268**(27): p. 19965-72.
140. Loo, T.W. and D.M. Clarke, *Mutations to amino acids located in predicted transmembrane segment 6 (TM6) modulate the activity and substrate specificity of human P-glycoprotein.* Biochemistry, 1994. **33**(47): p. 14049-57.
141. Chen, G., et al., *Multidrug-resistant human sarcoma cells with a mutant P-glycoprotein, altered phenotype, and resistance to cyclosporins.* J Biol Chem, 1997. **272**(9): p. 5974-82.
142. Crowley, E., et al., *Transmembrane helix 12 modulates progression of the ATP catalytic cycle in ABCB1.* Biochemistry, 2009. **48**(26): p. 6249-58.
143. Crowley, E., et al., *Transmembrane helix 12 plays a pivotal role in coupling energy provision and drug binding in ABCB1.* FEBS J, 2010. **277**(19): p. 3974-85.
144. Rothnie, A., et al., *The topography of transmembrane segment six is altered during the catalytic cycle of P-glycoprotein.* J Biol Chem, 2004. **279**(33): p. 34913-21.
145. Rothnie, A., et al., *The coupling mechanism of P-glycoprotein involves residue L339 in the sixth membrane spanning segment.* FEBS Lett, 2005. **579**(18): p. 3984-90.
146. Storm, J., et al., *Residue G346 in transmembrane segment six is involved in inter-domain communication in P-glycoprotein.* Biochemistry, 2007. **46**(35): p. 9899-910.
147. Loo, T.W. and D.M. Clarke, *The transmembrane domains of the human multidrug resistance P-glycoprotein are sufficient to mediate drug binding and trafficking to the cell surface.* J Biol Chem, 1999. **274**(35): p. 24759-65.

148. Loo, T.W., M.C. Bartlett, and D.M. Clarke, *Simultaneous binding of two different drugs in the binding pocket of the human multidrug resistance P-glycoprotein.* J Biol Chem, 2003. **278**(41): p. 39706-10.
149. Loo, T.W., M.C. Bartlett, and D.M. Clarke, *Substrate-induced conformational changes in the transmembrane segments of human P-glycoprotein. Direct evidence for the substrate-induced fit mechanism for drug binding.* J Biol Chem, 2003. **278**(16): p. 13603-6.
150. Rosenberg, M.F., et al., *Repacking of the transmembrane domains of P-glycoprotein during the transport ATPase cycle.* EMBO J, 2001. **20**(20): p. 5615-25.
151. Chufan, E.E., H.M. Sim, and S.V. Ambudkar, *Molecular basis of the polyspecificity of P-glycoprotein (ABCB1): recent biochemical and structural studies.* Adv Cancer Res, 2015. **125**: p. 71-96.
152. Loo, T.W. and D.M. Clarke, *Cross-linking of human multidrug resistance P-glycoprotein by the substrate, tris-(2-maleimidoethyl)amine, is altered by ATP hydrolysis. Evidence for rotation of a transmembrane helix.* J Biol Chem, 2001. **276**(34): p. 31800-5.
153. Loo, T.W., M.C. Bartlett, and D.M. Clarke, *ATP hydrolysis promotes interactions between the extracellular ends of transmembrane segments 1 and 11 of human multidrug resistance P-glycoprotein.* Biochemistry, 2005. **44**(30): p. 10250-8.
154. Lugo, M.R. and F.J. Sharom, *Interaction of LDS-751 and rhodamine 123 with P-glycoprotein: evidence for simultaneous binding of both drugs.* Biochemistry, 2005. **44**(42): p. 14020-9.
155. Shapiro, A.B. and V. Ling, *Positively cooperative sites for drug transport by P-glycoprotein with distinct drug specificities.* Eur J Biochem, 1997. **250**(1): p. 130-7.
156. Shapiro, A.B., et al., *Stimulation of P-glycoprotein-mediated drug transport by prazosin and progesterone. Evidence for a third drug-binding site.* Eur J Biochem, 1999. **259**(3): p. 841-50.
157. Martin, C., et al., *Communication between multiple drug binding sites on P-glycoprotein.* Mol Pharmacol, 2000. **58**(3): p. 624-32.
158. Chufan, E.E., et al., *Multiple transport-active binding sites are available for a single substrate on human P-glycoprotein (ABCB1).* PLoS One, 2013. **8**(12): p. e82463.
159. Shapiro, A.B. and V. Ling, *ATPase activity of purified and reconstituted P-glycoprotein from Chinese hamster ovary cells.* J Biol Chem, 1994. **269**(5): p. 3745-54.
160. Shapiro, A.B. and V. Ling, *Reconstitution of drug transport by purified P-glycoprotein.* J Biol Chem, 1995. **270**(27): p. 16167-75.
161. Shapiro, A.B. and V. Ling, *Extraction of Hoechst 33342 from the cytoplasmic leaflet of the plasma membrane by P-glycoprotein.* Eur J Biochem, 1997. **250**(1): p. 122-9.
162. Shapiro, A.B. and V. Ling, *Effect of quercetin on Hoechst 33342 transport by purified and reconstituted P-glycoprotein.* Biochem Pharmacol, 1997. **53**(4): p. 587-96.
163. Spoelstra, E.C., et al., *Kinetics of daunorubicin transport by P-glycoprotein of intact cancer cells.* Eur J Biochem, 1992. **207**(2): p. 567-79.

164. Spoelstra, E.C., et al., *The multidrug-resistance-reverser verapamil interferes with cellular P-glycoprotein-mediated pumping of daunorubicin as a non-competing substrate.* Eur J Biochem, 1994. **221**(1): p. 363-73.
165. Shapiro, A.B., A.B. Corder, and V. Ling, *P-glycoprotein-mediated Hoechst 33342 transport out of the lipid bilayer.* Eur J Biochem, 1997. **250**(1): p. 115-21.
166. Martinez, L., et al., *Understanding polyspecificity within the substrate-binding cavity of the human multidrug resistance P-glycoprotein.* FEBS J, 2014. **281**(3): p. 673-82.
167. Dolghih, E., et al., *Predicting binding to p-glycoprotein by flexible receptor docking.* PLoS Comput Biol, 2011. **7**(6): p. e1002083.
168. Bikadi, Z., et al., *Predicting P-glycoprotein-mediated drug transport based on support vector machine and three-dimensional crystal structure of P-glycoprotein.* PLoS One, 2011. **6**(10): p. e25815.
169. Pajeva, I.K., et al., *Interactions of the multidrug resistance modulators tariquidar and elacridar and their analogues with P-glycoprotein.* ChemMedChem, 2013. **8**(10): p. 1701-13.
170. Shapiro, A.B. and V. Ling, *Transport of LDS-751 from the cytoplasmic leaflet of the plasma membrane by the rhodamine-123-selective site of P-glycoprotein.* Eur J Biochem, 1998. **254**(1): p. 181-8.
171. Swartz, D.J., et al., *Replacing the eleven native tryptophans by directed evolution produces an active P-glycoprotein with site-specific, non-conservative substitutions.* Sci Rep, 2020. **10**(1): p. 3224.
172. Pawagi, A.B., et al., *Transmembrane aromatic amino acid distribution in P-glycoprotein. A functional role in broad substrate specificity.* J Mol Biol, 1994. **235**(2): p. 554-64.
173. Sharom, F.J., et al., *Exploring the structure and function of the P-glycoprotein multidrug transporter using fluorescence spectroscopic tools.* Semin Cell Dev Biol, 2001. **12**(3): p. 257-65.
174. Qu, Q. and F.J. Sharom, *Proximity of bound Hoechst 33342 to the ATPase catalytic sites places the drug binding site of P-glycoprotein within the cytoplasmic membrane leaflet.* Biochemistry, 2002. **41**(14): p. 4744-52.
175. Qu, Q. and F.J. Sharom, *FRET analysis indicates that the two ATPase active sites of the P-glycoprotein multidrug transporter are closely associated.* Biochemistry, 2001. **40**(5): p. 1413-22.
176. Lugo, M.R. and F.J. Sharom, *Interaction of LDS-751 with P-glycoprotein and mapping of the location of the R drug binding site.* Biochemistry, 2005. **44**(2): p. 643-55.
177. Sharom, F.J., M.R. Lugo, and P.D. Eckford, *New insights into the drug binding, transport and lipid flippase activities of the p-glycoprotein multidrug transporter.* J Bioenerg Biomembr, 2005. **37**(6): p. 481-7.
178. Martin, C., et al., *The molecular interaction of the high affinity reversal agent XR9576 with P-glycoprotein.* Br J Pharmacol, 1999. **128**(2): p. 403-11.
179. Ferry, D.R., M.A. Russell, and M.H. Cullen, *P-glycoprotein possesses a 1,4-dihydropyridine-selective drug acceptor site which is allosterically coupled to a vinca-alkaloid-selective binding site.* Biochem Biophys Res Commun, 1992. **188**(1): p. 440-5.
180. Kenakin, T., *Allosteric modulators: the new generation of receptor antagonist.* Mol Interv, 2004. **4**(4): p. 222-9.

181. Martin, C., et al., *Drug binding sites on P-glycoprotein are altered by ATP binding prior to nucleotide hydrolysis.* Biochemistry, 2000. **39**(39): p. 11901-6.
182. Garrigos, M., L.M. Mir, and S. Orlowski, *Competitive and non-competitive inhibition of the multidrug-resistance-associated P-glycoprotein ATPase--further experimental evidence for a multisite model.* Eur J Biochem, 1997. **244**(2): p. 664-73.
183. Pascaud, C., M. Garrigos, and S. Orlowski, *Multidrug resistance transporter P-glycoprotein has distinct but interacting binding sites for cytotoxic drugs and reversing agents.* Biochem J, 1998. **333 (Pt 2)**: p. 351-8.
184. Taylor, A.M., et al., *Detailed characterization of cysteine-less P-glycoprotein reveals subtle pharmacological differences in function from wild-type protein.* Br J Pharmacol, 2001. **134**(8): p. 1609-18.
185. Storm, J., et al., *Cytosolic region of TM6 in P-glycoprotein: topographical analysis and functional perturbation by site directed labeling.* Biochemistry, 2008. **47**(12): p. 3615-24.
186. Liu, R., A. Siemiarczuk, and F.J. Sharom, *Intrinsic fluorescence of the P-glycoprotein multidrug transporter: sensitivity of tryptophan residues to binding of drugs and nucleotides.* Biochemistry, 2000. **39**(48): p. 14927-38.
187. Rigaud, J.L., M.T. Paternostre, and A. Bluzat, *Mechanisms of membrane protein insertion into liposomes during reconstitution procedures involving the use of detergents. 2. Incorporation of the light-driven proton pump bacteriorhodopsin.* Biochemistry, 1988. **27**(8): p. 2677-88.
188. Chifflet, S., et al., *A method for the determination of inorganic phosphate in the presence of labile organic phosphate and high concentrations of protein: application to lens ATPases.* Anal Biochem, 1988. **168**(1): p. 1-4.
189. Russell, P.L. and F.J. Sharom, *Conformational and functional characterization of trapped complexes of the P-glycoprotein multidrug transporter.* Biochem J, 2006. **399**(2): p. 315-23.
190. Kodan, A., et al., *Improved expression and purification of human multidrug resistance protein MDR1 from baculovirus-infected insect cells.* Protein Expr Purif, 2009. **66**(1): p. 7-14.
191. Losada-Perez, P., et al., *Dielectric constant of fluids and fluid mixtures at criticality.* Phys Rev E Stat Nonlin Soft Matter Phys, 2010. **81**(4 Pt 1): p. 041121.
192. Tamaki, A., et al., *The controversial role of ABC transporters in clinical oncology.* Essays Biochem, 2011. **50**(1): p. 209-32.
193. Sun, J., et al., *A systematic analysis of FDA-approved anticancer drugs.* BMC Syst Biol, 2017. **11**(Suppl 5): p. 87.
194. Subramanian, N., et al., *Identification of Possible Binding Sites for Morphine and Nicardipine on the Multidrug Transporter P-Glycoprotein Using Umbrella Sampling Techniques.* J Chem Inf Model, 2015. **55**(6): p. 1202-17.
195. Dey, S., et al., *A single amino acid residue contributes to distinct mechanisms of inhibition of the human multidrug transporter by stereoisomers of the dopamine receptor antagonist flupentixol.* Biochemistry, 1999. **38**(20): p. 6630-9.
196. Zhang, J., et al., *Interaction of P-glycoprotein with anti-tumor drugs: the site, gate and pathway.* Soft Matter, 2015. **11**(33): p. 6633-41.
197. Loo, T.W., M.C. Bartlett, and D.M. Clarke, *The drug-binding pocket of the human multidrug resistance P-glycoprotein is accessible to the aqueous medium.* Biochemistry, 2004. **43**(38): p. 12081-9.

198. Ward, A., et al., *Flexibility in the ABC transporter MsbA: Alternating access with a twist.* Proc Natl Acad Sci U S A, 2007. **104**(48): p. 19005-10.
199. Alam, A., et al., *Structural insight into substrate and inhibitor discrimination by human P-glycoprotein.* Science, 2019. **363**(6428): p. 753-756.
200. Nosol, K., et al., *Cryo-EM structures reveal distinct mechanisms of inhibition of the human multidrug transporter ABCB1.* Proc Natl Acad Sci U S A, 2020. **117**(42): p. 26245-26253.
201. Ferreira, R.J., M.J. Ferreira, and D.J. dos Santos, *Molecular docking characterizes substrate-binding sites and efflux modulation mechanisms within P-glycoprotein.* J Chem Inf Model, 2013. **53**(7): p. 1747-60.
202. Blott, E.J., C.F. Higgins, and K.J. Linton, *Cysteine-scanning mutagenesis provides no evidence for the extracellular accessibility of the nucleotide-binding domains of the multidrug resistance transporter P-glycoprotein.* EMBO J, 1999. **18**(23): p. 6800-8.
203. Senior, A.E., M.K. al-Shawi, and I.L. Urbatsch, *ATP hydrolysis by multidrug-resistance protein from Chinese hamster ovary cells.* J Bioenerg Biomembr, 1995. **27**(1): p. 31-6.
204. Sauna, Z.E. and S.V. Ambudkar, *About a switch: how P-glycoprotein (ABCB1) harnesses the energy of ATP binding and hydrolysis to do mechanical work.* Mol Cancer Ther, 2007. **6**(1): p. 13-23.
205. Lawson, J., M.L. O'Mara, and I.D. Kerr, *Structure-based interpretation of the mutagenesis database for the nucleotide binding domains of P-glycoprotein.* Biochim Biophys Acta, 2008. **1778**(2): p. 376-91.
206. Loo, T.W., M.C. Bartlett, and D.M. Clarke, *Methanethiosulfonate derivatives of rhodamine and verapamil activate human P-glycoprotein at different sites.* J Biol Chem, 2003. **278**(50): p. 50136-41.
207. Locher, K.P., *Mechanistic diversity in ATP-binding cassette (ABC) transporters.* Nat Struct Mol Biol, 2016. **23**(6): p. 487-93.
208. Xu, Y., A. Seelig, and S. Berneche, *Unidirectional Transport Mechanism in an ATP Dependent Exporter.* ACS Cent Sci, 2017. **3**(3): p. 250-258.
209. Wang, L. and Y. Sun, *Efflux mechanism and pathway of verapamil pumping by human P-glycoprotein.* Arch Biochem Biophys, 2020. **696**: p. 108675.
210. Subramanian, N., et al., *Probing the Pharmacological Binding Sites of P-Glycoprotein Using Umbrella Sampling Simulations.* J Chem Inf Model, 2019. **59**(5): p. 2287-2298.
211. Zhang, J., et al., *Drug promiscuity of P-glycoprotein and its mechanism of interaction with paclitaxel and doxorubicin.* Soft Matter, 2014. **10**(3): p. 438-45.
212. Cui, W., et al., *Unraveling the allosteric inhibition mechanism of PTP1B by free energy calculation based on umbrella sampling.* J Chem Inf Model, 2013. **53**(5): p. 1157-67.
213. Chang, S.Y., et al., *Molecular insight into conformational transmission of human P-glycoprotein.* J Chem Phys, 2013. **139**(22): p. 225102.
214. Wise, J.G., *Catalytic transitions in the human MDR1 P-glycoprotein drug binding sites.* Biochemistry, 2012. **51**(25): p. 5125-41.
215. Prajapati, R. and A.T. Sangamwar, *Translocation mechanism of P-glycoprotein and conformational changes occurring at drug-binding site: Insights from multi-targeted molecular dynamics.* Biochim Biophys Acta, 2014. **1838**(11): p. 2882-98.

216. McCormick, J.W., P.D. Vogel, and J.G. Wise, *Multiple Drug Transport Pathways through Human P-Glycoprotein.* Biochemistry, 2015. **54**(28): p. 4374-90.
217. Eytan, G.D., et al., *Efficiency of P-glycoprotein-mediated exclusion of rhodamine dyes from multidrug-resistant cells is determined by their passive transmembrane movement rate.* Eur J Biochem, 1997. **248**(1): p. 104-12.
218. Loo, T.W. and D.M. Clarke, *Recent progress in understanding the mechanism of P-glycoprotein-mediated drug efflux.* J Membr Biol, 2005. **206**(3): p. 173-85.
219. Loo, T.W. and D.M. Clarke, *Do drug substrates enter the common drug-binding pocket of P-glycoprotein through "gates"?* Biochem Biophys Res Commun, 2005. **329**(2): p. 419-22.
220. Loo, T.W., M.C. Bartlett, and D.M. Clarke, *Suppressor mutations in the transmembrane segments of P-glycoprotein promote maturation of processing mutants and disrupt a subset of drug-binding sites.* J Biol Chem, 2007. **282**(44): p. 32043-52.
221. Loo, T.W., M.C. Bartlett, and D.M. Clarke, *Identification of residues in the drug translocation pathway of the human multidrug resistance P-glycoprotein by arginine mutagenesis.* J Biol Chem, 2009. **284**(36): p. 24074-87.
222. O'Mara, M.L. and A.E. Mark, *The Effect of Environment on the Structure of a Membrane Protein: P-Glycoprotein under Physiological Conditions.* J Chem Theory Comput, 2012. **8**(10): p. 3964-76.
223. Seelig, A., *P-Glycoprotein: One Mechanism, Many Tasks and the Consequences for Pharmacotherapy of Cancers.* Front Oncol, 2020. **10**: p. 576559.
224. Ferreira, R.J., M.J. Ferreira, and D.J. Dos Santos, *Do drugs have access to the P-glycoprotein drug-binding pocket through gates?* J Chem Theory Comput, 2015. **11**(10): p. 4525-9.
225. Loo, T.W., M.C. Bartlett, and D.M. Clarke, *Val133 and Cys137 in transmembrane segment 2 are close to Arg935 and Gly939 in transmembrane segment 11 of human P-glycoprotein.* J Biol Chem, 2004. **279**(18): p. 18232-8.
226. Sharom, F.J., *The P-glycoprotein efflux pump: how does it transport drugs?* J Membr Biol, 1997. **160**(3): p. 161-75.
227. Raviv, Y., et al., *Photosensitized labeling of a functional multidrug transporter in living drug-resistant tumor cells.* J Biol Chem, 1990. **265**(7): p. 3975-80.
228. Higgins, C.F. and M.M. Gottesman, *Is the multidrug transporter a flippase?* Trends Biochem Sci, 1992. **17**(1): p. 18-21.
229. Sharom, F.J., *Complex Interplay between the P-Glycoprotein Multidrug Efflux Pump and the Membrane: Its Role in Modulating Protein Function.* Front Oncol, 2014. **4**: p. 41.
230. Omote, H. and M.K. Al-Shawi, *A novel electron paramagnetic resonance approach to determine the mechanism of drug transport by P-glycoprotein.* J Biol Chem, 2002. **277**(47): p. 45688-94.
231. Katzir, H., et al., *Role of the plasma membrane leaflets in drug uptake and multidrug resistance.* FEBS J, 2010. **277**(5): p. 1234-44.
232. Oliveira, A.S., A.M. Baptista, and C.M. Soares, *Conformational changes induced by ATP-hydrolysis in an ABC transporter: a molecular dynamics study of the Sav1866 exporter.* Proteins, 2011. **79**(6): p. 1977-90.
233. Chakraborty, S., B. Asgeirsson, and B.J. Rao, *A measure of the broad substrate specificity of enzymes based on 'duplicate' catalytic residues.* PLoS One, 2012. **7**(11): p. e49313.

234. Bankstahl, J.P., et al., *Tariquidar and elacridar are dose-dependently transported by P-glycoprotein and Bcrp at the blood-brain barrier: a small-animal positron emission tomography and in vitro study.* Drug Metab Dispos, 2013. **41**(4): p. 754-62.
235. Vahedi, S., E.E. Chufan, and S.V. Ambudkar, *Global alteration of the drug-binding pocket of human P-glycoprotein (ABCB1) by substitution of fifteen conserved residues reveals a negative correlation between substrate size and transport efficiency.* Biochem Pharmacol, 2017. **143**: p. 53-64.
236. Sajid, A., et al., *Evidence for the critical role of transmembrane helices 1 and 7 in substrate transport by human P-glycoprotein (ABCB1).* PLoS One, 2018. **13**(9): p. e0204693.
237. Loo, T.W. and D.M. Clarke, *Mapping the Binding Site of the Inhibitor Tariquidar That Stabilizes the First Transmembrane Domain of P-glycoprotein.* J Biol Chem, 2015. **290**(49): p. 29389-401.
238. Martin, C., C.F. Higgins, and R. Callaghan, *The vinblastine binding site adopts high- and low-affinity conformations during a transport cycle of P-glycoprotein.* Biochemistry, 2001. **40**(51): p. 15733-42.
239. Subramanian, N., K. Condic-Jurkic, and M.L. O'Mara, *Structural and dynamic perspectives on the promiscuous transport activity of P-glycoprotein.* Neurochem Int, 2016. **98**: p. 146-52.
240. Bonito, C.A., et al., *Theoretical insights on helix repacking as the origin of P-glycoprotein promiscuity.* Sci Rep, 2020. **10**(1): p. 9823.
241. Ferreira, R.J., M.J. Ferreira, and D.J. Dos Santos, *Assessing the Stabilization of P-Glycoprotein's Nucleotide-Binding Domains by the Linker, Using Molecular Dynamics.* Mol Inform, 2013. **32**(5-6): p. 529-40.
242. Sajid, A., et al., *Reversing the direction of drug transport mediated by the human multidrug transporter P-glycoprotein.* Proc Natl Acad Sci U S A, 2020. **117**(47): p. 29609-29617.
243. van Wonderen, J.H., et al., *The central cavity of ABCB1 undergoes alternating access during ATP hydrolysis.* FEBS J, 2014. **281**(9): p. 2190-201.
244. Chufan, E.E., K. Kapoor, and S.V. Ambudkar, *Drug-protein hydrogen bonds govern the inhibition of the ATP hydrolysis of the multidrug transporter P-glycoprotein.* Biochem Pharmacol, 2016. **101**: p. 40-53.
245. Berridge, G., et al., *The nucleotide-binding domains of P-glycoprotein. Functional symmetry in the isolated domain demonstrated by N-ethylmaleimide labelling.* Eur J Biochem, 2003. **270**(7): p. 1483-92.
246. Davidson, A.L. and H. Nikaido, *Purification and characterization of the membrane-associated components of the maltose transport system from Escherichia coli.* J Biol Chem, 1991. **266**(14): p. 8946-51.
247. Ko, Y.H. and P.L. Pedersen, *The first nucleotide binding fold of the cystic fibrosis transmembrane conductance regulator can function as an active ATPase.* J Biol Chem, 1995. **270**(38): p. 22093-6.
248. Nikaido, K., P.Q. Liu, and G.F. Ames, *Purification and characterization of HisP, the ATP-binding subunit of a traffic ATPase (ABC transporter), the histidine permease of Salmonella typhimurium. Solubility, dimerization, and ATPase activity.* J Biol Chem, 1997. **272**(44): p. 27745-52.
249. Sonveaux, N., et al., *Ligand-mediated tertiary structure changes of reconstituted P-glycoprotein. A tryptophan fluorescence quenching analysis.* J Biol Chem, 1999. **274**(25): p. 17649-54.

250. Subramanian, N., et al., *Understanding the accumulation of P-glycoprotein substrates within cells: The effect of cholesterol on membrane partitioning.* Biochim Biophys Acta, 2016. **1858**(4): p. 776-82.
251. Ferreira, R.J., M.J. Ferreira, and D.J. dos Santos, *Do adsorbed drugs onto P-glycoprotein influence its efflux capability?* Phys Chem Chem Phys, 2015. **17**(34): p. 22023-34.